TECHNISCHE UNIVERSITÄT MÜNCHEN

Institute for
Experimental Physics E21

Annual Report 2004

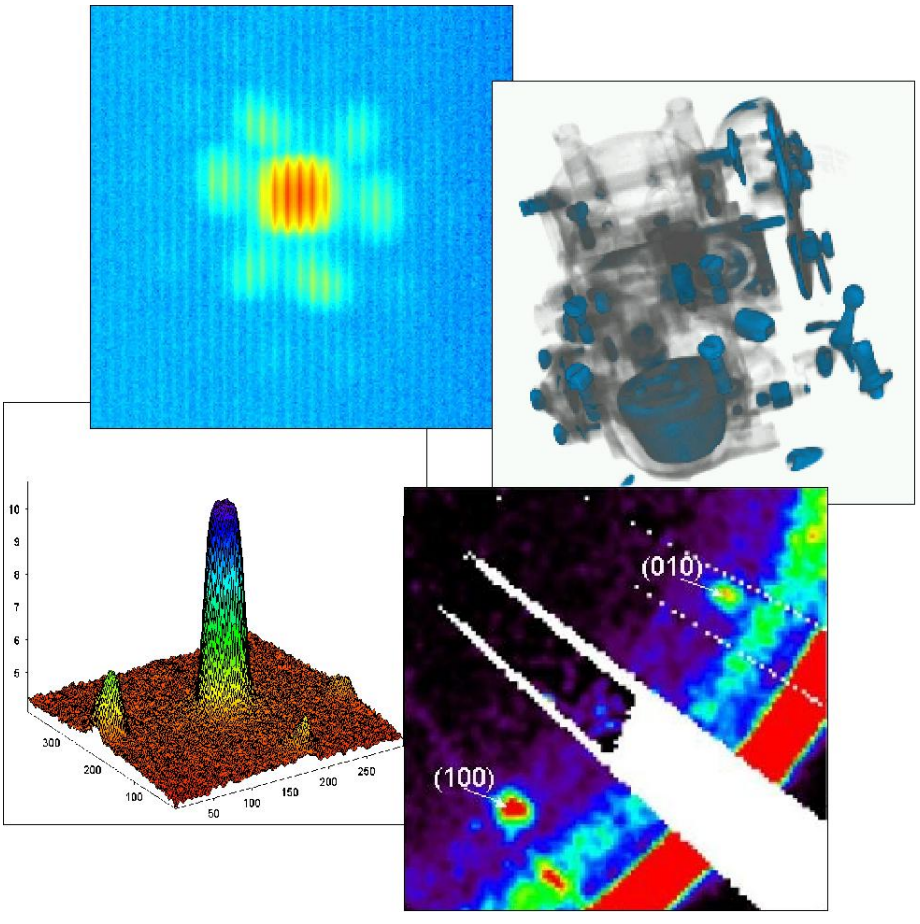

Annual Report 2004

of the Institute for Experimental Physics E21
Prof. Dr. P. Böni
Technische Universität München

Annual Report 2004
of the Institute for Experimental Physics E21
published: Feb. 2005
Layout by Nikolas Arend, Florian Grünauer
Edited by Nikolas Arend
http://www.ph.tum.de/lehrstuehle/E21

Technische Universität München
James-Franck-Straße
D-85747 Garching

Phone: +49-89-289-14711
Fax: +49-89-289-14713

Contents

Preface

The most exciting event in the year 2004 was of course the initial operation of the new neutron source FRM-II on March 2 2004. Thanks to the very accurate flux calculations it took only two hours to attain a self-sustained chain reaction at the precalculated position of the control rod, demonstrating that the details of the fission process are very well understood. It was within a week that the ANTARES beam line of E21 was able to produce the first radiographies at a reactor power of 50 kW within 30 seconds, demonstrating that for radiography the FRM-II provides a flux gain of approximately 400 and significantly better resolution compared to the "Atom Egg". At the same time we also succeeded in extracting a monochromatic beam of very cold neutrons from beam line MIRA and produced the first reflection measurements from a supermirror that was manufactured at TUM. The commissioning of the reactor advanced rather quickly and full power was reached on August 25 2004.

In Summer 2004 the in-pile positron source NEPOMUC was set into operation at the nominal reactor power of 20 MW, providing a high flux of $\simeq 10^8$ moderated positrons at an energy of 1 keV. Within the course of a diploma work first spatially resolved defect densities in brass were determined. Unfortunately, no polarised neutrons could be delivered to the zero-field spin-echo spectrometer RESEDA due to problems with the shielding of neutron guide NL5. We are looking forward to the beam lines PANDA (cold triple-axis) as well as REFSANS (reflectometer), where E21 has a share of 10% of the beam time, to become operational in early 2005.

Another highlight of 2004 was the organisation of the International Topical Meeting on Neutron Radiography ITMNR-5 in Garching by the Department of Radiochemistry (RCM) and E21 of the Physics Department. 92 scientist from 22 countries contributed 64 papers for a very lively and successful conference. It was professionally organised by Thomas Bücherl from RCM and Burkhard Schillinger from E21/FRM-II. The refereed proceedings will soon appear in a special issue of Nuclear Instruments and Methods in Physics Research (NIMA).

Last year we had some important changes in staff positions. Thanks to the excellent support of the Ministry for Culture and Science of Bavaria and the Hochschulleitung of TUM we succeeded to fill the permanent C3 position of E21 by Prof. Dr. Christian Pfleiderer on Dec. 22 2004 (see article on the next page) within a very short time. We are extremely happy to welcome him at E21 and hope that we can quickly provide excellent working conditions allowing him to continue his widely appreciated research projects in low temperature physics. On the one hand we are sad about losing two excellent scientists in E21 due to the retirement of Dr. E. Steichele in late 2003 and Prof. Dr. K. Böning in Summer 2004. On the other hand we are happy that they are going to share their expertise in neutron optics and reactor technology with us in the future. In particular, we are very pleased that Klaus was willing to continue his teaching duties. We wish them many more enjoyable and rewarding years.

Besides instrumentation, E21 was very active in doing science. Within the course of a diploma work we succeeded in observing the flux line lattice in Nb and the incommensurate scattering in MnSi using MIRA at FRM-II. Of course, most experiments were still conducted at other neutron sources, namely GKSS, ISIS, PSI, ILL, Dubna and IPNS. We thank these institutions for collaborating with E21. Highlights within these collaborations were the observation of inelastic scattering at the silent Bragg peaks in the spin density wave state of Cr and chiral scattering in an artificial multilayer. Our scientific results are reported in more than 20 publications and were presented during the occasion of more than 40 conference and seminar contributions.

Garching, January 2005

Peter Böni

Appointment of Prof. C. Pfleiderer, PhD, at E21

Christian Pfleiderer, born in 1965, studied Physics at the University of Tübingen and the University of Denver. In 1994 he earned a doctorate in Physics at the University of Cambridge. From 1994 to 1996 Christian Pfleiderer was employed as post-doctoral fellow and engineer for cryo-physics at the CEA Grenoble. Since 1996 he has worked as scientific assistant at the Universität Karlsruhe, followed by a recent appointment as head of group of a team of young scientists at the Universität Karlsruhe funded by the Helmholtzgemeinschaft Deutscher Forschungszentren. His main research activities concern the experimental investigation of magnetic metals under extreme conditions (low temperatures, high pressure and strong magnetic field) with a special interest in quantum phase transitions und the emergence of novel electronic states. Examples include the metallic state itself as well as novel forms of magnetic order and superconductivity.

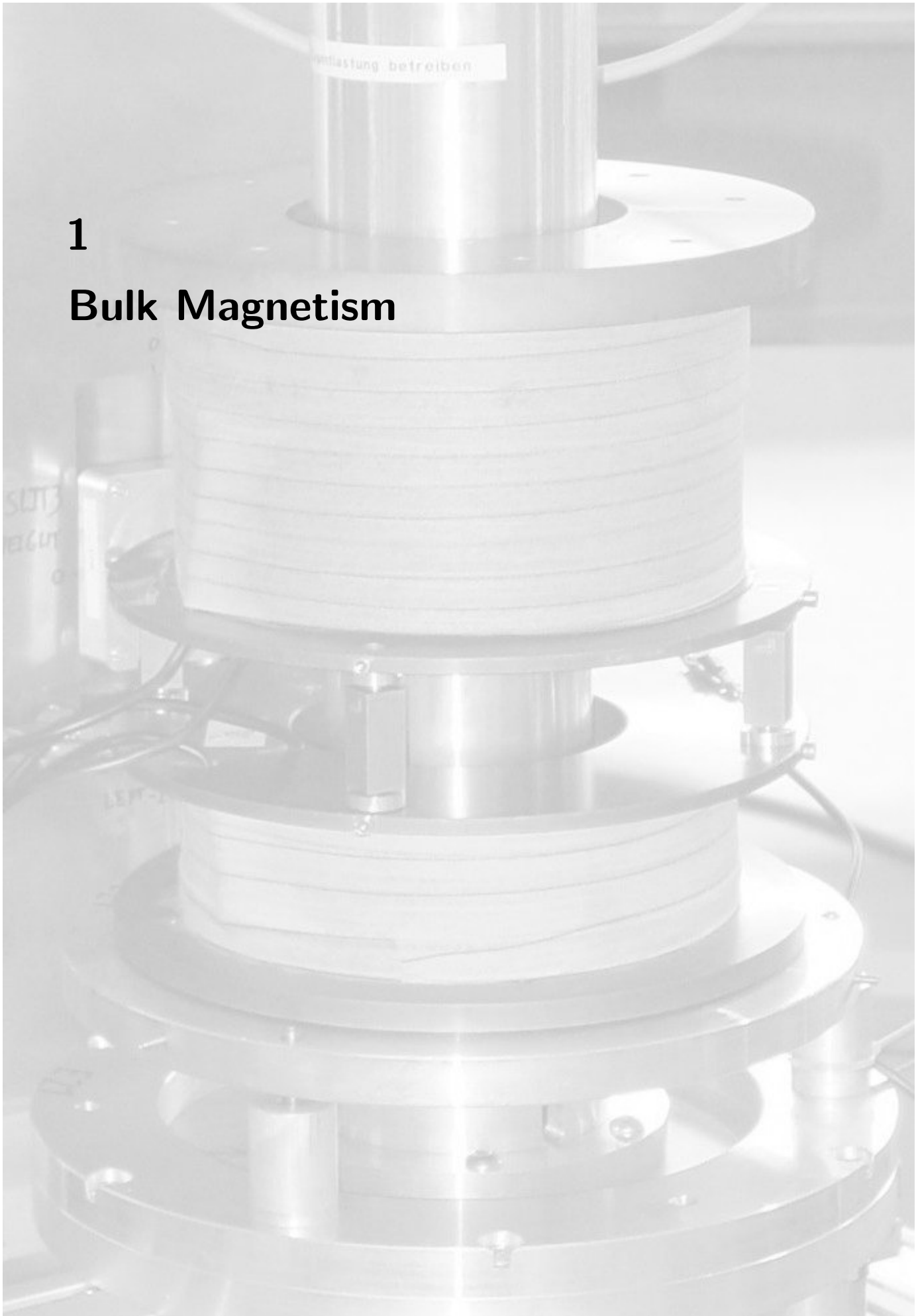

1
Bulk Magnetism

1.1 Reinvestigation of magnetic critical phenomena in MnSi

D. Lamago [1, 2], **R. Georgii** [1, 2], **P. Böni** [1], **H. Eckerlebe** [3], **K. Pranzas** [3], **A.I. Okorokov** [4], **Yu.O. Chetverikov** [4]

[1] *Technische Universität München, Physics Department, Institute E21, D-85747 Garching, Germany*
[2] *Technische Universität München, ZWE FRM-II, D-85747 Garching, Germany*
[3] *GKSS Forschungszentrum, 21502 Geesthacht, Germany*
[4] *Petersburg Nuclear Physics Institute 188350, Russia*

The predictions of Kawamura [1] on the existence of new universality classes for magnetic systems with chiral symmetry motivated several theoretical and experimental investigations of critical phenomena in helical magnets. In spite of some experimental validation of the hypothesis of new chiral universality classes, the Kawamuras predictions are still subject of controversy. Azaria et al. [2] suggest that the lack of universality of experimental results on Ho, Dy and Tb can be understood as the consequence of a tricritical mean-field behavior for the Heisenberg-like spin-order. Experimental and theoretical investigations of the magnetic critical behavior in the intermetallic compound MnSi could help to explain the phase transitions in helimagnets since MnSi is known as a typical chiral magnet and exhibits a complex magnetic transition at 29 K. Here we report on critical small angle polarized neutron scattering measurements of a single crystal of MnSi. A precise alignment of the single crystal allows to study the critical behavior of each magnetic satellite separately and thus to evaluate with high accuracy the critical exponents of the phase transition. The measuremnents were performed at the GKSS research center (SANS-2) and at the FRM-II (MIRA).

The high quality single crystal was oriented in such a way that two axes [111] were set in a plane perpendicular to the incident beam. The possibility to rotate the sample was given by a low temperature piezo-rotator of *Attocube Systems*. The sample could be rotated only around the vertical axis, it was not possible to tilt the sample. This set-up allowed us to select a magnetic satellite of interest and then to perform a field and/or a temperature scan. In our previous experiment it was quite difficult to satisfactorily align the crystal since there were no goniometer available.

Fig. 1 displays a typical diffraction pattern of a helical magnet at zero field for $T = 17$ K. We denote the appearance of four magnetic peaks due to the reflection of the chiral vectors collinear to the two [111] axes.

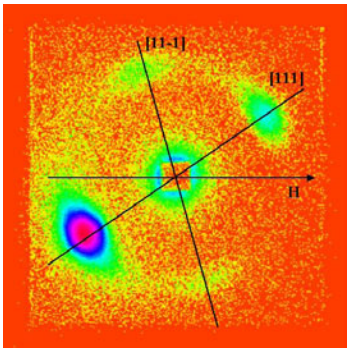

Figure 1: SANS scattering patterns observed in MnSi at zero field for $T = 17$ K.

There are no additional peaks as in our previous measurements, which indicates a better crystal orientation. First measurements on the Instrument MIRA at the FRM-2 display a similar scattering pattern (see Fig. 2).

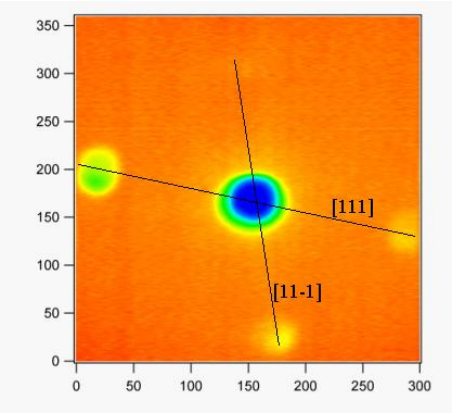

Figure 2: Scattering patterns observed in MnSi on the instrument MIRA at zero field for $T = 27$ K.

.

The sample was then rotated in such a way that only the magnetic satellites along one of the [111] direction were visible (not shown). It should be noticed that the other peaks were not dissolved completely since it was not possible to tilt the sample. In this geometry we used polarised neutrons and changed the magnetic field from $H = 0$ to 600 mT. As soon as a magnetic field is applied, the selected satellites move towards the direction of the field so that at $H_c = 350$ mT the peaks collapses to the direction of the magnetic field and only one satellite is visible as shown in Fig.3 (case with flipper on).

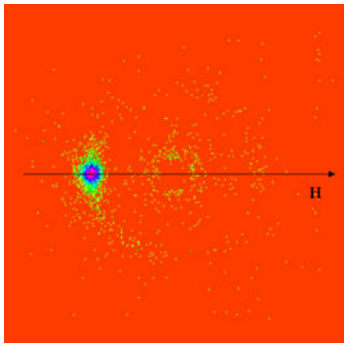

Figure 3: SANS scattering patterns at $H = 350$ mT for $T = 17$ K.

The intensity of this peak begin to decrease with further increase of the magnetic field and finally vanished, i.e. no scattering is observed anymore. From the dependence of the scattering intensity with the reduced magnetic field $I \propto (H - H_C)^{\beta}$, we find the critical exponent $\beta = 0.23 \pm 0.013$ of the phase transition due to the wave-vector rotation towards the [111] direction.

References

[1] H. Kawamura. *J. Appl. Phys.*, 63:3086, 1988.
[2] P. Azaria, B. Delamotte, and T. Jolicoeur. *J. Appl. Phys.*, 69:8, 1991.

1.2 The influence of pressure on the spin excitations in MnSi

D. Lamago [1, 2], **C. Pfleiderer** [3, 7], **P. Böni** [1], **B. Roessli** [4], **L. Pintschovius** [5], **D. Reznik** [5, 6]
[1] *Technische Universität München, Physics Department, Institute E21, D-85747 Garching, Germany*
[2] *Technische Universität München, ZWE FRM-II, D-85747 Garching, Germany*
[3] *Physikalisches Institut, Universität Karlsruhe, D-76128 Karlsruhe, Germany*
[4] *Laboratory for Solid State Physics, ETH Zürich, CH-8093 Zürich, Switzerland*
[5] *Forschungszentrum Karlsruhe, Institut für Festkörperphysik, D-76021 Karlsruhe, Germany*
[6] *Laboratoire Léon Brillouin, CEA Saclay, F-91191 Gif-sur-Yvette Cedex, France*
[7] *now at: Technische Universität München, Physics Department, Institute E21, D-85747 Garching, Germany*

The behaviour of the critical fluctuations of MnSi at ambient pressure has been studied in great detail in the past. Ishikawa et al. [1] established that the fluctuations well above T_c may be viewed as ferromagnetic paramagnons. Using polarised neutron diffraction it was recently found that the fluctuations are sensitive to the DM-interaction near T_c [2] and exhibit chirality. First neutron diffraction studies as function of pressure up to 20 kbar established, on the one hand the existence of large ordered moments far into the non-Fermi-Liquid (NFL) phase, despite, on the other hand, clear signatures of vanishing bulk long range order at P_c seen in the susceptibility and resistivity [3]. In contrast to conventional three-dimensional order, however, these moments are arranged in a highly unusual pattern giving rise to Bragg intensity on a tiny sphere in reciprocal space implying partial magnetic order. The goal of this experiment was to investigate the pressure dependence of the spin waves below p_c and to search for the spin excitations above p_c in order to understand the unusual quasi-static order in the NFL phase.

A high-quality single crystal of MnSi (diameter $\sim$ 6 mm, length $\sim$ 2 cm) was investigated at ambient pressure and in the pressure cell. The cell was not loaded to the maximum pressure on purpose. From the temperature dependence of the satellite intensity at high pressure (not shown), we conclude that the pressure was close to 8 kbar (disappearence of the magnetic satellite intensity at $T = 18$ K) according to the previously established pressure-temperature phase diagram.

Q-scans through the 110-Bragg peak at ambient pressure were performed and are shown in Fig. 1.

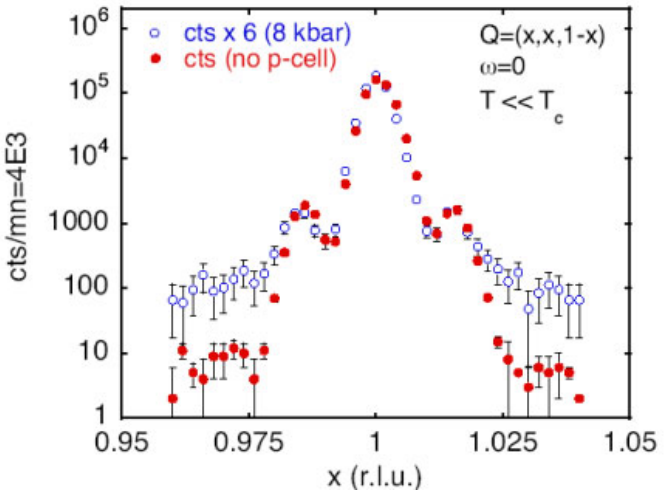

Figure 1: Neutron scattering intensity of the (110) nuclear Bragg peak and the magnetic sattlites of MnSi at ambient pressure and at $p = 8$ kbar, where the data at 8 kbar have been multiplied by a factor of 6.

The satellite intensity at 8 kbar remains unchanged within the experimental error indicating that the ordered moment does not decrease with pressure. A constant energy scan at 0.5 meV (see Fig. 2) shows a broad square peak in the zero pressure scan due to inelastic magnetic scattering, which was the focus of the experiment.

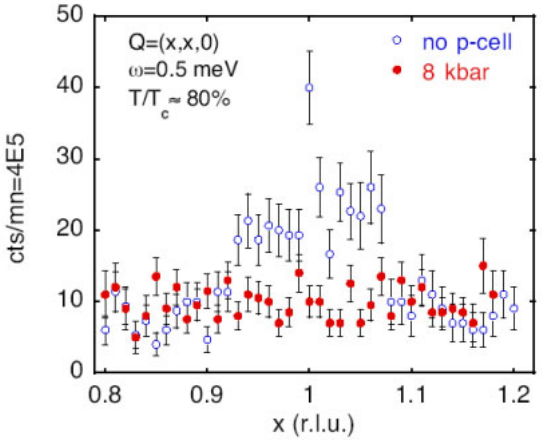

Figure 2: Neutron scattering intensity through the magnetic sattelite at a constant energy transfer $\omega = 0.5$ meV of the same sample with a pressure cell (8 kbar) and without pressure cell.

This result agrees with previous studies [4]. However, we do not observe a magnetic signal at elevated pressure. This is not necessarily due to the absence of this signal, but may be simply due to the absorbtion of the pressure cell because the background is not reduced. We note that the signal to be expected in MnSi is comparatively small since the magnetic moment is just 0.4 μ_B which, above the critical pressure p_c is moreover spread over a certain volume in reciprocal space. Considering the fact that the counting time of the scans we performed were 13 minutes per point, we conclude that the measurements of the magnetic excitations in MnSi under pressure are unfeasible with the current pressure cell. Use of a moderately less absorbing pressure cell material may already proof to resolve this problem. At the same time we are able to conclude, that the newly developed cell promises to be very useful for measurements on other materials having a moderately larger inelastic signal.

References

[1] Y. Ishikawa et al. *Phys. Rev. B*, 31:5884, 1985.
[2] B. Roessli et al. *Phys. Rev. Lett.*, 88:237204, 2002.
[3] C. Pfleiderer et al. *Nature*, 427:227, 2004.
[4] B. Roessli et al. *Physica B*, 345:124–127, 2004.

1.3 Spin wave damping in the isotropic Heisenberg antiferromagnet $RbMnF_3$

Sebastian Stüber [1], **Mechthild Enderle** [2], **Severian Gvasaliya** [3]
[1] *Technische Universität München, Physics Department, Institute E21, D-85747 Garching, Germany*
[2] *Institut Laue-Langevin, BP 156, Grenoble, 38042, France*
[3] *Laboratory for Neutron Scattering ETH & PSI, CH-5232 Villigen PSI, Switzerland*

As $RbMnF_3$ is a simple cubic antiferromagnet, ordering below the Néel temperature $T_N = 83$ K with moments along the [111] direction [1], its spin dynamics have already been studied in the 1970's [2]. However because of limited energy resolution (0.2 meV), these measurements remain deficient, especially for low temperatures.

Neutron Resonance Spin Echo (invented by R. Golub and R. Gähler [3] in 1987, for an introduction see, e.g., [4]) now offers the possibility to significantly improve the available data, as it increases energy resolution by at least an order of magnitude, compared to the stated limitations of standard triple axis spectrometry.

The main scientific case is to check the compliance between theory and experiment, which has been started by S. Rezende and R. White [5]. They did numerical calculations based on four-magnon exchange scattering as dominant relaxation channel for $q \neq 0$ magnons. As can be seen in fig. 1, a safe assessment for lower temperatures ($T < 0.4\,T_N$) cannot be made.

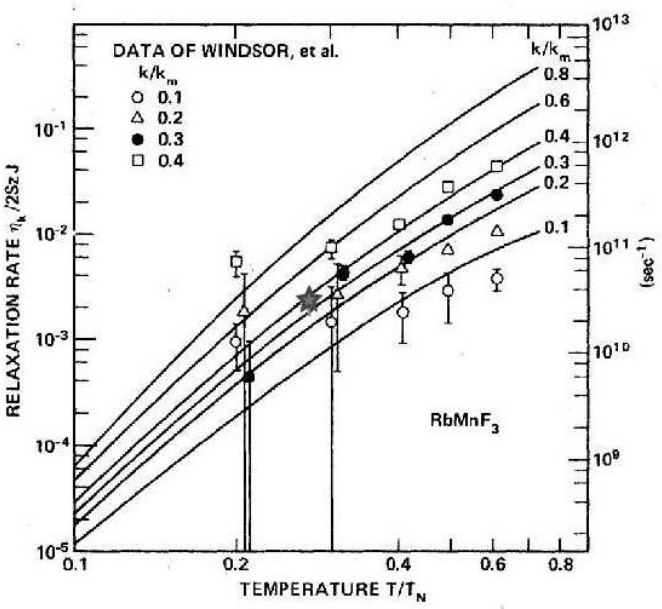

Figure 1: Relaxation rate (in units of $2SzJ$) vs. reduced temperature [5]. The star indicates the recent result of the ZETA measurements for $k = 0.4\,k_m$.

The star in fig. 1 is the result of measurements done at the Institut Laue-Langevin (ILL) in Grenoble, France, using the ZETA option [6] for IN20. Several spin echo times for the transverse magnon at $Q = (-0.4\,-0.4\,+0.6)$ were measured for two temperatures, at 2 K with no intrinsic line width, and at 24 K. The data has been corrected for beam efficiency and mosaicity effects. The results are shown in fig. 2.

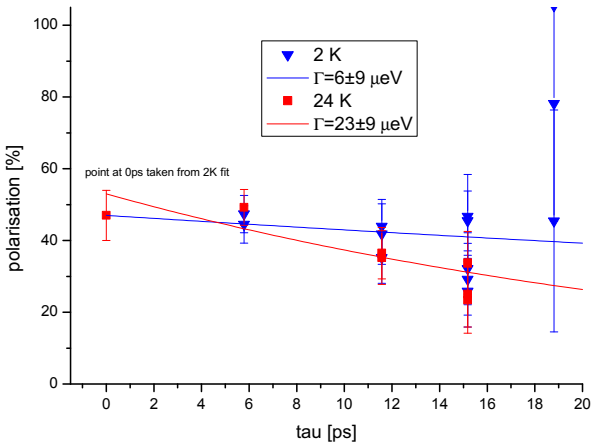

Figure 2: Normalized polarisation vs. spin echo time for $Q = (-0.4 - 0.4 + 0.6)$, $E = 5.18$ meV.

The error for high spin echo times is rather large, because of the mosaicity of the probe (16') and problems with the resonance circuits, but normalizing the 24 K data to the 2 K data yields the same line broadening of about 17 μeV. This first new data point in fig. 1 is in good agreement with Rezende and White's theoretical prediction for this Q value and seems to be more reliable than the data of Windsor et al. [2], included in the picture.

In following experiments at the FRM-II and the ILL, we want to extend the available data, allowing a more detailed comparison with the theoretical predictions.

References

[1] D. Teaney, M. Freiser, and R. Stevenson. *Phys. Rev. Lett.*, 9:212–4, 1962.
[2] C. Windsor, D. Saunderson, and E. Schedler. *Phys. Rev. Lett.*, 37(13):855–8, 1976.
[3] R. Golub and R. Gähler. *Phys. Lett. A*, 123:43–8, 1987.
[4] *Scattering*, pages 1264–86. San Diego: Academic Press, 2002.
[5] S. Rezende and R. White. *Phys. Rev. B*, 18(5):2346–9, 1978.
[6] S. Klimko. *ZETA, A zero field spin echo method for very high resolution study of elementary excitations and first application.* PhD thesis, Fakultät für Physik, Technische Universität Berlin, 2003.

1.4 Anti-Renormalization of Paramagnetic Fluctuations in $CsMnBr_3$

P. Böni [1], **B. Roessli** [2], **Ch. Reich** [1], **E. Rastelli** [3]
[1] *Technische Universität München, Physics Department E21, D-85747 Garching, Germany*
[2] *Laboratory for Neutron Scattering ETH & PSI, CH-5232 Villigen PSI, Switzerland*
[3] *Dipartimento di Fisica dell'Università, I-43100 Parma, Italy*

The critical behavior of the spin-wave dispersion in the triangular antiferromagnet $CsMnBr_3$ was investigated in the paramagnetic phase using inelastic neutron scattering. Unexpectedly, we find an anti-renormalisation of the excitations. We speculate that a description of the spin dynamics in terms of an extension of an approach for an $S = 1/2$ model for a Heisenberg chain to $S = 5/2$ may be more appropriate to explain our results.

3D-ordered systems forming spin chains with antiferromagnetic coupling usually exhibit an energy gap in their dispersion relation. An energy gap was also observed in $CsMnBr_3$ in the ordered state [1, 2] and was interpreted in terms of an effective Hamiltonian with XY-like anisotropy

$$H = 2J_{ab}\sum_i \vec{S}_i \cdot \vec{S}_{i+1} + 2J_c \sum_i \vec{S}_i \cdot \vec{S}_{i+1} + D\sum_i (S_i^z)^2 \quad (1)$$

with an in-plane exchange $J_{ab} = 1.7 \pm 0.1$ μeV and an out-of-plane exchange $J_c = 0.89 \pm 0.01$ meV. The effective single ion anisotropy parameter $D = 12 \pm 1$ μeV leads to a confinement of the spins to the a-b-plane. It is expected that the energy gap decreases when approaching $T_N = 8.3$ K from below.

In order to study the renormalisation of the spin wave branches and the critical scattering near T_N we have performed inelastic neutron scattering experiments in the paramagnetic phase of $CsMnBr_3$ using the spectrometer TASP at SINQ. Unexpectedly, we found indications for an increase of the energy gap of the optic in-plane and the out-of-plane modes [3].

A representative measurement at (0 0 1) and $T = 25$ K is shown in Fig. 1. The central peak consists of quasielastic scattering and incoherent scattering. The spin wave peak at finite energy was fitted by means of a damped harmonic oscillator function that was convoluted with the resolution function of the spectrometer.

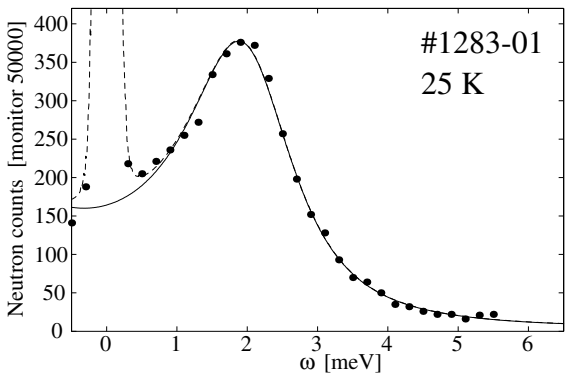

Figure 1: Neutron scattering data measured at (0 0 1) *showing a spin wave peak that moves to higher E with increasing T. The solid line is a fit to the experimental data using a DHO-function.*

Between $20 \leq T \leq 40$ K the gap at (0 0 1) can be parametrized by

$$E_g = 0.729 \text{ meV} + 0.058 \cdot T, \quad (2)$$

where E_g is measured in meV and T in K [4]. The fits clearly show that the energy gap increases with increasing T. This is a very peculiar behavior because usually the gap decreases with increasing T.

In Fig. 2 we have plotted the fitted linewidths Γ_q of the excitations. Interestingly there is no q-dependence observed. Γ_q increases also with increasing T as somehow expected and the T-dependence can be parametrized by

$$\Gamma_q = 0.328 \text{ meV} + 0.027 \cdot T. \quad (3)$$

Clearly, for the T-range investigated the excitations are significantly under-damped $\Gamma_q/E_g < 2$, i.e. the hardening of the energy-gap is a real effect [4]. For completeness we point out that an increase of E_g has also been observed at other positions in reciprocal space, in particular also at the magnetic zone centre ($\frac{1}{3}$ $\frac{1}{3}$ 1) [3].

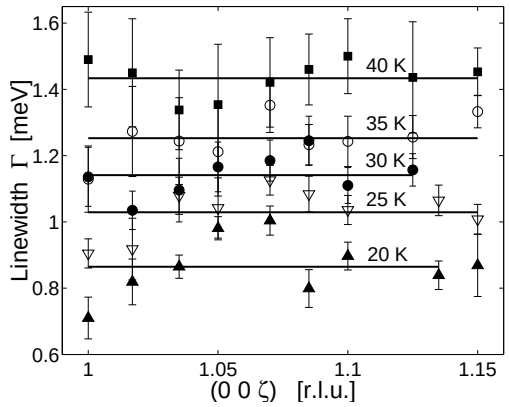

Figure 2: The figure shows that the linewidths increase with increasing T. However, for a fixed temperature they are independent of q. The lines represent the average linewidths at different temperatures. Note that the zero of the vertical scale is suppressed.

The results for the quantum linear antiferromagnetic chain coupled by exchange does not assure an upward renormalisation of the magnetic excitations [3]. Therefore, an extension of an approach for an $S = 1/2$ model for a Heisenberg chain to $S = 5/2$ may be more appropriate to explain our results [5].

References

[1] B. D. Gaulin et al. *J. Appl. Phys.*, 61:3409, 1987.
[2] U. Falk et al. *Phys. Rev. B*, 35:4888, 1987.
[3] Ch. Reich et al. *Phys. Rev. Lett.*, 91:157203, 2003.
[4] P. Böni et al. *Physica B*, 350:59–62, 2004.
[5] E. Rastelli. , *private communication.*

1.5 Polarized SANS measurements of the flux line lattice in Niobium

Sebastian Mühlbauer [1], **Robert Georgii** [1, 2]
[1] Technische Universität München, Physics Department, Institute E21, D-85747 Garching, Germany
[2] Technische Universität München, ZWE FRM-II, D-85747 Garching, Germany

Intention

Magnetic structures of superconductors have great importance in helping to understand the mechanism of superconductivity, especially of the modern cuprate superconductors like YBaCuO. These superconductors belong to the so called type II superconductors, which are penetrated by external fields in the region of $H_{c1} < H < H_{c2}$ in form of flux or vortex lines. The ideal flux line lattice (FLL) is described by a hexagonal symmetry that may be disturbed owing to e. g. the crystal lattice of the bulk superconductor, possible crystal defects, lattice distortions or the surface roughness of the material. As the critical field or current density is lowered near to such crystal anomalies, they act as pinning centres for flux lines [1].

Experiments

The flux line lattice (FLL) of a superconducting niobium single crystal has been measured in SANS (small angle neutron scattering) geometry on the instrument MIRA at the FRM II. With SANS, especially using long wavelengths, it is possible to gain direct information about the magnetic structure of the sample.

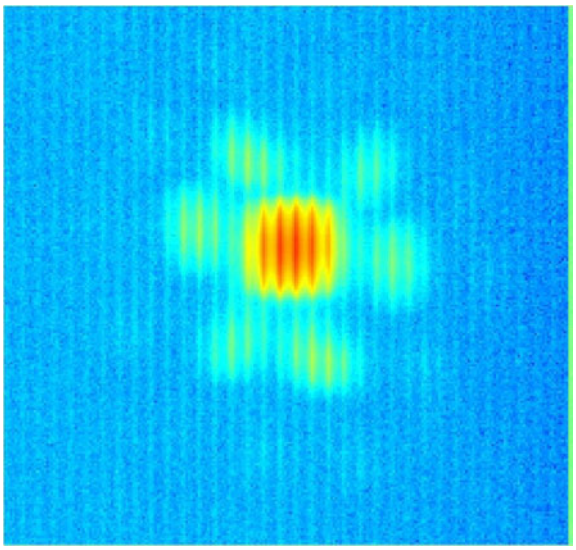

Figure 1: SANS picture of the FLL of niobium on MIRA. The sixfold symmetry is observed. The first order peaks are centered around the direct beam, second order peaks are visible, but of low scattering intensity. The lined structure results from the anode wires of the detector.

Experimental setup

To provide a suitable sample environment for the FLL measurements, a pair of Helmholtz Coils with current supply and a closed cycle cryostat with temperature controller were adapted to MIRA. The temperature can be driven from 3.5 K to ambient temperature (stability below 0.02 K), and a magnetic field up to 0.15 T can be applied parallel and vertical to the neutron beam (see Fig. 2).

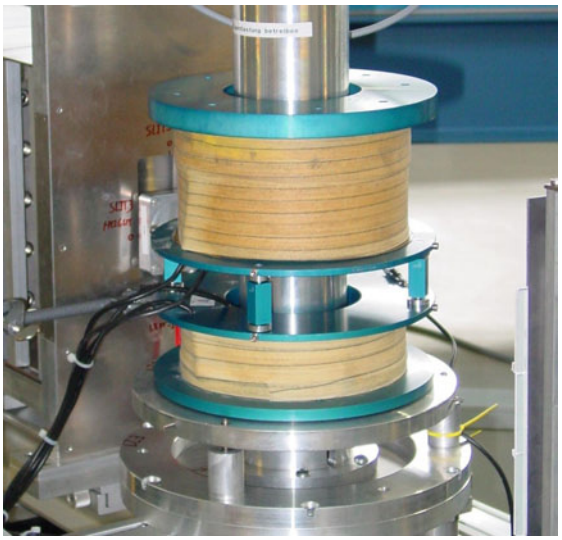

Figure 2: The closed cycle cryostat mounted together with the small Helmholtz coil system on the sample table on MIRA

Results

With a two dimensional position sensitive detector, the scattered intensity was recorded. In order to put the sample in the Shubnikov-phase, a external magnetic field, oriented parallel to the incident neutron beam, was applied. The field strength was varied from zero to 0.15 T, the temperature range was 3.5 K to 9.5 K. For a incident wavelength of 10 Å the observed magnetic peaks show a six-fold symmetry (separated by 60°), corresponding to $|Q| \approx 0.01$ Å at 6.5 K and 0.15 T (see Fig. 1).

Outlook

In addition to the conducted SANS experiments in 2004, it is planned to do polarized SANS on the sample in order to get a deeper insight in the chirality of the FLL. It is also planned to investigate the vortex behavior near to the critical field H_{c2}. The latter experiment shall add information whether a melting transition of the FLL takes place at H_{c2} [2]. Niobium was chosen because of its well known beaviour, to get used to the instrument´s capabilities for future measurements on high T_c superconductors.

References

[1] W. Buckel. Supraleitung. *VCH*, 71(3):307–11, 1993.
[2] J. W. Lynn. Vortex dynamics and melting in niobium. *Phys. Rev. Lett.*, 72(21):3413–3416, 1994.

1.6 Magnetic excitations near magnetic phase transition in the singlet ground state system PrNi

E.S. Clementyev [1], **N.N. Tiden** [2], **P.A. Alekseev** [2], **V.N. Lazukov** [2]
[1] *Physics Department, Institute E21, Technical University of Munich, D-85748 Garching, Germany*
[2] *Russian Research Centre Kurchatov Institute, 123182 Moscow, Russia*

PrNi ($T_C = 21$ K) belongs to the class of singlet ground state ferromagnetic systems (Pr_3Tl, $PrAl_2$, PrNi). It's possible to describe the magnetic ordering in such systems by the concept of induced magnetism [1]. The recent study [2] of the magnetic neutron scattering spectra of PrNi single crystal shows that the observed excitations are qualitatively described within the framework of the mean field random phase approximation with two excited crystal field (*CF*) levels at $E = 2.3$ meV and 3.8 meV and the exchange coupling between the nearest neighbour Pr ions from two sublattices. Nevertheless the lack of detailed experimental information does not allow more accurate model calculations for the magnetic dynamics in PrNi. The measurements of PrNi single crystal have been performed in the $[0, 1, 0]$ and $[1, 1, 0]$ directions. Constant-Q scans have been measured at $T = 23$ K for fixed final neutron energy 8.05 meV and energy resolution at the elastic line ~ 0.5 meV.

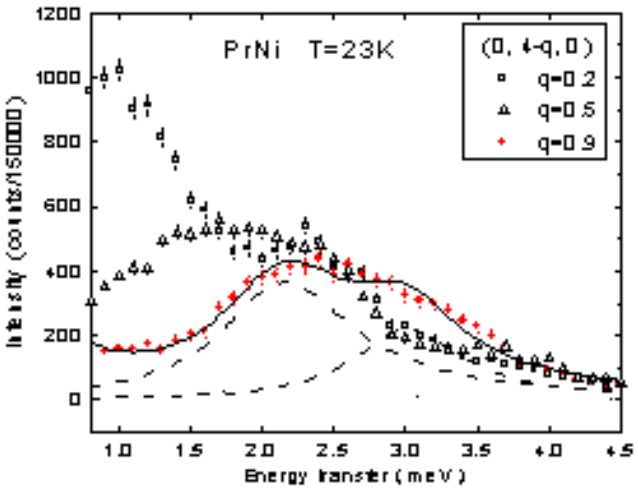

Figure 1: The neutron scattering spectra of PrNi measured at $T = 23$ K along the [0 1 0] crystallographic direction. Lines - approximation by sum of three Lorentzian functions. See details in the text.

Typical neutron spectra of $PrNi$ are shown in Fig. 1. Two dispersive magnetic modes have been observed. The obtained spectra have been approximated by a sum of three Lorentzian spectral functions multiplied by the temperature factor (solid line), two of them correspond to the magnetic scattering from the magnetic excitons (dashed lines) and the last one with the energy position near zero simulates background scattering and possible quasielastic-like (QE) signal (dotted line).

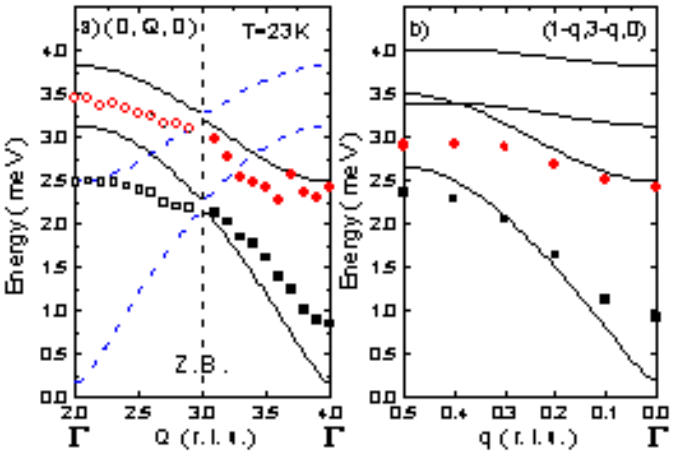

Figure 2: Magnetic excitation dispersion curves along $[0, x, 0]$ - (a) and $[x, x, 0]$ - (b) directions. See details in the text.

The energy dispersions for the mentioned excitons are presented in Fig. 2a - for the $[0, x, 0]$ direction and 2b - for the $[x, x, 0]$ direction from $Q = (1, 3, 0)$. Notation used in Fig. 2: lines - model calculations; dashed lines - zero intensity modes; open symbols - results of the previous measurements [2], filled symbols - present data. We observe a strong softening (Fig. 2a) for both modes by approaching the zone center $Q = (0, 4, 0)$ which is expected for the acoustic modes. In this direction the acoustic magnetic modes have not been observed before in PrNi. Moreover, the acoustic brunch from the 3.8 meV *CF* excitation has never been seen before. The dispersion curves for the $[x, x, 0]$ direction are shown in Fig. 2b. Here we see the soft mode at $Q = (1, 3, 0)$. To sum up current measurements provide very useful quantitative information on the magnetic excitations in PrNi and might allow a good model description of the soft mode driven magnetic ordering in this system.

References

[1] B.R. Cooper. In R.J. Elliot, editor, *Magnetic Properties of Rare Earth Metals*, chapter 2. Plenum Press, 1972.
[2] P.A. Alekseev, E.S. Clementyev, P. Allenspach, and V.N. Lazukov. *JETP Lett.*, 76:99, 2002.

1.7 High energy excitations in single-Q chromium

E. Clementyev [1], **P. Böni** [1], **H. Woo** [2], **T. Perring** [2], **G. Shirane** [3], **M. Fujita** [4], **S. Hayden** [5]

[1] *Physics Department, Institute E21, Technical University of Munich, D-85748 Garching, Germany*
[2] *ISIS, Rutherford Appleton Laboratory, Chilton, Didcot OX11 0QX, United Kingdom*
[3] *Brookhaven National Laboratory, Physics Department, Upton, NY 11974, USA*
[4] *Institute for Chemical Research, Kyoto University, Gokashou, Uji 611-0011, Japan*
[5] *H.H. Wills Physics Laboratory, Bristol University, Tyndall Ave., Bristol BS8 1TL, UK*

The dynamics of the spin density wave (*SDW*) in Cr continues to be one of the most fascinating subjects in magnetism (see [1] and references therein). The main aim of the experiment was to map out the high energy magnetic response in chromium around the silent and allowed incommensurate Bragg positions. In addition a puzzling phason peak near 60 meV has been studied. A single-Q single crystal of Cr was aligned in the [1 0 0]/[0 1 0] scattering plane. The measurements have been performed both in the transverse *SDW* and longitudinal *SDW* phases in the temperature range 60 K to 230 K. The scans were carried out with incident energies between 110 and 240 meV. Fig. 1 shows the global map of intensity measured at $E_i = 240$ meV and $T = 60$ K. The magnetic contribution is clearly seen around $Q = (-1, 0, 0)$ and $(0, 1, 0)$.

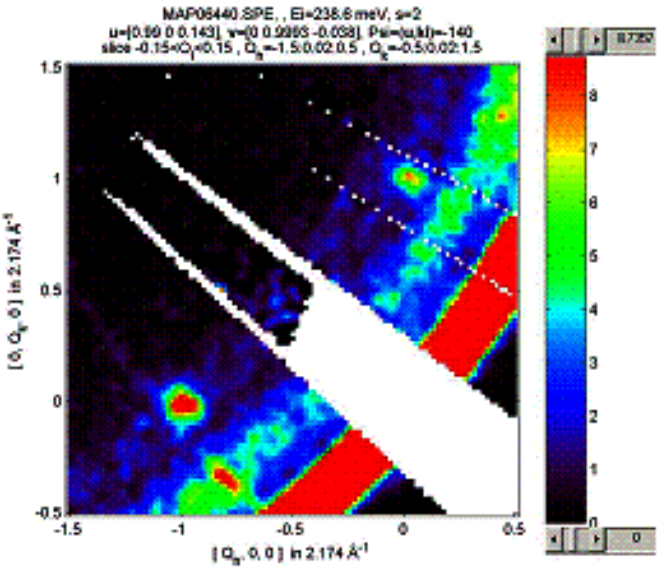

Figure 1: Map of intensity in $(h\,k\,0)$ plane for $T = 60$ K.

We have collected many intensity maps zooming into the $Q = (-1, 0, 0)$ and $(0, 1, 0)$ spots using $h-k$, $h-l$ and $k-l$ cuts in the 3-dimensional Q-space. The $k-l$ cuts provided valuable experimental information in the silent magnetic plane. Fig. 2 shows the energy dependence of the incommensurate peaks in Cr for the allowed modes and Fig. 3 for the silent modes.

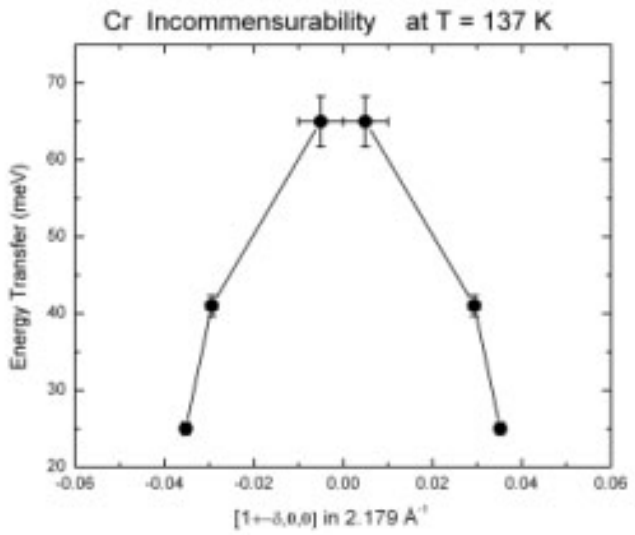

Figure 2: The energy positions of the allowed peaks in Cr in the $TSDW$ phase measured at $T = 137$ K.

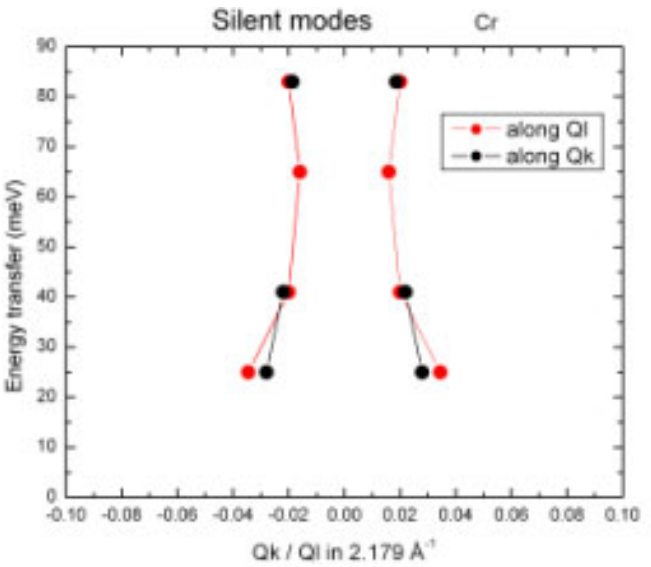

Figure 3: The energy positions of the incommensurate peaks in the silent plane at $T = 137$ K.

The double-phonon scattering at $E = 60$ meV (the arc connecting the points $Q = (-1, 0, 0)$ and $(0, 1, 0)$, see Fig. 1) is sizable and its energy is just the same as the energy of the phason peak. Due to these facts the occurrence of this peak requires further careful data treatment.

References

[1] E. Fawcett. *Rev. Mod. Phys.*

1.8 Phase diagram of the spin chain compounds $Ca_{2+x}Y_{2-x}Cu_5O_{10}$

Verena Kargl [1], **Peter Böni** [1], **Alex Mirmelstein** [2]
[1] *Technische Universität München, Physics Department, Institute E21, D-85747 Garching, Germany*
[2] *Institute of Metal Physics, Russian Academy of Science, GSP-170 Ekaterinburg 620219, Russia*

Introduction

Charge ordering within spin chains are one of the central issuses in investigating low dimensional magnetic systems. The cuprate $Ca_{2+x}Y_{2-x}Cu_5O_{10}$ allows hole doping with a raising Ca/Y ratio from the formal Cu-valence of +2 to +2.34 [1]. Undoped $Ca_2Y_2Cu_5O_{10}$ exhibits a second order phase transition from the paramagnetic to the antiferromagnetic state. Below its ordering temperature T_N the material is characterized as a 3D antiferromagnet. Increasing x leads to a lowering of the ordering temperature.

Experiments

Ceramic samples of various doping concentrations of $Ca_{2+x}Y_{2-x}Cu_5O_{10}$ were investigated by means of elastic neutron scattering as well as specific heat measurements in order to construct a phase diagram by determining the ordering temperature [2]. Neutron experiments were performed on the cold triple axis spectrometer TASP, PSI, (80'-80'-sample-80', $k_f = 1.97$ Å fixed), whereas specific heat was measured at E21, TUM, using a conventional calorimeter (Physical Property Measurement System by Quantum Design).

Results

In order to determine the ordering temperature by elastic neutron scattering the sublattice magnetization $M(T)$ of the (0 0 1) integrated intensity of $Ca_2Y_2Cu_5O_{10}$ and $Ca_{2.5}Y_{1.5}Cu_5O_{10}$ was measured. T_N was derived from the data by least square fitting using the scaling law $M(T) \sim (1 - T/T_N)^\beta$ in the temperature range $0.8\ T_N \leq T \leq T_N$. Data evaluation yields an order temperature of 28.6(1) K and 26.2(2) as well as the critical exponents $\beta = 0.31(2)$ and 0.42(6), respectively. The critical temperature of undoped $Ca_2Y_2Cu_5O_{10}$ compares well with earlier works [3, 4]. Within the error bars, the former exponent is compatible with 3D Ising or XY behaviour, whereas the latter can be attributed to 3D Heisenberg behaviour.

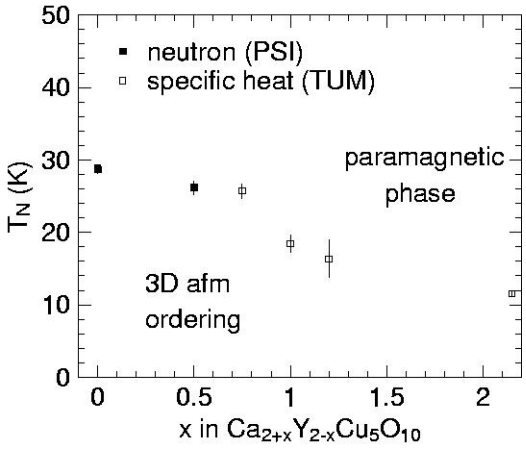

Figure 1: Phase diagram of $Ca_{2+x}Y_{2-x}Cu_5O_{10}$ in zero field.

As alternative technique for determining the ordering temperature specific heat was measured by the relaxation method [5]. The second order phase transition from the paramagnetic to the afm state is characterized by a λ-type singularity in C/T diverging at T_N. Undoped $Ca_2Y_2Cu_5O_{10}$ exhibits a sharp transition, whereas with raising x the λ-peak broadens. The ordering temperature can be found as the inflection point the λ-type singularity of C/T(T). Doping obviously leads to the reduction of long range correlations and the ordering temperature. T_N obtained by neutron diffraction and by calorimetric measurements coincides for the investigated samples (see Fig. 1).

The field dependence of the ordering temperature of the parent compound $Ca_2Y_2Cu_5O_{10}$ was investigated by specific heat measurements up to 9T. By applying a magnetic field the λ-anomality broadens. In addition, the maximum of the measured specific heat is decreasing as well as shifting to lower temperatures (see Fig. 2). However, no shift of the ordering temperature with applied magnetic field was found up to 9T. This finding is in agreement with bulk measurements of single crystal $Ca_2Y_2Cu_5O_{10}$ [6] reporting only at 10 T a significant decrease of the ordering temperature T_N.

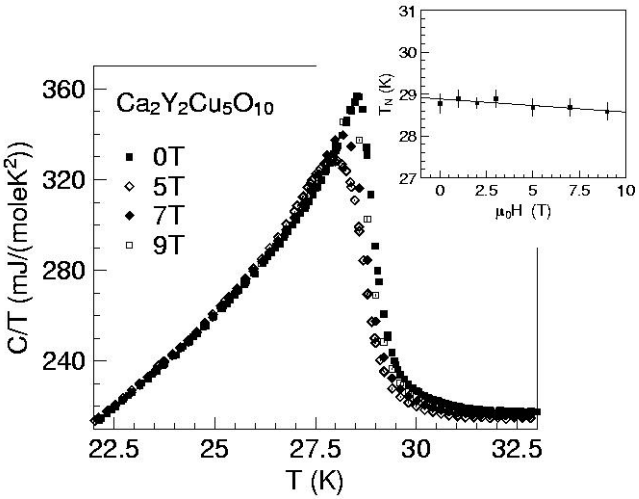

Figure 2: Specific heat of undoped $Ca_2Y_2Cu_5O_{10}$ in various fields. The inset shows the field dependence of the ordering temperature.

References

[1] A. Hayashi et al. *Physical Review B*, 58:2678, 1996.
[2] V. Kargl et al. *Physica B, accepted*, 2004.
[3] H. F. Fong et al. *Physical Review B*, 59:6873, 1999.
[4] M. Matsuda et al. *J. Phys. Soc. Jn.*, 68:269, 1999.
[5] J. S. Hwang et al. *Rev. Sci. Instrum.*, 68:94, 1997.
[6] K. Kudo et al. *J. Phys.: Cond. Mat., in press*, 2004.

2

Multilayers and Interfaces

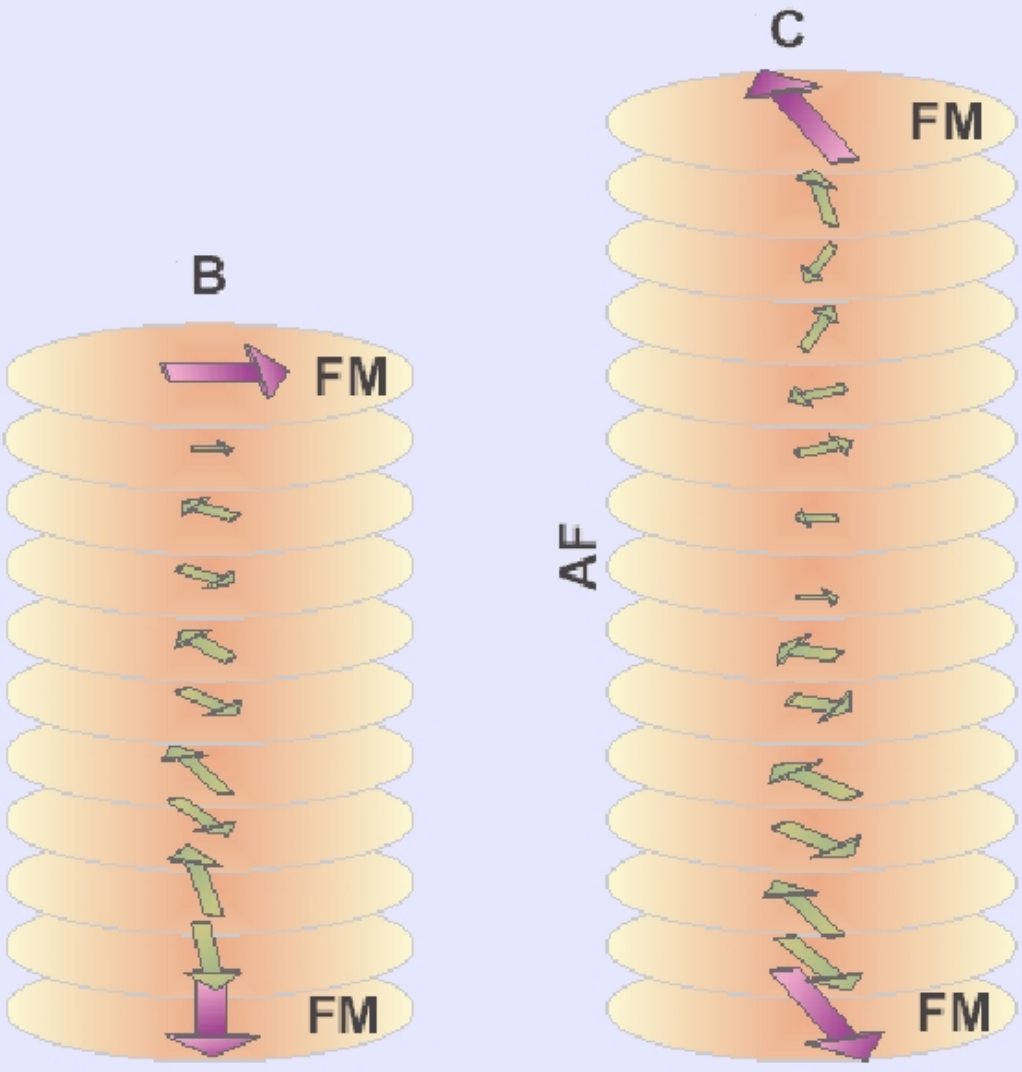

2.1 Influence of roughness on the magnetization reversal of FM/AF/FM trilayers

V. R. Shah [1], **C. Schanzer** [1], **H. B. Braun** [2], **P. Böni** [1]
[1] *Physics Department, Institute E21, Technical University of Munich, D-85747 Garching, Germany*
[2] *Department of Mathematical Physics, University College Dublin, Dublin 4, Ireland*

We have examined the possible interlayer exchange between two ferromagnets (FM) mediated by an antiferromagnet (AF) with varying thickness. The bulk magnetization measurements showed a clear AF thickness dependence [1]. In order to quantify the role of roughness induced dipolar (Néel's „orange-peel") coupling and to establish the interfacial exchange we performed off-specular x-ray reflectometry (XRR), AFM and field cooling experiments. From AFM and off-specular XRR we obtained the length scale of the roughness oscillation that amounts to be ≈ 4 μm. Fig. 1, shown below, reveals the intensity map of 2D reciprocal space of the trilayer $t_{NiO} = 60$ nm.

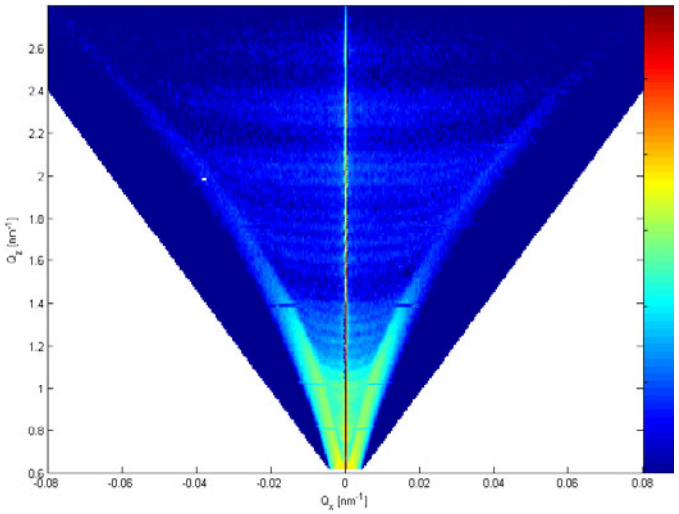

Figure 1: 2D reciprocal space map of the specular and off-specular x-ray reflectivity of the $t_{NiO} = 60$ nm sample. The pattern of the diffuse signal significantly reproduces the specular features. This indicates a high vertical correlation of the interfaces in the sample representing a conformal interface profile.

Assuming conformal interfaces with a sinusoidal roughness profile in a FM1/NM/FM2 system (NM = nonmagnetic), the magnetic field (Néel's „orange-peel field") H_N acting on the free layer (FM2) from the pinned layer (FM1) across the NM spacer is given by [2]

$$H_N = \frac{\pi^2}{\sqrt{2}} \cdot \left(\frac{h^2}{\lambda t_F}\right) \cdot M_S \cdot \exp(-2\pi\sqrt{2} t_S/\lambda) \qquad (1)$$

where h represents the amplitude of the roughness oscillation, t_F is the thickness of the free layer and M_S represents the saturation magnetization of the pinned layer. The r.m.s. roughness of the samples are typically in the range of 0.3 - 3 nm for t_{NiO} ranging from 1.5 - 100 nm, as obtained from the specular reflectivity analysis. These values give rise to Néel fields H_N of the order of 1-3 Oe in this t_{NiO} interval.

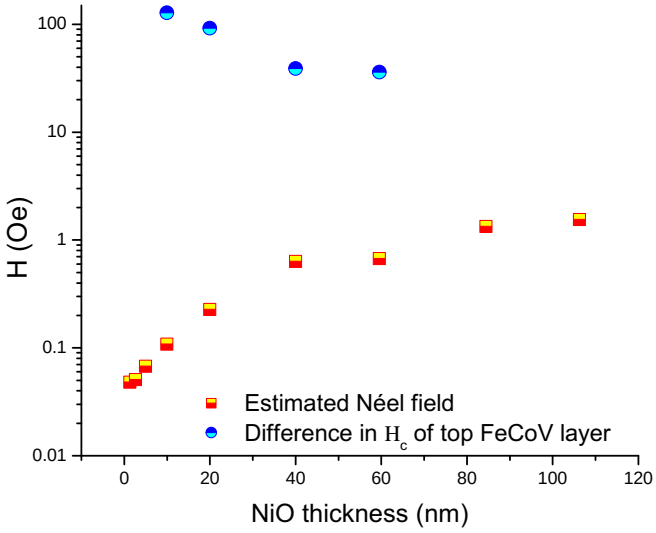

Figure 2: Contribution of the Néel „orange-peel" field in comparison to the change in coercivity of the top FeCoV layer when deposited on top of NiO with various thicknesses.

Field cooling experiments from 300 K to 2 K in a state of antiparallel orientation of the adjacent FeCoV layers revealed the opposite nature of exchange bias at the two interfaces. This experiment confirms that the interfacial exchange exists and being established according to orientation of the FM. These results indicate that the observed magnetic behaviour can not be explained as an effect due to the dipolar coupling originating from the roughness. Moreover, roughness induced bi-quadratic exchange may result in a perpendicular coupling between the FM layers. Our PNR results do not support this possibility. Further detailed PNR and magnetization investigations [1, 3] suggest an interlayer coupling mediated by NiO accommodating a spin-twist within its internal spin structure.

References

[1] V. R. Shah, C. Schanzer, P. Böni, and H. B. Braun. *J. Magn. Magn. Mater.* in press.
[2] B. D. Schrag, A. Anguelouch, S. Ingvarsson, Gang Xiao, Yu Lu, P. L. Trouilloud, A. Gupta, R. A. Wanner, W. J. Gallagher, P. M. Rice, and S. S. P. Parkin. *Appl.Phys. Lett*, 77:2373, 2000.
[3] C. Schanzer, V. R. Shah, T. Gutberlet, M. Gupta, P. Böni, and H. B. Braun. *Physica B.* in press.

2.2 Investigation of interlayer exchange in FM/AF/FM trilayers

V. R. Shah [1], **C. Schanzer** [1], **T. Gutberlet** [2], **M. Gupta** [2], **M. Horisberger** [2], **H. B. Braun** [3], **P. Böni** [1]

[1] *Physics Department, Institute E21, Technical University of Munich, D-85747 Garching, Germany*
[2] *Laboratory for Neutron Scattering, ETHZ & PSI, CH-5232 Villigen PSI, Switzerland*
[3] *Department of Mathematical Physics, University College Dublin, Dublin 4, Ireland*

FM/AF interfaces have attracted a lot of attention owing to their exchange bias phenomenon [1]. Recent theories and experimental observations suggest that the internal spin structure of the antiferromagnet is no longer rigid but is modified by the interfacial exchange leading to partial domain walls (DW) within the AF [2, 3]. Further in trilayers of FM/AF/FM, a more complicated scenario is foreseen. Theoretical investigations predict an AF thickness dependence on the magnetic properties and an interlayer exchange coupling accomplished by means of a twist in the AF spins [4]. We investigated the AF thickness dependence of the magnetization reversal by bulk and layer resolved magnetization measurements in FeCoV (20 nm)/NiO (t_{NiO} nm)/FeCoV (20 nm) trilayers.

Bulk magnetization measurements exhibited three distinct reversal regimes. For $t_{NiO} < 20$ nm, the two FM layers shows a combined reversal process whereas, for 20 nm $< t_{NiO} <$ 40 nm, a small step appears that widens as t_{NiO} increases. From $t_{NiO} \approx 40$ nm onwards the step remains the same in size indicacting the establishment of a 180° orientation between the two FM layers. We performed layer resolved magnetometry by PNR during the magnetization reversal. Fig. 1 shows the PNR of selected samples and the inset shows the magnetization profile of each layer obtained from the simultaneous modeling of the NSF and SF reflectivities.

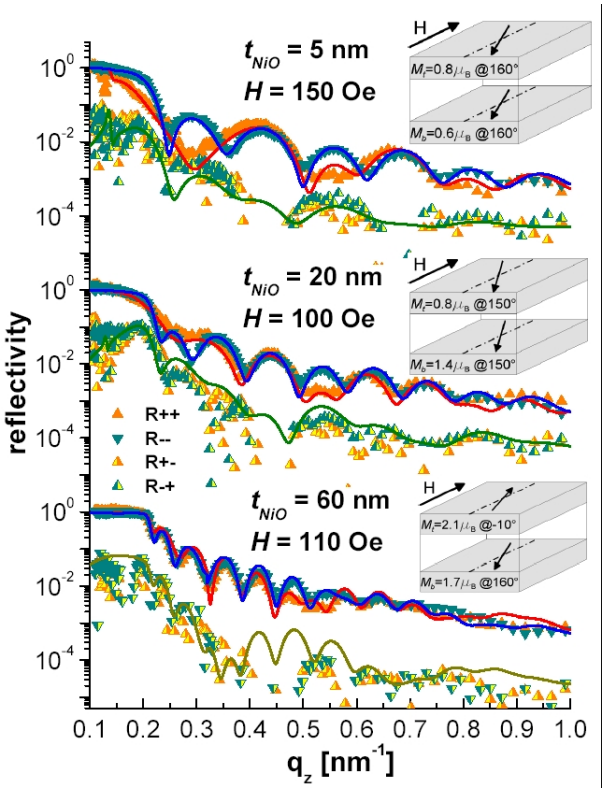

Figure 1: Polarized neutron reflectivities of t_{NiO} = 5, 20 and 60 nm samples during the magnetization reversal. The symbols and lines represent the experimental data and computed reflectivities, respectively. The resultant spin configurations are shown in the insets.

Clearly, PNR reveals that the two FM layers rotate in unison during the magnetization reversal at low t_{NiO} cases whereas a twist angle between the two FM layers is formed as t_{NiO} increases reaching $\approx 180°$ at around $t_{NiO} = 40$ nm. Theoretical predictions [5] suggest that when the AF thickness is $\ll \delta_0$ ($= \pi \cdot \sqrt{\frac{A}{K}}$, where A and K are the exchange and anisotropy constants of the AF, respectively), the AF remains in a uniform state. Here, when the AF is coupled to a FM at both ends, AF spins follows the rotation of the FM moments resulting in a single uniform rotation of both FM layers. As the AF thickness increases and becomes comparable to δ_0, the AF exhibits critical angle regimes where the AF sublattice moments can be twisted up to 180°. A schematic illustration of the partial DW formation in a FM/AF/FM trilayer is depicted in Fig. 2. It has been reported that, in NiO films, a realistic estimate of 180° DW width is 40 nm [5] that coincides with the observation of a full plateau region in the trilayer case. Supported from our PNR observations, we believe that partial DW formation in NiO is responsible for the magnetization behaviour of the trilayer samples.

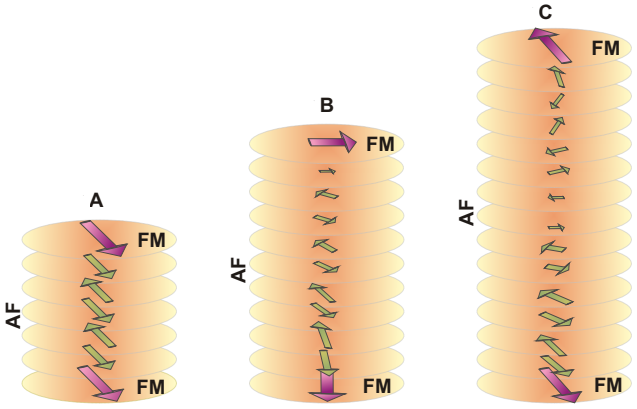

Figure 2: Illustration of partial DW formation in the AF. (A) when t_{AF} is very small, the AF follows the rotation of the FM, (B) when t_{AF} is sufficiently large, the AF moments start to exhibit spin twist and (C) the maximum twist is accommodated by the formation of a 180° DW.

References

[1] A. E. Berkowitz and Kentaro Takano. *J. Magn. Magn. Mater*, 200:552, 1999.
[2] D. Mauri, H. C. Siegmann, P. S. Bagus, and E. Kay. *J. Appl.Phys.*, 62:3047, 1987.
[3] A. Scholl, M. Liberati, E. Arenholz, H. Ohldag, and J. Stöhr. *Phys. Rev. Lett*, 92:247201, 2004.
[4] Haiwen Xi and Robert. M. White. *Phys. Rev. B*, 62:3933, 2000.
[5] M. D. Stiles and R. D. McMichael. *Phys. Rev. B*, 59:3722, 1999.

2.3 Temperature dependence of exchange bias of polycrystalline NiO/FeCoV bilayers

C. Schanzer [1], **V.R. Shah** [1], **P. Böni** [1]
[1] *Technical University Munich, Faculty for Physics E21, D-85747 Garching, Germany*

Interfaces of ferromagnetic (FM)/antiferromagnetic (AF) nanostructures are well known for their exchange bias properties, which manifests as a shift of the magnetic hysteresis by an exchange field H_E [1]. Fundamentally, exchange bias is described as an exchange interaction between the interfacial spins of FM and AF but a detailed understanding of the role of these spins and possibly the AF internal spin structure is still lacking. In our investigation of FM/AF/FM trilayers [2, 3] we separately analyse FM/AF and AF/FM bilayer counterparts for the individual properties of the two FM layers, respectively the two interfaces. Here we report the temperature dependence of magnetic properties of NiO(t_{NiO})/FeCoV(20 nm) bilayers.

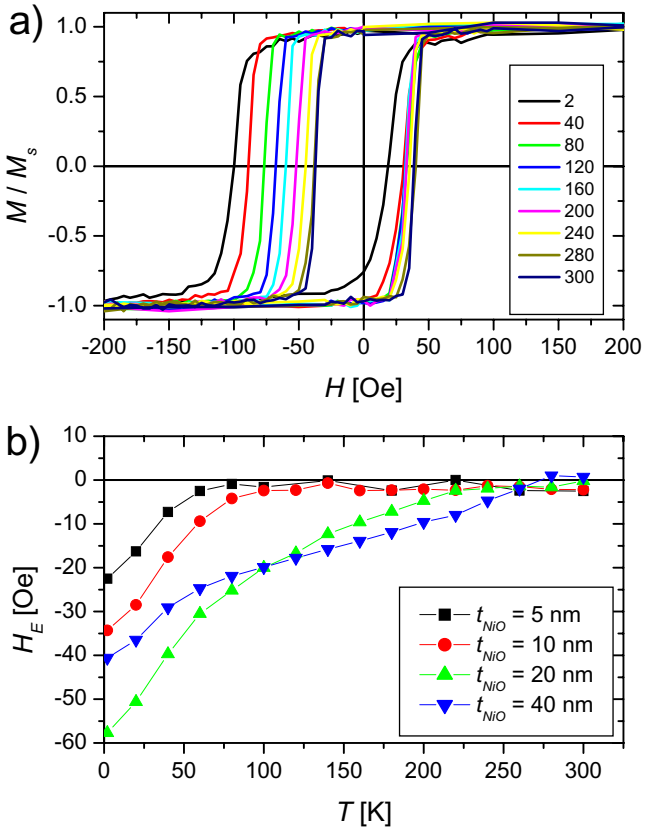

Figure 1: a) MH-loops of a NiO (40 nm)/FeCoV(20 nm) bilayer at various temperatures after field cooling in an applied field of +1000 Oe to 2 K; b) temperature dependence of the exchange field H_E for various thicknesses of NiO layers, as determined from the shift of the hysteresis.

A series of bilayers with FeCoV on top of NiO is prepared by DC magnetron sputtering. Besides the layers are textured in the growth direction the grains exhibit polycrystalline distribution in the film plane [4]. DC magnetisation loops are measured by the extraction technique using a Quantum Design Physical Property Measurement System. In order to investigate the temperature dependence of exchange bias the samples are field cooled at +1000 Oe down to 2 K. At this temperature, prior to measurement of the MH-loop the magnetic field is cycled five times from +1000 to -1000 Oe and vice versa in order to remove training effects. This procedure reduces H_E about ≈15 Oe. Then the MH-loop is measured at various constant temperatures from 2 K to 300 K. Fig. 1a) shows the MH-loops for $t_{NiO} = 40$ nm. The shift of the loop with respect to $H = 0$, namely the exchange field H_E, decreases with increasing temperature. The temperature dependence of H_E is plotted for various NiO thicknesses in Fig. 1b). The blocking temperature T_B, below which exchange bias sets in, is estimated from $H_E(T)$ where H_E approaches zero. The dependence of T_B on the AF thickness t_{AF} is shown in fig 2.

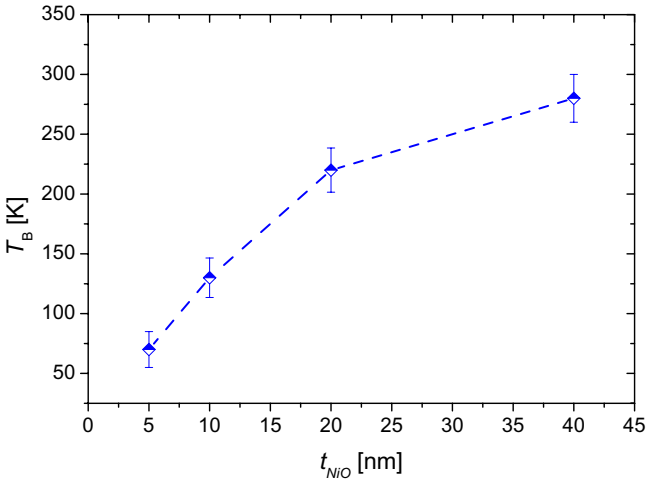

Figure 2: Dependence of the blocking temperature on the thickness of NiO in NiO(t_{NiO})/FeCoV(20 nm) bilayers.

Xi et al. [5] investigated the dependence of blocking temperature on t_{AF} in exchange coupled polycrystalline FM/AF bilayers in terms of a thermal fluctuation model. Our experimental results show a rather similar dependence of T_B on t_{AF} but with some discrepancy remaining. This is most likely because of the influence of other parameters which might vary with t_{AF} in our real samples, like grain size or Néel temperature. These parameters are also considered separately in the work of Xi. A combined analysis of all parameters is rather complex. Therefore microstructural investigations are in progress in order to confirm the contributions to the observed exchange bias properties.

References

[1] W.H. Meiklejohn and C.P. Bean. *Phys. Rev.*, 102:1413, 1956.
[2] V.R. Shah, C. Schanzer, P. Böni, and H. B. Braun. *J. Magn. Magn. Mater.* in press.
[3] C. Schanzer, V.R. Shah, T. Gutberlet, M. Gupta, P. Böni, and H. B. Braun. *Physica B.* in press.
[4] V.R. Shah, C. Schanzer, P. Böni, and H.B. Braun. *Kluwer Academic, NATO ASI series.* submitted.
[5] H. Xi, R.M. White, Z. Gao, and S. Mao. *J. Appl. Phys.*, 92:4828, 2002.

2.4 Investigation of non-collinear magnetization in FM/AF/FM trilayers by PNR

C. Schanzer [1], **V.R. Shah** [1], **T. Gutberlet** [2], **M. Gupta** [2], **M. Horisberger** [2], **P. Böni** [1], **H.B. Braun** [3]

[1] *Technical University Munich, Faculty for Physics E21, D-85747 Garching, Germany*
[2] *ETHZ&PSI, Laboratry for Neutron Scattering, CH-5232 Villgen PSI, Switzerland*
[3] *University College Dublin, Department of Mathematical Physics, Dublin 4, Irland*

We examined the magnetic depth profile during the magnetisation reversal of FeCoV (FM) / NiO (AF) / FeCoV (FM) trilayers for various NiO thicknesses by polarised neutron reflectivity. Using neutrons polarised within the film plane, we were able to distinguish simultaneous and separate magnetisation reversal of the two FM layers for small and large NiO thickness, respectively [1] . A direct observation of the spin twist was possible by means of selecting the neutron polarisation perpendicular to the magnetic moment of the sample. Our results confirm the role of AF in mediating the interlayer exchange according to the recent theoretical predictions.

In FM/AF/FM trilayers, a possible interlayer exchange coupling, accommodated by a twist of the AF spins has been proposed from macroscopic magnetisation measurements [2]. The twist angle between the FM layer magnetisations is found to depend linearly on the AF thickness. The angle reaches 180° for AF thickness larger than a domain wall width.

Polarised neutron scattering is most sensitive to the chirality of magnetisation when the neutrons are polarised either parallel or antiparallel to the propagation direction of the magnetic spiral [3]. In this geometry all magnetic scattering is spin flip scattering and an asymmetry in the spin flip (SF) signal will arise if the magnetic structure is chiral. As the magnetisation of FeCoV layers is confined in the plane of the films, a neutron polarisation perpendicular to the film plane is necessary. This is in contrast to the conventional geometry for polarised neutron reflectometry. The particular setup could be realised at the AMOR reflectometer by providing a small perpendicular magnetic field over a finite sample region. An appropriate overlap of the perpendicular field at the sample with the guide field of the incident and reflected beam enabled an adiabatic transformation of the neutron polarisation from in-plane to perpendicular and vice versa. PNR with a perpendicular neutron polarisation was performed on sputter deposited trilayers of FeCoV (20 nm) / NiO (t_{NiO}) / FeCoV (20 nm) with t_{NiO} = 5, 20, 40, 60, 80 nm. During the experiment the samples were at remanence after magnetising to the desired states during the magnetisation reversal. This process was done externally in an in-plane magnetic field. A Q range of 0.1-0.5 nm^{-1} was covered by measuring the reflected TOF spectrum at an angle of incidence of 0.6°. Instrumental contributions have been excluded by inverting the incident polarisation. The expected inversion of the spin flip asymmetry was obtained confirming the success of the experiments and non-collinear structure. Fig. 1 shows selected results for thin and thick NiO spacer layer cases. An asymmetry of the spin flip signal was observed for thick NiO layers ($t_{NiO} \geq 20$ nm). The results confirm that for thin NiO layers ($t_{NiO} <$ 20 nm) the magnetisation of the FeCoV layers reverses together due to a strong coupling mediated by the NiO layer. For thicker NiO the coupling presumably relaxes by accommodating a spin twist up to 180° in NiO [4, 1].

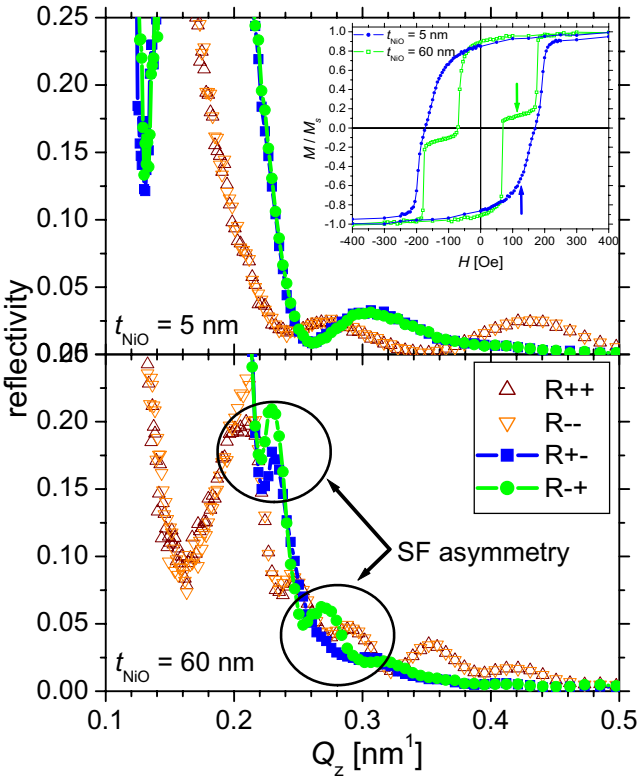

Figure 1: PNR with neutron polarisation perpendicular to the sample of FeCoV/NiO/FeCoV trilayers with t_{NiO} = 5 and 60 nm. The samples were at remanent magnetisation after magnetising to a state as indicated by the arrows in the M-H loop (inset figure). For t_{NiO} = 60 nm the circles mark regions of strong spin flip asymmetry, due to a non-collinear arrangement of the magnetisation of top and bottom FeCoV layers. No asymmetry is present for t_{NiO} = 5 nm indicating a nearly collinear magnetisation state of the two FeCoV layers.

Acknowledgment

This research project has been supported by the European Commission under the 6th Framework Programme through the Key Action: Strengthening the European Research Area, Research Infrastructures. Contract no.: RII3-CT-2004-505925

References

[1] C. Schanzer, V.R. Shah, T. Gutberlet, M. Gupta, P. Böni, and H. B. Braun. *Physica B.* in press.
[2] F.Y. Yang and C.L. Chien. *Phys. Rev. Lett.*, 85:2597, 2000.
[3] F. Tasset, P.J. Brown, E. Lelièvre-Berna, T. Roberts, S. Pujol, J. Allibon, and E. Bourgeat-Lami. *Physica B*, 267-268:69, 1999.
[4] V.R. Shah, C. Schanzer, P. Böni, and H. B. Braun. *J. Magn. Magn. Mater.* in press.

2.5 First neutron reflectometry results from the new instrument MIRA at FRM-II

C. Schanzer [1], **V.R. Shah** [1], **Robert Georgii** [1, 2], **S. Mühlbauer** [1], **P. Böni** [1]
[1] *Technical University Munich, Faculty for Physics E21, D-85747 Garching, Germany*
[2] *Technical University Munich, ZWE FRM-II, D-85747 Garching, Germany*

Neutron reflectometry is a powerful tool to probe the depth profile of thin films and multilayers. In additon, using polarised neutrons the magnetic depth profile of ferromagnetic nanostructures can be unraveled. Here, we report the first reflectivity experiments performed at the new instrument MIRA at the new high flux neutron source FRM-II. MIRA is designed as a versatile instrument to provide various options for different types of experiments. One option of MIRA is as a reflectometer using a monochromatic beam from a mica crystal. At present, MIRA is ready for unpolarised neutron reflectivity measurements, which is used the first time to measure reflectivity on a Ni single film and on FeCoV (20 nm)/NiO (t_{NiO})/FeCoV (20 nm) trilayers in order to test the structural layer model as obtained from X-ray reflectivity (XRR).

Prior to the reflectivity experiments the instrument including the sample stage was aligned. In particular, the design of the sample stage allows to change samples without the necessity of a new alignment. From neutron reflectivity on a Ni single film (fig. 1) we obtained the characteristics of the neutron beam: $\lambda = 0.98$ nm, $\Delta\lambda = 0.02$ nm, $\Delta\theta = 0.06°$.

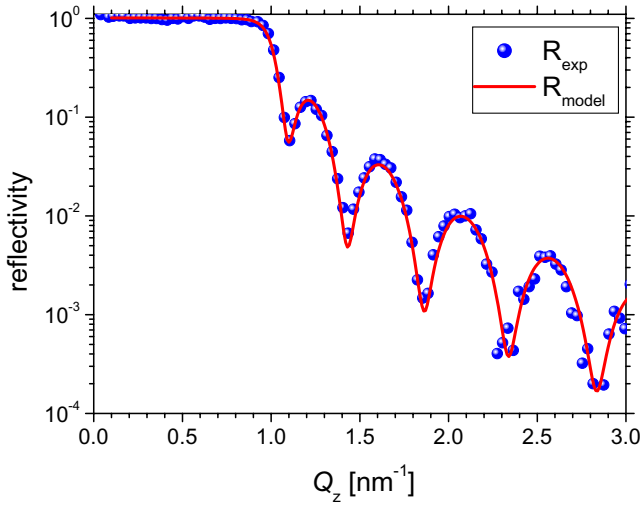

Figure 1: Neutron reflectivity of Ni single film (t_{Ni} = 52.55 nm). The symbols represent the experimental data whereas the solid line shows the computed reflectivity.

Fig. 2 shows the neutron reflectivities of FeCoV/NiO/FeCoV trilayers. The agreement of experimental and computed reflectivities is satisfactory. Some discrepancies are remaining as the model reflectivities include only a contribution from an average magnetisation of the ferromagnetic FeCoV layers. This may not be completely real since the magnetic field environment was not ready at the time of the experiments and therefore the magnetic state of the samples could not be defined absolutely. Nevertheless these first results obtained from MIRA confirm our structural layer model, which is the basis for the analysis of polarised neutron reflectivity measurements performed at the AMOR reflectometer at PSI [1, 2]. In addition to the successful test of the layer profile of our samples we could establish the reflectometry option of MIRA. It is a promising instrument especially once polarised neutrons are available allowing to investigate magnetic structures in detail.

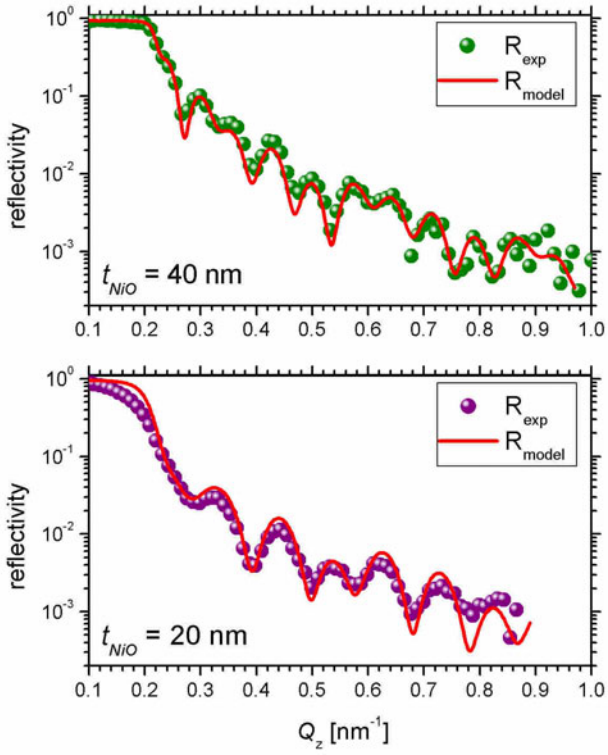

Figure 2: Neutron reflectivity of FeCoV (20 nm)/NiO (t_{NiO})/FeCoV (20 nm) trilayers. The structural parameters, as obtained from the refinement of the X-ray reflectivity, are directly used to calculate the nuclear SLD profile of the trilayers for neutrons. From the combination of nuclear and magnetic contributions to the scattering length the model reflectivities are calculated.

References

[1] V.R. Shah, C. Schanzer, P. Böni, and H. B. Braun. *J. Magn. Magn. Mater.* in press.
[2] C. Schanzer, V.R. Shah, T. Gutberlet, M. Gupta, P. Böni, and H. B. Braun. *Physica B.* in press.

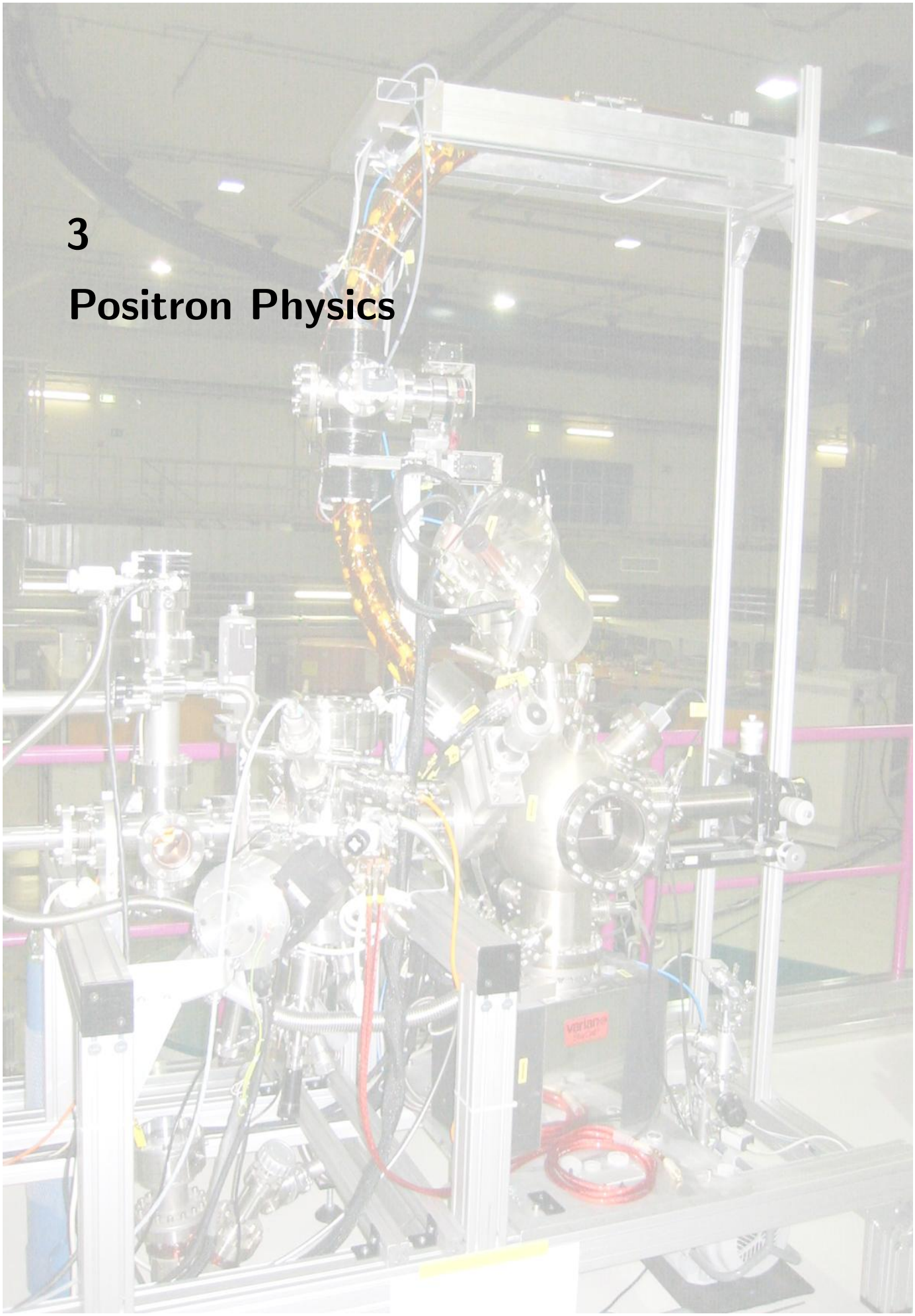

3

Positron Physics

3.1 First Positrons at NEPOMUC

Christoph Hugenschmidt [1, 2], **Reinhard Repper** [2], **Benno Straßer** [2], **Martin Stadlbauer** [1], **Klaus Schreckenbach** [1, 2]

[1] *Technische Universität München, Physics Department, Institute E21, D-85747 Garching, Germany*
[2] *Technische Universität München, ZWE FRM-II, D-85747 Garching, Germany*

NEPOMUC – Neutron Induced Positron Source Munich

The intense positron source NEPOMUC is based on absorption of high-energy prompt γ-rays from thermal neutron capture in ^{113}Cd [1]. For this purpose, a cadmium cap is placed inside the tip of the inclined beam tube SR 11 in the heavy water moderator tank (see Fig. 1). Inside the cadmium cap a structure of platinum foils is mounted in order to convert the high-energy γ-radiation into positron-electron pairs. Due to the negative positron work function, moderation in annealed platinum leads to emission of monoenergetic positrons.

After acceleration to an energy between a few eV and 1 keV by electrical lenses the positron beam is magnetically guided in a solenoid field of typically 7 mT. The beam passes three bents in the biological shield of the reactor in order to eliminate background of fast neutrons and γ-radiation.

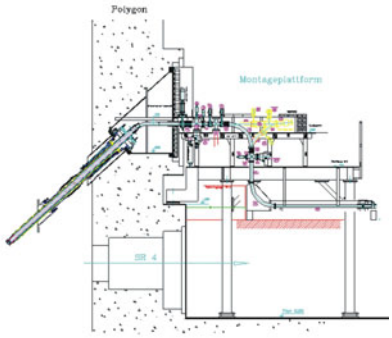

Figure 1: Cross sectional view of the inclined beamtube SR 11: The in-pile positron source is mounted inside the tip. After acceleration the positron beam is magnetically guided to the platform outside the biological shield of the reactor.

Beam Diagnostic Instruments

Intensity and positron beam profile measurements were preformed at the first accessible position outside the biological shield. A movable aluminium plate and an aperture were mounted inside the vacuum beamline in order to vary the beam profile. NaI-scintillators were positioned perpendicular to the movable Al-plate. Hence, the beam intensity could be determined by the detection of the 511 keV γ-radiation of positrons that annihilate at the aluminium plate, which acts as positron target when it is positioned in the beam line.

The beam profile is determined with a micro channel plate (MCP) detector and a CCD-camera. Electrons were repelled by a negative voltage at the MCP-entrance in order to obtain an almost background free signal of positrons hitting the MCP-detector.

Positron Intensity and Beam Profile Measurements

In April 2004 first positrons were detected at low reactor power of 15 kW. Hence, beam parameters such as magnetic solenoid and correction fields as well as acceleration voltages could be optimized. Fig. 2 shows the raw data of the detected γ-radiation. The photopeak and Compton events due to the 511 keV annihilation radiation are clearly visible. The background accords to a measurement without magnetic guiding field, which was expected to be very low due to the massive heavy concrete shield around the beam tube.

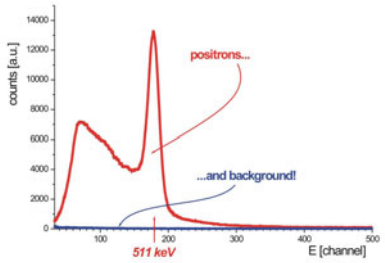

Figure 2: Detection of positrons: Photopeak and Compton events due to the 511 keV annihilation radiation.

In summer 2004 intensity measurements were performed at the nominal reactor power of 20 MW. Due to limitations of the applied voltage the maximum primary beam energy was set to 1 keV, which perfectly fits the Coincident Doppler broadening experiment (see [2]). The highest measured intensity was about 10^8 moderated positrons per second. The intensity profile of the monoenergetic positron beam at 1 keV was recorded in a longitudinal magnetic field of 6 mT with the MCP-detector. The beam shows a slightly elliptical contour with an estimated diameter of about 6-8 mm (see Fig. 3).
In another experiment the positron beam was extracted at much lower energy of 30 eV in order to accomplish the requirements of the PAES (Positron annihilation induced Auger-electron spectroscopy) facility [3]. For both energies, 30 eV as well as 1 keV, the positron beam was guided to the instruments on the experimental platform.

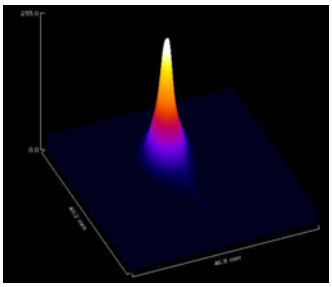

Figure 3: Intensity profile of the monoenergetic positron beam at 1 keV and a longitudinal magnetic field of 6 mT. The beam diameter amounts to about 7 mm.

References

[1] C. Hugenschmidt, G. Kögel, R. Repper, K. Schreckenbach, P. Sperr, B. Straßer, and W. Triftshäuser. *Nucl. Instr. Meth. B*, 221:160–164, 2004.
[2] M. Stadlbauer. Aufbau eines ortsauflösenden Doppler-Koinzidenzspektrometers zur Untersuchung der Positronenzerstrahlung. Diplomarbeit, TU München, 2004.
[3] B. Straßer, C. Hugenschmidt, and K. Schreckenbach. *Mat. Sci. For.*, 363-365:686–688, 2001.

3.2 The Positron Beam Facility NEPOMUC and its Instrumentation

Christoph Hugenschmidt [1, 2], **Benno Straßer** [2], **Martin Stadlbauer** [1], **Klaus Schreckenbach** [1, 2]

[1] *Technische Universität München, Physics Department, Institute E21, D-85747 Garching, Germany*
[2] *Technische Universität München, ZWE FRM-II, D-85747 Garching, Germany*

In summer 2004 the in-pile positron source NEPOMUC of the new Munich research reactor FRM II was set into operation at the nominal reactor power of 20 MW. The largest section of the positron beam facility was completed and extended by an additional beam switch in order to connect two spectrometers for positron experiments: positron annihilation induced Auger electron spectroscopy (PAES) [1] and coincident Doppler-broadening spectroscopy (CDB) [2].

NEPOMUC – Neutron Induced Positron Source Munich and the beam facility

The moderated positrons are accelerated to an energy between a few eV and 1 keV by electrical lenses. In the beam tube SR 11 the positron beam is magnetically guided in a solenoid field of typically 7 mT to the experimental platform. An overview of the positron beam facility is given in Fig. 1. The beam line consists of stainless steel vacuum tubes, computer controlled valves and pumping units as well as magnetic field coils. Straight sections are μ-metal shielded and correction coils are mounted at the bent parts of the beam line in order to adjust the positron beam and to minimize transport loss.

NEPOMUC's Instrumentation

In the present arrangement of NEPOMUC's instrumentation the monoenergetic positron beam is magnetically guided to a CDB facility and to a PAES analysis chamber. These facilities were constructed in the lab of E21 and transferred to the reactor in 2004. It is planned to use an additional open beam port for fundamental research with the high intense positron beam. In 2005 it is planned to install an apparatus for the production of the negatively charged positronium (Ps^-), which is presently operated at the Max-Planck-Institute for nuclear physics [3]. Two positron lifetime experiments (PLEPS and SPM) will be transferred from the Universität der Bundeswehr to the reactor in the beginning of 2005 [4].

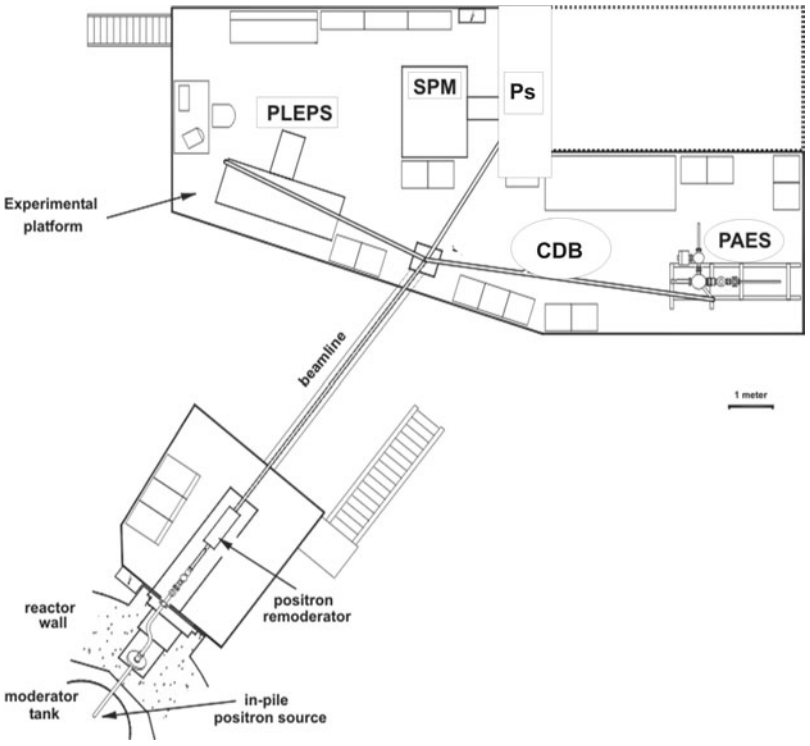

Figure 1: Overview of the positron beam facility NEPOMUC. First installed experiments are a CDB spectrometer and a PAES analysis chamber, which are built and operated by E21/TUM. The positron lifetime experiments PLEPS and SPM (Universität der Bundeswehr, München) as well as the (Ps^-)-apparatus (MPI for nuclear physics, Heidelberg) will be transferred to the reactor in 2005

References

[1] C. Hugenschmidt, B. Straßer, and K. Schreckenbach. *Radiat. Phys. Chem.*, 68:627–629, 2003.

[2] M. Stadlbauer. Aufbau eines ortsauflösenden Doppler-Koinzidenzspektrometers zur Untersuchung der Positronenzerstrahlung. Diplomarbeit, TU München, 2004.

[3] D. Schwalm, F. Fleischer, M. Lestinsky, K. Degreif, G. Gwinner, V. Liechtenstein, F. Plenge, and H. Scheit. *Nucl. Instr. Meth. B*, 221:185–194, 2004.

[4] C. Hugenschmidt, G. Kögel, R. Repper, K. Schreckenbach, P. Sperr, B. Straßer, and W. Triftshäuser. *Nucl. Instr. Meth. B*, 221:160–164, 2004.

3.3 Development of a Coincident Doppler Spectrometer with Spacial Resolution at the Intense Positron Source NEPOMUC

Martin Stadlbauer [1], **Christoph Hugenschmidt** [1, 2], **Klaus Schreckenbach** [1, 2]
[1] *Technische Universität München, Physics Department, Institute E21, D-85747 Garching, Germany*
[2] *Technische Universität München, ZWE FRM-II, D-85747 Garching, Germany*

A CDB-spectrometer was developed in order to enable elemental specific defect spectroscopy by positron annihilation in matter. If a positron is implanted into a metallic sample it thermalizes within picoseconds. After diffusion through hundreds of lattice constants, it annihilates with an electron in the sample into 2 γ-Quanta with energies of 511 keV. Due to the electron momenta the emitted γ-radiation is Doppler shifted. The Doppler shift decreases, if the positron is trapped at a defect due to the lower annihilation probability with core electrons which have high momenta. Hence defects can be studied by measuring the Doppler-broadened 511 keV annihilation line [1]. Moreover, the accurate measurement of high Doppler shifts, i.e. high electron momenta, reveals chemical info at the annihilation site [2]. Our new Doppler spectrometer with two facing germanium detectors allows to focus the positron beam NEPOMUC and to position the sample in vacuum in order to measure Doppler spectra with spacial resolution of about 2 mm.

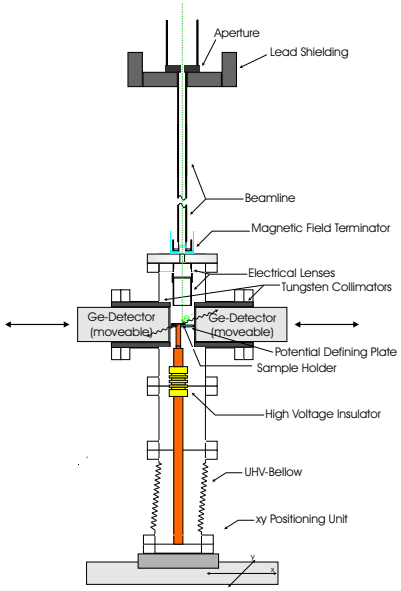

Figure 1: Scheme of the CDB experiment.

Experimental Setup

The positron beam is guided in an evacuated tube along a longitudinal magnetic guiding field. The intensity as well as the diameter of the beam is determined by a 2 mm aperture. In order to vary the penetration depth of the positrons, the sample potential can be chosen between 0 and -20 kV. Consequently there exists an electric field in the vacuum chamber which would disturb magnetic focussing. For this reason the magnetic field of the beam tube is screened by μ-metal and the positrons are nonadiabatically released from the guiding field by a magnetic field terminator. An electric focussing unit consisting of an Einzel lens forms the positron beam and reduces it to a diameter of about 2 mm.
The spacial resolution is achieved by positioning the sample in the vacuum chamber perpendicular to the beam direction. The translation of the sample holder is accomplished with a stepper motor controlled positioning unit. Fig. 1 shows a cross sectional view of the sample chamber.

First Measurements

In order to measure the diameter of the positron beam, a sample was prepared which consists of tungsten stripes glued on aluminium. Since the electron momenta of aluminium and tungsten are different, the shape of the annihilation line of both materials is unequal. Hence, the varying broadness of the annihilation line reveals the beam structure, when the sample position is varied and the positron beam crosses the border between aluminium and tungsten. These measurements show, that the beam consists of an intense centre of about 2 mm diameter which is surrounded by a bigger halo, what was ascertained by the comparison with a theoretically supposed homogeneous beam.
The next measurement was performed with a thermally treated brass sample. It was heated on one end to about 800 K and cooled on the other side. The achieved spectra of four different positions on the sample were normalized to annealed zinc and compared with pure copper. As Fig. 2 shows, the curves of copper and zinc differ strongly in the region of high Doppler shift, i.e. $E > 513$ keV, as a consequence of the different electron momentum distribution in both materials. The four curves of the brass sample are approaching the copper curve as the position of the positron beam reaches the heated side of the sample.
One possible reason for this behaviour is the decrease of the zinc concentration in heated brass due to the low vapour pressure of zinc. In addition the observed behaviour may also be a consequence of a partially annealing during the heating process which would lead to different defect densities.
Further measurements will be performed in order to investigate the contribution of varying defect concentrations.

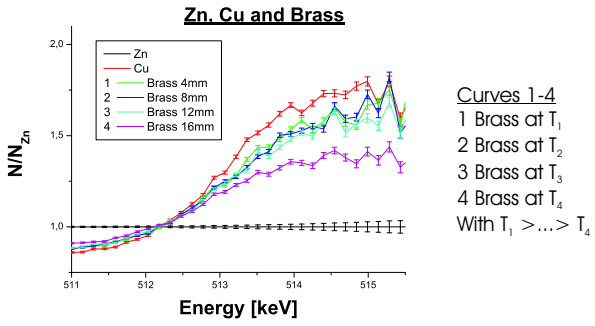

Figure 2: Annihilation spectra of pure copper, zinc and thermally treated brass.

References

[1] P.J. Schulz and K.G. Lynn. *Rev. Mod. Phys.*, 60:701–773, 1988.
[2] P. Asoka-Kumar, M. Alatalo, V. J. Ghosh, A. C. Krusemann, B. Nielsen, and K. G. Lynn. *Phys. Rev. Let.*, 77:2097–2100, 1996.

3.4 Positron remoderation facility for the slow positron beam at FRM-II

Christian Piochacz [1], **Christoph Hugenschmidt** [1, 2], **Klaus Schreckenbach** [1, 2]
[1] *Technische Universität München, Physics Department, Institute E21, D-85747 Garching, Germany*
[2] *Technische Universität München, ZWE FRM-II, D-85747 Garching, Germany*

Recently the intense positron source at the FRM-II has been set into operation[1]. In order to enhance the brightness of the beam, a positron remoderator will be installed. The idea of using remoderation for brightness enhancement was first mentioned by [1]. For the remoderation process, positrons are guided and focused on a solid, where they stop and thermalize. There is a certain possibility, that thermalized positrons drift to the surface where they leave the solid with a sharp energy and a small angular divergency. The whole process depends on the properties of the solid, which is used for moderation. Materials, such as tungsten, nickel and platinum are known to be effidient for moderating positrons. There are basically two possibilities for remoderating a positron beam, depending on which surface the positrons are emitted: reflection or transmission geometry. The moderator, which is currently built works in transmission geometry with a 100 nm thin tungsten singel crystalline foil. The moderated positrons leave the foil surface with an energy of about 3 eV and an angular spread of about 8°.

Setup

The positons are focused by adiabatic magnetic field compression, i.e. the postirons follow the compressed magnetic field by a gyration motion leading to a smaller beam. The increasing magnetic field is archieved by conventional copper coils whereas the high magnetic field of about 300 mT is realized by a water cooled copper coil. The positrons leave the high magnetic field after moderation non-adiabatically in order to conserve the small diameter of the beam. This magnetic field termination is implemented by an aperture made of mu-metal.

Advantages of the chosen design

Transmission remoderators require much simpler beam guiding fields unlike the reflection geometry solutions. Due to the small beam diameter after moderation the termination of the magnetic field is done just by an aperture made of mu-metal. Beams with a great transversal impulse and/or a broad energy spread can be focused and hence remoderated. This is more difficult with electric or magnetic lenses and would lead to complex lens systems in order to avoid lens aberrations. The working parameters of the moderator (e.g. coil currents) depend not or only in a simple way on the properties of the primary beam.

State of the work

Simulations of the magnetic and electric field properties have been done. According to the optimised results geometry of the vacuum system, magentic coils and electrical electrodes have been constructed. Recently the whole remoderation facility has been setup. First measurements of the magnetic field assert the results of the field simulations. Now we are ready to test the focusing behaviour with an electron beam. After the installation of the W(100) remoderation foil the system will be tested at the positron beam facility at the FRM-II.

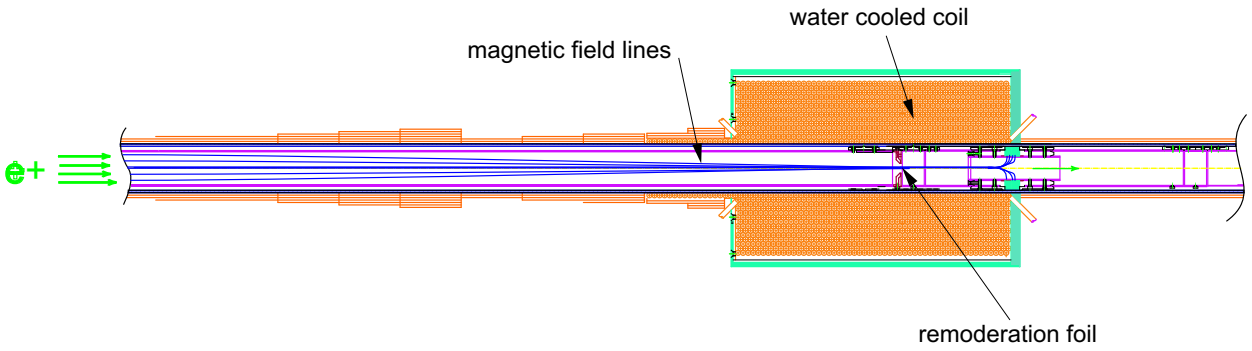

Figure 1: Cross-sectional view of the positron beam remoderator, which will be installed at the positron beam facility at the FRM-II in Munich. The primary beam from the left is focused by the compressed magnetic field lines. After moderation the positrons leave the area of high magnetic field non-adiabatically in oder to conserve the small diameter of the beam. The moderating foil (100 nm W(100)) is near the centre of the big coil block. The magnetic field lines (blue) are only schematically.

References

[1] A.P. Mills Jr. Brightness enhancement of slow positron beam. *Appl. Phys.*, 23:189, 1980.

[1] see contribution in this issue

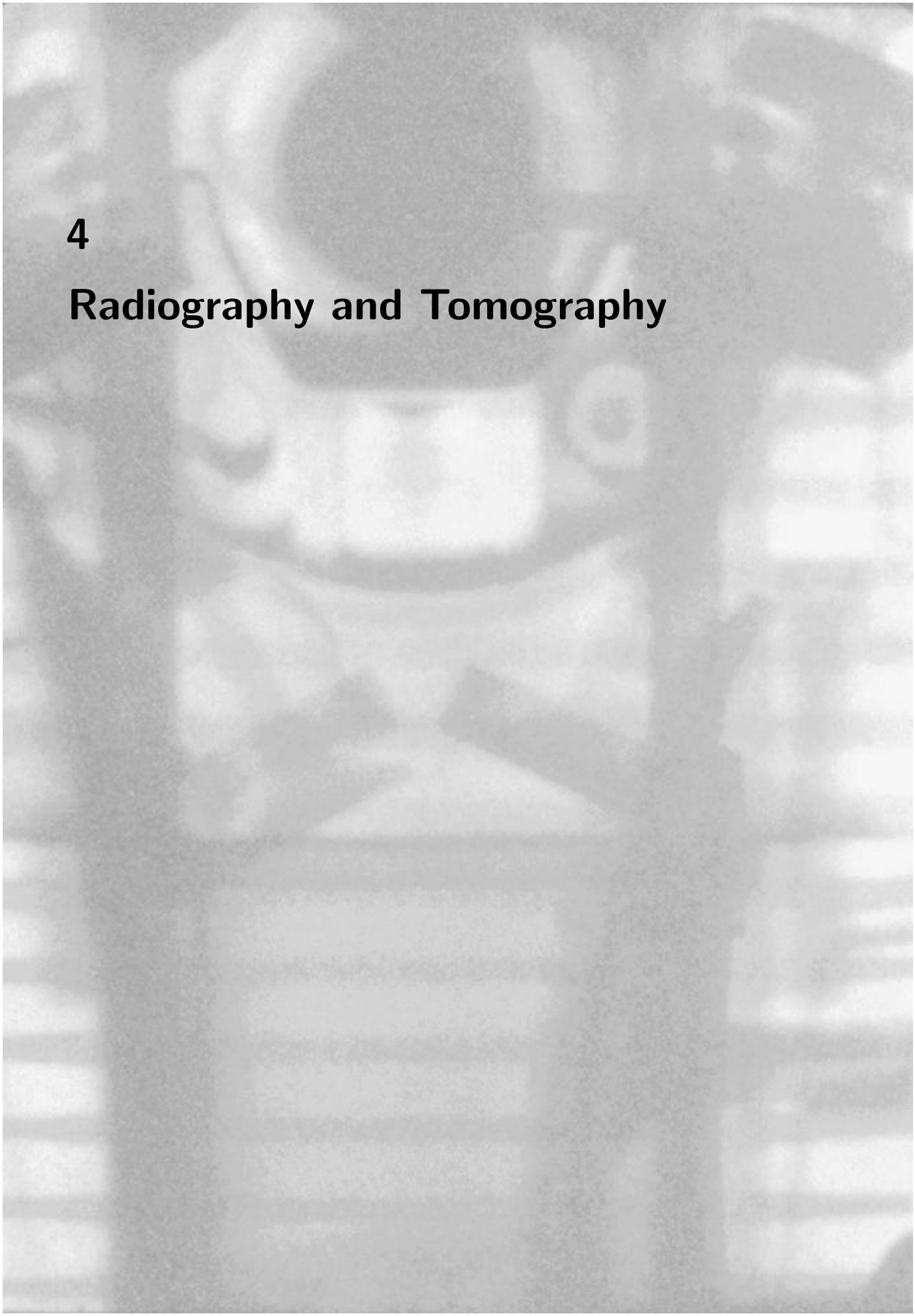

4
Radiography and Tomography

4.1 Investigation of a focusing parabolic guide by radiography methods

N. Kardjilov [2], **P. Böni** [1], **A. Hilger** [2], **M. Strobl** [2], **W. Treimer** [2]
[1] *Technische Universität München, Physics Department E21, D-85747 Garching, Germany*
[2] *BENSC, Hahn-Meitner-Institut, Glienickerstrasse 100, D-14109 Berlin, Germany*

We show that neutrons can be very efficiently focused by using parabolic neutron guides leading to gains of more than 50 on areas as small as 1 mm^2. The advantages are i) ease of implementation, ii) improved signal to noise ratio, and iii) largest gain at focal point.

The aim of the experiment was to investigate the focusing properties of a new type of focusing neutron guide (trumpet) with parabolically shaped walls. The device was manufactured by SwissNeutronics and placed at the beam line V12b. The guide had a length of 445 mm with an entrance area of 16×16 mm^2 and an output area of 4×4 mm^2 [1]. The interior surfaces were coated with supermirror $m = 3$ and due to their parabolic shape it was expected that an incident parallel beam can be focused onto a single spot in the focal point.

To quantify the performance of the device, the neutron intensity distribution at different distances behind the guide was recorded by means of a standard radiography detector described in [2]. The experiments were performed at the V12b instrument with a preliminary monochromatization of the incident cold neutron beam by a Si (1 1 1) perfect crystal monochromator with $\lambda = 5.2$ Å. A sketch of the experimental arrangement is shown in Fig. 1.

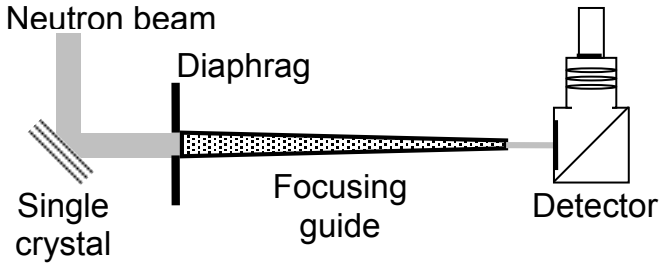

Figure 1: Layout of the experiment at beam line V12b.

The beam divergence of approximately 0.5° was given by the Ni coating of the neutron guide at this beam line. The position of the guide in the beam was adjusted with an accuracy of 0.05° by a combination of a tilt and a rotation table. The distance between the radiography detector and the end of the guide was set with the help of a translation table.

The images were recorded at three different distances d behind the focusing guide (directly at the exit of the guide, at the focal point and at a large distance from the exit) and are shown in Fig. 2. The area of the beam spot at the focal point (the picture in the middle) was estimated to be of the order of approximately 1 mm^2.

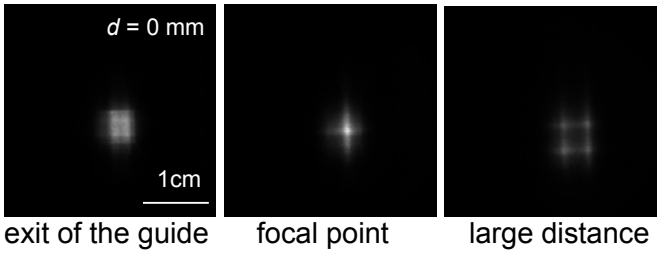

Figure 2: Radiography images of the intensity distribution at different distances behind the focusing guide.

The intensity gain was calculated as the flux ratio of the images with and without the utilization of the focusing guide. The result as a function of the distance behind the guide for two monochromators with a different energy acceptance: Si (1 1 1) with $\triangle\lambda/\lambda \simeq 10^{-3}$ and C(200) with $\triangle\lambda/\lambda \simeq 10^{-2}$ are shown in Fig. 3.

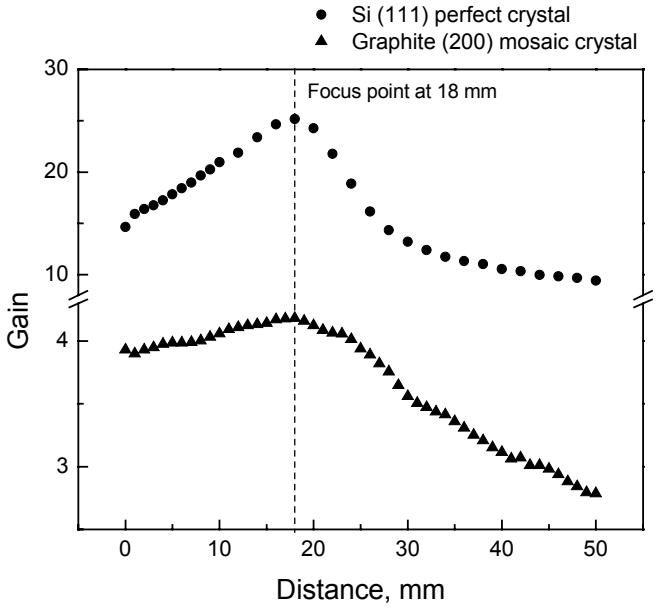

Figure 3: The measured intensity gain for two monochromators.

The large intensity gains are comparable to a Kumakhov lens [1].

References

[1] T. Hils, P. Böni, and J. Stahn. *Physica B*, 350:166–168, 2004.
[2] http://www.ndandm.com/products.htm#readout.

4.2 Neutron Radioscopy at FRM-II

Johannes Brunner [1], **Burkhard Schillinger** [1, 2]
[1] *Technische Universität München, Physics Department, Institute E21, D-85747 Garching, Germany*
[2] *Technische Universität München, ZWE FRM-II, D-85747 Garching, Germany*

Neutron radioscopy is an imaging technique, which allows the observation of dynamic processes. At today's neutron sources the accumulation time for a neutron radiography is typically in the range of seconds. In the case of cyclic processes it is possible to reach the millisecond time scale or below by stroboscopic imaging. Gating the detector by an image intensifier and the accumlation of identical frames lead to neutron radiographies of a good quality and can be obtained in spite of the low neutron flux at that time scale.
A very suited sample for the described method is a running combustion engine. Neutrons have an excellent penetration capability for many metallic materials, especially aluminium, and a high sensitivity for hydrogenous substances as oil, thus repetitive processes inside of a combustion engine can be visualized with a time scale down to 100 μs.

Figure 1: Diesel combustion engine for the neutron radioscopy at FRM-II

Before the comissioning of the FRM-II the explained technique was tested in a series of experiments at NEUTRA, PSI, Switzerland and at Neutrograph, ILL, France.
After the first neutrons March 10th, October 20th of this year the first neutron radioscopy experiment of a running combustion engine, Fig. 1, was launched at the Antares setup at FRM-II (Fig. 2). Every frame of the movie lasts one millisecond and consists of 1500 accumulations. The field of view of 144 $\times$ 144 mm, see Fig. 3, shows the movement of the piston and the valves in real time. The spatial resolution [1] resulted to be 1.0 mm, which can be explained by the beam divergency and the large object detector distance of 450 mm. The relative noise in the open beam under that conditions was measured to be 2.5%. The neutron tomography station Antares is well suited for neutron radioscopy because of its high neutron flux and the small beam divergency.

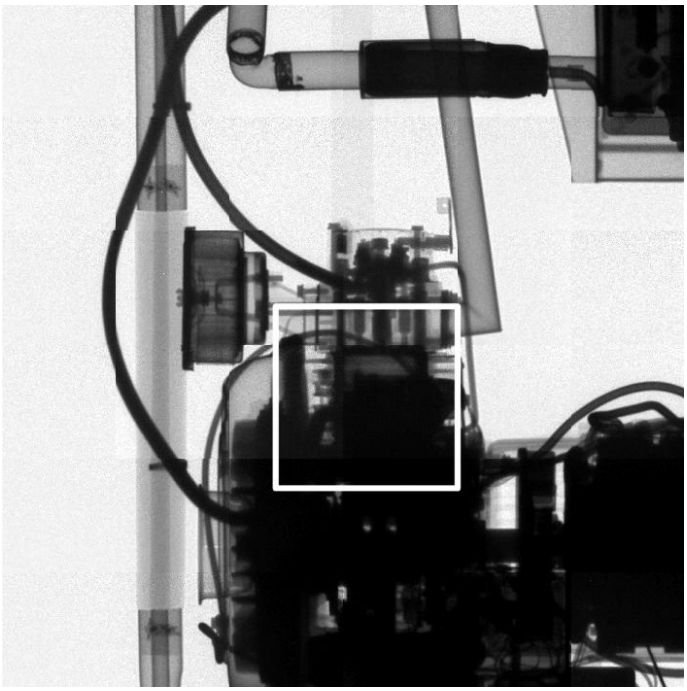

Figure 2: Composed neutron radiography of the combustion engine in Fig. 1

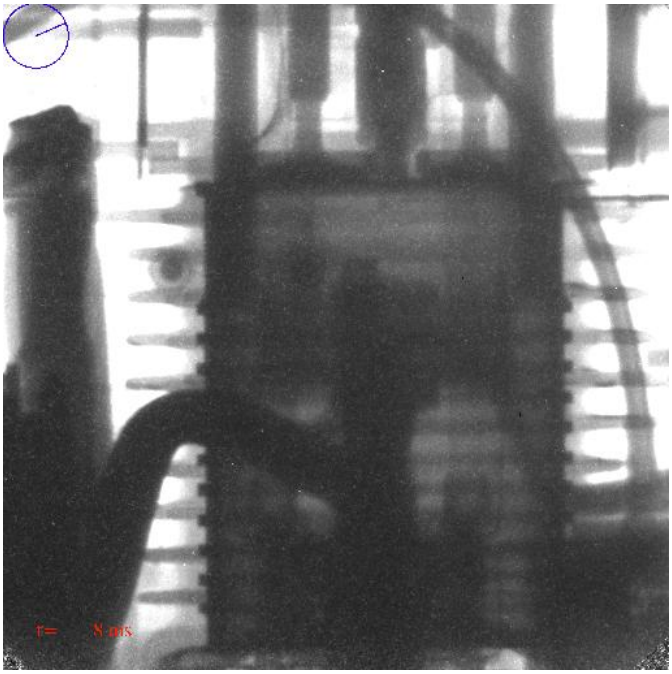

Figure 3: Single frame of the neutron radioscopy movie

References

[1] J. Brunner, M. Engelhardt, G. Frei, A. Gildemeister, E. Lehmann, A. Hillenbach, and B. Schillinger. Characterization of image quality in neutron radiography. *Proceedings of the International Topical Meeting of Neutron Radiography ITMNR 2004, Munich*, 2004.

4.3 Coded masks in neutron radiography

F. Grünauer [1]

[1] *Technische Universität München, Physics Department, Institute E21, D-85747 Garching, Germany*

Nearly all neutron radiography facilities use a setup similar to a single pinhole camera. With such facilities a compromise between high flux at the detector plane and high spatial resolution has to be made: High resolution can be obtained with a small aperture diameter D and a large distance L between aperture and object. As flux at the object plane is proportional to $(D/L)^2$, high resolution needs a long exposure time and yields a poor signal to noise ratio. Low L/D ratios provide a low noise level but the resulting image is blurred. Investigations were carried out by Monte Carlo simulations whether other configurations can overcome the single pinhole dilemma. In X-ray astronomy ring shaped masks, random array masks, uniformly redundant array (URA) masks, etc. are used to overcome the problem. The simulations show, that these types of apertures are less advantageous in neutron radiography, where large and structured objects are in the focus of interest. However it could be shown, that a multiple pinhole mask with minimized autocorrelation (Fig. 1; non redundant array) together with an improved reconstruction algorithm, provide significant better results. This new approach with regard to neutron radiography was introduced at FRM-II. The following example shows a radiography of an arrangement of Ge-crystals (Fig. 2). The setup is used as monochromator at the powder diffractometer SPODI.

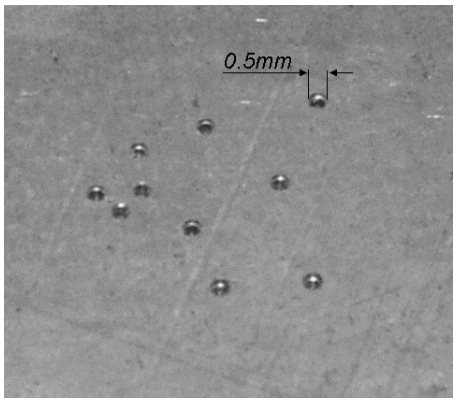

Figure 1: Multiple pinhole aperture

Figure 2: Setup at the powder diffractometer SPODI

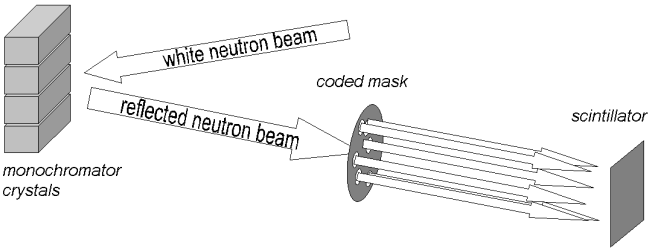

Figure 3: Schematic overview of the setup

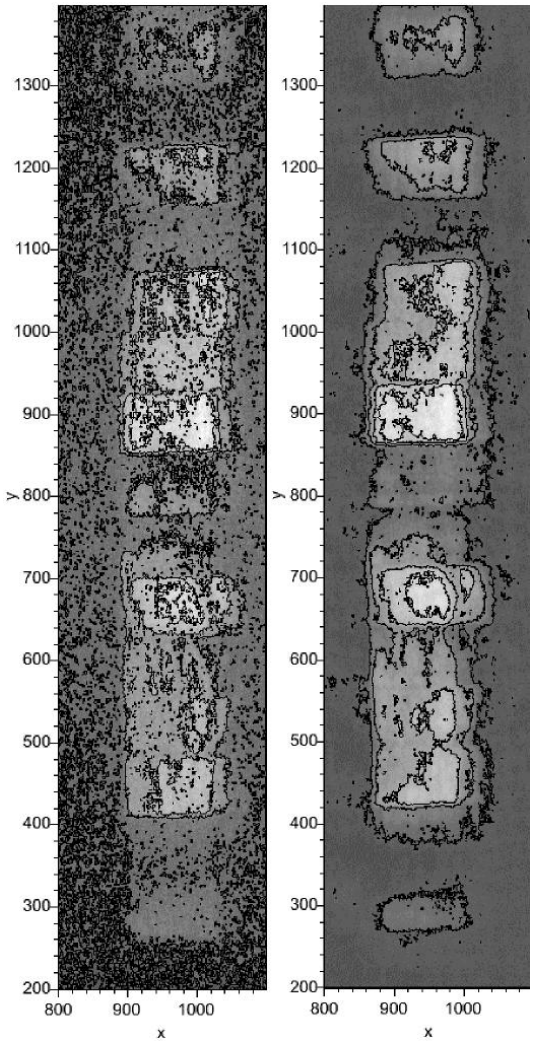

Figure 4: Left hand side: Projection of the monochromator crystals using a single hole aperture (hole diameter = 0.5 mm). Right hand side: Reconstruction of the projection obtained by the coded 10 hole aperture (hole diameter = 0.5 mm). In both cases the exposure time was 8280 s.

The example shows, that the signal to noise ratio of a neutron radiography can be increased without major loss of resolution (Fig. 4). This can be useful for several applications in neutron radiography, e.g. in phase contrast radiography, where the necessity of a very small aperture limits intensity, or in dynamic radiography, where exposure time is limited by the observed process.

4.4 Non-destructive testing with phase contrast radiography at ANTARES

Eberhard Lehmann [1], **Klaus Lorenz** [2], **Erich Steichele** [2], **Peter Vontobel** [1]
[1] *Paul-Scherrer-Institut, CH-5232 Villigen, Switzerland*
[2] *Technische Universität München, Physics Department, Institute E21, D-85747 Garching, Germany*

The refractive index $n = 1 - \delta - \mathrm{i}\beta$ of a material consists in general of a real and an imaginary part. The imaginary part causes the attenuation of the neutron beam, what is used in conventional radiographies to visualize the structure of an object. The real part leads to a phase shift φ of the neutron with regard to propagation in free space. At edges and interfaces this leads to great deviations of the wavefronts of an incoming wave. If the detector has a certain distance from the object (in the near field region), an increase in the contrast at edges and interfaces occurs [1]. This interference effect is the so called phase contrast.

Experimental setup

To get phase contrast, the radiography setup has to fulfill two basic requirements:

1. High transversal spatial coherence
   This can be realized easily with a pinhole and a large distance between the pinhole and the object.

2. Detector plane in the near field region
   The distance between sample and detector must not be to small (else you get only absorption contrast) and it must not be too large (else you come in the fresnel region).

At ANTARES the high lateral coherence is achieved by inserting an aperture with a very small pinhole in the neutron beam. If the diameter of the pinhole is D and the distance between pinhole and sample is L, the lateral coherence length is $l_{coh} = (L/D)\,\lambda$, where λ is the wavelength of the neutrons. To be able to vary this parameter easily, an aperture wheel was constructed for the ANTARES facility (see Fig. 1). With this revolver-like device, eight different apertures can be positioned quickly and precisely in the neutron beam. Besides the single pinholes with different diameters, coded apertures are used in the aperture wheel. With the help of these multi-hole apertures, the exposure time for phase contrast radiographies can be reduced.

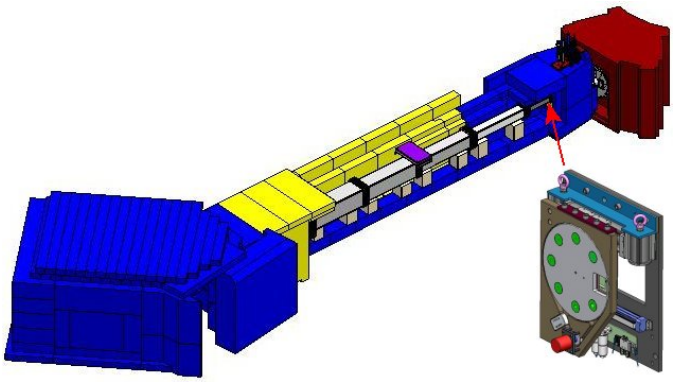

Figure 1: Implementation of the aperture wheel in ANTARES.

Applications of phase contrast imaging

The enhanced contrast at edges and interfaces in phase contrast images can be very useful for the non-destructive testing of objects, especially for materials with low attenuation coefficients like aluminium.

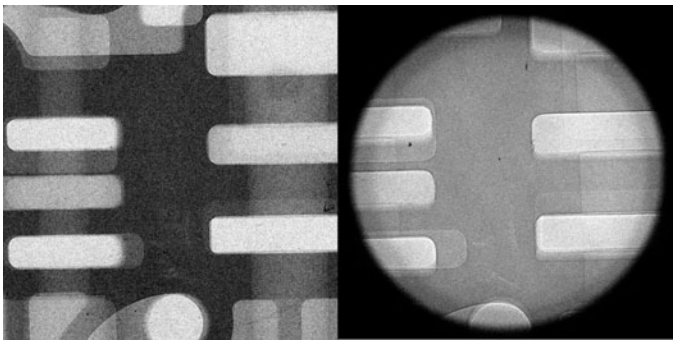

Figure 2: Comparison of a conventional radiography (left) and a phase contrast radiography (right) of a cast aluminum sample.

The additional contrast at edges is only one feature of this non-interferometric technique. It also allows the measurement of the phase shift φ the neutrons experienced on their way through the sample. The technique to do this phase retrieval is based on the transport-of-intensity-equation (TIE) [2]. Therefore at least two phase contrast radiographies in different sample-to-detector-distances z have to be done. Out of these intensity distributions $I_z(X, Y)$ in the different detector planes, the phase shift is calculated with the TIE [3]. For this phase retrieval, the neutrons do not have to be monochromatic [4]. With this technique it becomes possible to get contrast even between materials with a similar attenuation coefficient (see Fig. 3).

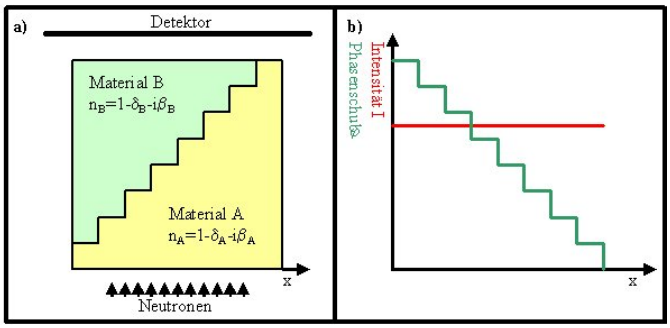

Figure 3: An example for the application of quantitative phase contrast imaging.

References

[1] Cowley. *Diffraction Physics*. Oxford University Press, 1975.
[2] M. R. Teague. *J. Opt. Soc. Am.*, 73:1434–1441, 1983.
[3] B. E. Allman, P. J. McMahon, K. A. Nugent, D. Paganin, D. L. Jacobson, M. Arif, and S. A. Werner. *Nature*, 408:158–159, 2000.
[4] P. J. McMahon, B. E. Allman, D. L. Jacobson, M. Arif, S. A. Werner, and K. A. Nugent. *Phys. Rev. Lett.*, 91, 2003.

4.5 First results of the radiography and tomography facility ANTARES

Burkhard Schillinger [1, 2], **Johannes Brunner** [1], **Elbio Calzada** [1, 2], **Florian Grünauer** [1], **Klaus Lorenz** [1], **Martin Mühlbauer** [1], **Michael Schulz** [1]

[1] *Technische Universität München, Physics Department, Institute E21, D-85747 Garching, Germany*
[2] *Technische Universität München, ZWE FRM-II, D-85747 Garching, Germany*

Abstract

In 2004, the reactor FRM-II was finally commissioned and the first fuel cycle was completed. The huge number of radiation protection tasks made a very difficult balance between commissioning the reactor itself and clearing all instruments at each new power level, so the instruments did not receive all the measurement time they required, and many test measurements could only be performed in a rudimentary way yet.
The Neutron radiography and tomography facility ANTARES produced first results in the categories of neutron radiography, neutron computed tomography, stroboscopic imaging and also the first test image with the additionally installed 300 kV X-ray tube. The phase contrast imaging mode yet has to be tested in 2005.

Neutron radiography measurements

On March 22, the very first neutron radiography images were recorded at a reactor power of only 50 kW, which equals 1/400 of the nominal power of 20 MW. With the 4 cm diameter collimator and $L/D = 400$, the flux was approx. 2.5×105 n/cm^{2}s, requiring a measurement time of approx. 50 seconds for the full dynamic range of the CCD detector.
The employed standard detector was a cooled CCD camera with 2048×2048 pixels, combined with a mirror and scintillation screen. Fig. 1 shows the radiography of a carburettor.

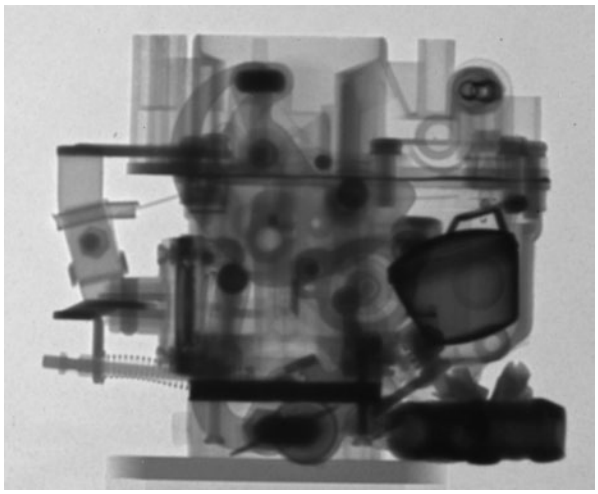

Figure 1: The radiography of a carburettor.

During the low-power periods up to 6 MW, several radiography and tomography test experiments were performed with both the large collimator (4 cm diameter, $L/D = 400$) and the small collimator (2 cm diameter, $L/D = 800$). When power was raised to 9 MW, we encountered an unexpected complication: The evacuated flight tube contains a stripping frame made of borated polyethylene at the joint of two tube segments in order to strip thermal neutrons from the penumbra region of the beam to keep the incident thermal flux low on the blockhouse wall around the beam window. The borated polyethylene was expected to pass the remaining epithermal and fast part of the neutron beam, but it showed to act as a scatterer to such an extent that the gamma dose rate induced within the shielding surpassed the permitted level by a factor of eight on the outside when the large collimator was used. All subsequent experiments at higher power levels had thus to be performed only with the small collimator, which prevented the beam from touching the stripper window.

The polyethylene stripper frame has now been replaced by Boron-Aluminium after completion of the first fuel cycle.

Neutron tomography measurements

The first neutron tomography measurement was performed with the intensified 1024×1024 pixel CCD camera intended for stroboscopic imaging at a power of 200 kW only. Due to the low power and short available time, the axis of rotation and the CCD camera were not perfectly adjusted, slightly lowering the achieved tomography resolution.
Fig. 2 shows several views of a carburettor.

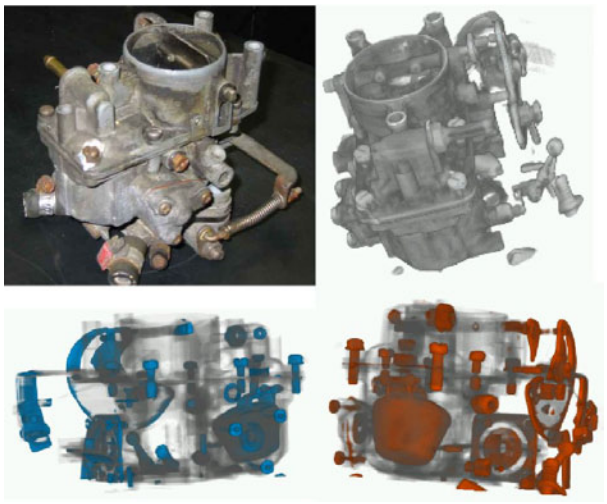

Figure 2: Several views of a carburettor.

Stroboscopic short-time imaging

For the recording of fast-moving objects, exposure times are required well below one millisecond. Even the FRM-II does not provide sufficient neutron flux for imaging in that time frame.
The only solution is stroboscopic imaging of repetitive motions with a gated integrating detector. At ANTARES, a cooled CCD camera with a gated image intensifier is coupled with appropriate sensor electronics that triggers the gate of the intensifier at identical time windows during the repetitive motion. This was demonstrated on a modified diesel generator (Fig. 3) running at 3000 rpm. The mounting frame of the generator and the respective connections were elongated in order to remove the exhaust and the fuel tank out of the beam path and to gain free access to the cylinder. Later

on, also the electric starter was removed. A remote magnetic switch allowed for stopping the engine from outside the blockhouse, the operation was controlled by a CCTV system. A special soot filter was mounted on the exhaust, the output was connected to the air exhaust of the experimental hall by a 20 m tube. A hall sensor was mounted in proximity to the camshaft of the engine to trigger the image intensifier. Several hundred time windows are integrated on the CCD chip before the image is read out.
By delaying the trigger signal in the computer, the time window can be shifted across the complete cycle of the repetitive motion, and the integrated images from consecutive time windows can be concatenated to form a movie covering a complete cycle.

A first movie was generated of the diesel engine running on its own power with a time window of 200 μs, using the small collimator (see above) with a flux of 2.5 $\cdot$ 107 n/cm^{2}s. The length of the time window still generated some motion unsharpness for the piston; better time resolution will be achieved in 2005, when the larger collimator can be used for more flux. Fig. 3 shows a photo of the diesel generator, Fig. 4 a mosaic of radiographs of the whole motor and Fig. 5 shows a single frame of the generated movie.

Figure 3: A photo of the diesel generator.

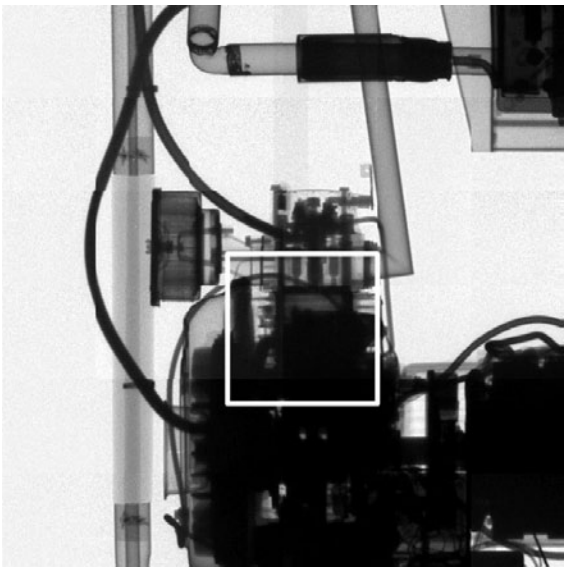

Figure 4: A mosaic of radiographs of the whole motor.

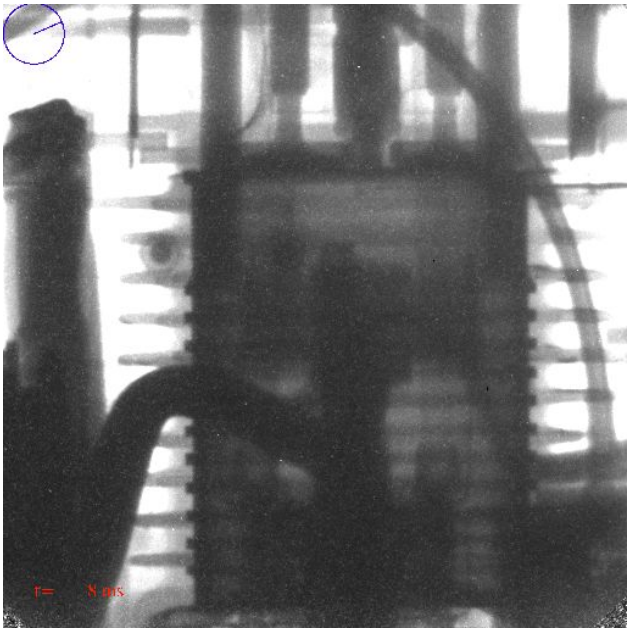

Figure 5: A single frame of the generated movie.

Small angle scattering tomography

A completely new approach for tomography measurements was suggested by Roland Gähler, ILL. Neutron computed tomography was used for the first time to detect small angle scattering due to texture alterations in Aluminium parts. In Aluminium aircraft components, holes intended for rivets are drilled with less than the required diameter, then they are widened with a thorn. At the edges, the Aluminium is compressed and deformed, the inner structure is altered. This is done to introduce compressive stress into the material to anticipate tensile stress from rivets in the hole.
The altered texture leads to increased small angle scattering, showing more attenuation around the hole edge. This effect is not visible at ordinarily drilled holes.

For these experiments, a neutron tomography was recorded of a sheet of Aluminium with drill hole with compressed edges. To make the effect of small angle scattering visible, the distance between the sample and detector was increased to 50 cms. Obtaining sharp images at this distance is onl possible at facilities with high L/D ratio like PSI and FRM-II.

To be able to detect these small effects at all, the obtained 3D data had to be visualised in the following way: The result of a tomography is a 3-dimensional matrix of density, or more accurately for neutrons, attenuation values for the different materials, which may be mapped to grey values in an image. If a 3-dimensional view is to be generated, the gray values in the image have to be additionally mapped with an opacity value to allow semi-transparent renderings of the matrix to allow a view into the interior of that matrix. Each material is represented by a certain attenuation range. For visualisation, different ranges may be mapped to different grey values, while at the same time ranges may be set opaque or completely transparent or invisible.

In order to detect the faint variations caused by small angle scattering, nearly the whole attenuation range of Aluminium was set to transparent, save for the most attenuating edge of that data range. This revealed two different structures

of increased small angle scattering in the sample: The Aluminium shows a wave structure from rolling out the sheet. One possible interpretation may be an uneven milling cylinder, another interpretation may be that the surfaces of Aluminium sheets are first milled with a large cylindrical milling cutter, the rolled out again; the variations may result from compressed milling traces. At the edges of the widened hole, a rim of increased attenuation is clearly visible.

With the permission of the sample owner, a second hole of equal diameter was drilled into the sample with a standard drill. The measurement was repeated with only half the distance to the detector, and with a second detector of less sensitivity and dynamic range, because the standard detector was not available at the time. The second measurement confirms the difference between the compressed and uncompressed rims, some increased attenuation at the second rim coincides with a wave of the rolling structure.
Fig. 6 shows a 3D view (a full tomography) of the Aluminium sheet with the widened and the ordinary holes.

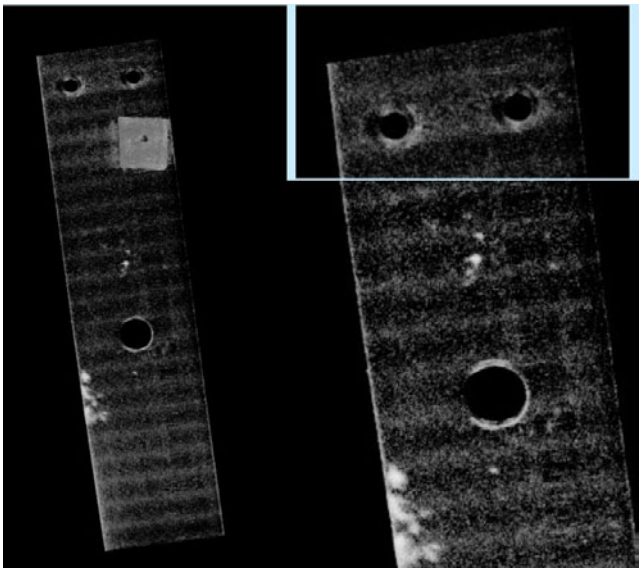

Figure 6: A 3D view of the Aluminium sheet with the widened and the ordinary holes.

This tomographic method may serve as a pre-examination tool for stress measurements, where regions of interest may be selected for consecutive quantitative measurements on a strain scanner, where the sample volume has to be scanned in quanta of a cubic millimetre.

Installation of the X-ray tube

Following the idea of the NEUTRA group at PSI, a retractable 300 kV X-ray tube was mounted after the secondary shutter before the beginning of the flight tube. The tube can be moved into the beam line when the neutron shutter is closed. The tube is more than 12 meters away from the detector position. This setup loses a lot of intensity, but has the great advantage of forming nearly the identical beam geometry as for neutron radiography. Using a Gadolinium-Oxisulfide scintillator, a common X-ray amplification foil which is sensitive for both neutrons and X-rays, enables the user for collecting matching datasets alternatively with X-rays and neutrons by the push of a button without the necessity of complicated registering (i.e. fitting the datasets over one another) of the calculated tomography volumes.
Some safety lights and switches still have to be installed for the final licensing, but Fig. 7 shows a photo of the X-ray tube in its retracted position before the flight tube, Fig. 8 already shows the first test measurement with X-rays during installation by the X-ray company. The carburettor (shown above as neutron radiography) is naturally very opaque for X-rays.

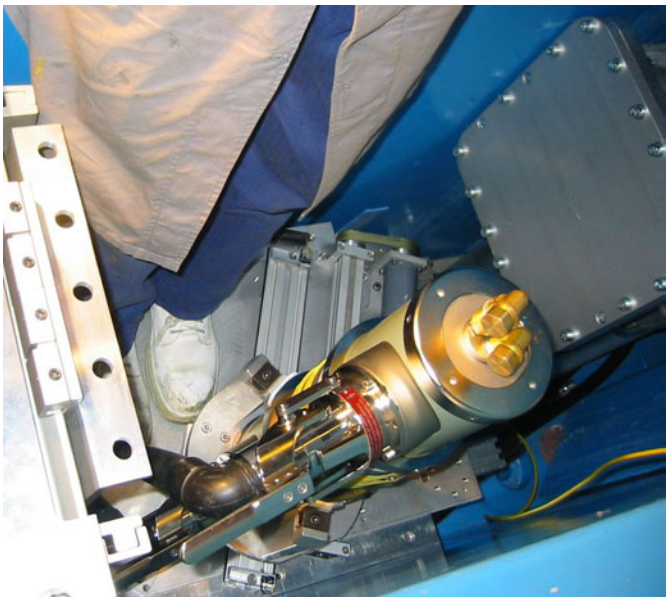

Figure 7: A photo of the X-ray tube in its retracted position.

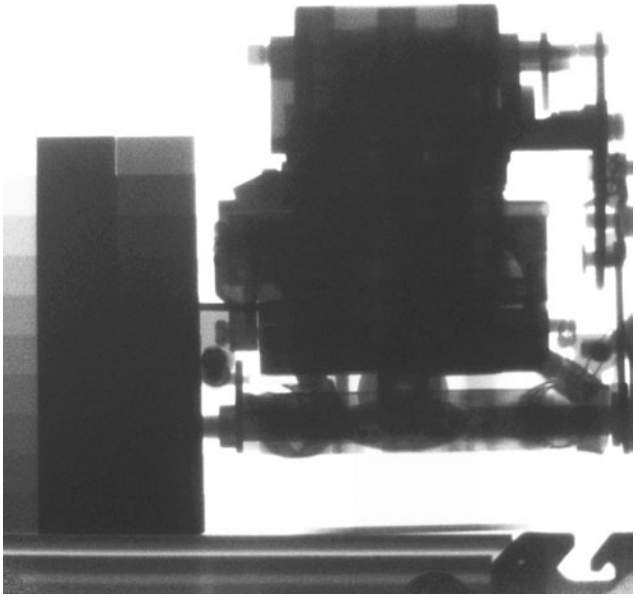

Figure 8: The first test measurement with X-rays during installation.

Selector wheel for phase contrast imaging

Between the secondary neutron shutter and the X-ray tube, a selector wheel (Fig. 9) has been installed that offers several different diaphragms for phase contrast imaging and coded aperture imaging.
Of eight possible positions, one is open for the full beam, two

contain coded masks and five contain smaller diaphragms from eight millimetres down to half a millimetre diameter, offering nominal L/D ratios from 2000 to 32000. For phase contrast imaging, a small hole diameter is required in order to achieve spatial coherence of the beam. A coherent beam will be diffracted at material edges which leads to visible edge enhancement.

Several successful phase contrast radiography measurements have been performed at PSI, with measurement times of about four hours. Since ANTARES will offer 40 to 100 times as much neutron flux, we will be able to do the worlds first phase contrast neutron computed tomography in 2005.

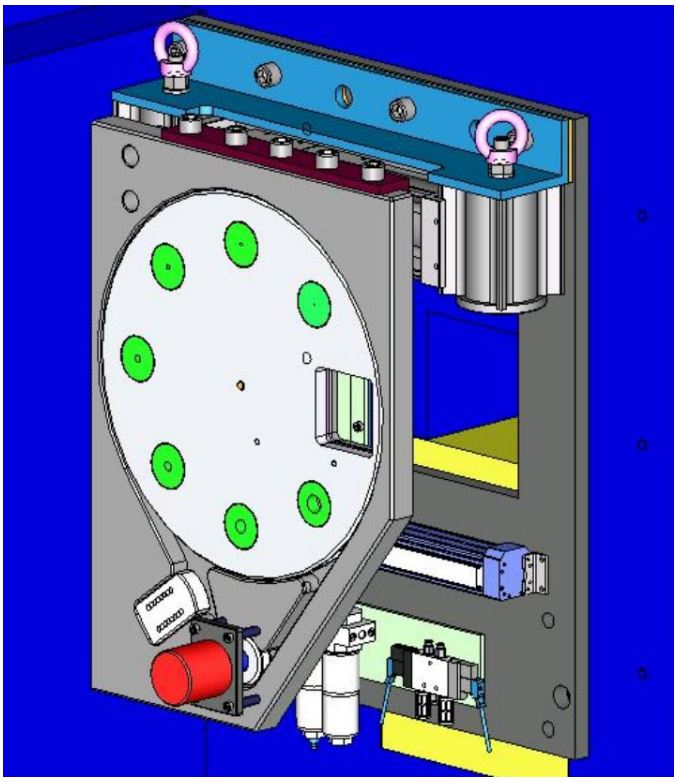

Figure 9: Drawing of the selector wheel.

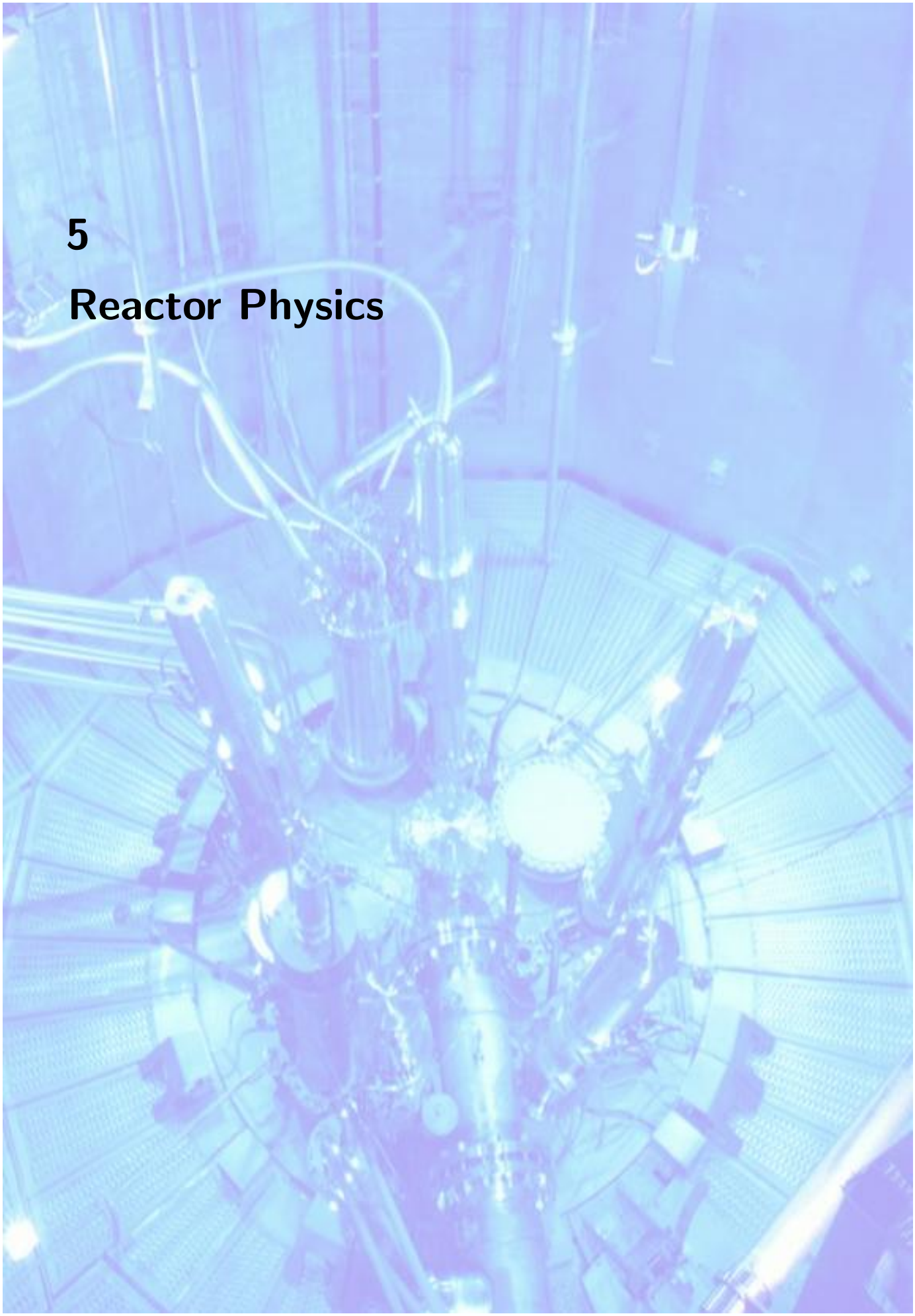

5
Reactor Physics

5.1 New high density fuel for the FRM-II

A. Röhrmoser [1], **W. Petry** [1], **K. Böning** [2], **N. Wieschalla** [2]
[1] *Technische Universität München, ZWE FRM-II, D-85747 Garching, Germany*
[2] *Technische Universität München, Physics Department, Institute E21, D-85747 Garching, Germany*

In 1998 the new "red-green"-Federal Government expressed its wish to take the FRM-II into operation with a fuel element with reduced enrichment - so far the scientific aims are met. Hearings with experts about the feasibility of the conversion have been organized by the Federal Ministry of Science and Education. In October 2001 an 'Agreement between the Federal Republic of Germany and the Free State of Bavaria on the conversion of FRM-II' has been written down and finally signed after granting the final license in May 2003. The compromise settled in this agreement is part of the final nuclear license - development of a new medium enriched (MEU, with not more than 50% U-235) fuel element until the end of the year 2010.
It is understood that the conversion should neither reduce the reactor safety nor degrade the neutron flux and reactor cycle time more than marginal.

Actual Schedule

Already in November 2001 TUM had established an international working group to study the possibility of a new fuel with up to now not qualified densities and reduced enrichment. The group consisted of representatives of the TUM (FRM-II), the fuel element manufacturer CERCA and the constructor of FRM-II, Framatome-ANP. In its kick-off meeting in July 2003 the group declared to accept the technological challenge of the development of a fuel with densities in the order of 8 g/cm^3 within the very short time limit of $7\frac{1}{2}$ years.
The project was broken down into three phases of $2\frac{1}{2}$ years duration each:

1. search for the fuel type, test irradiations
2. further test irradiations, final decision on the fuel type and design of the fuel element
3. fabrication of the fuel element and licensing

MEU Conversion FRM-II, Phase I

In program phase I the high density fuel shall be chosen or at least done a preselection. This first $2\frac{1}{2}$ years phase spreads from 7.2003 till 12.2005 and the following tasks are assigned to phase I:

1. calculations for the high density fuel(s) for FRM-II geometry
2. irradiations of MEU full size fuel plates
3. participation in international research programs

Calculations with UMo dispersion fuel, first results

Any scenario to convert the FRM-II has to keep the reactor power constant at 20 MW. Without changing the whole D_2O moderator tank with all its installations and its shutdown rods the core geometry must remain unchanged. This is necessary not only to avoid a complete new licensing procedure but also a reactor shutdown period of many years and costs of more than 150 million Euros as stated by a sharp estimation.
For an enrichment of 50% an advanced fuel with very high density is required when maintaining the dimensions of the HEU compact core fuel element of the FRM-II. The new uranium-molybdenum dispersion fuel (UMo-Al) presently under research worldwide promises realistic uranium densities of up to 8.0 g/cm^3. TUM did actual neutronics calculations for this fuel with the same procedures that led to the HEU design of FRM-II (criticality, burn up ...). The result was now that the density in the fuel must be at least 7.75 g/cm^3 with an enrichment of 50% U-235. When taking into account other aspects like the less fortunate power density distribution with UMo, the minium density can hardly be below 8.0 g/cm3. The core contains then 10.8 kg U-235 instead of 7.5 in the actual HEU case. The total U mass is 22 kg instead of 8 kg now. Necessary efforts to flatten the power distribution will reduce criticality.
One key point is the maximum of the fission density (FD) in the fuel. Because of the very inhomogeneous power and fission density in the plates maxima are reached only in very small areas of the plate. This is different from irradiation tests where the plates are much more homogeneously irradiated. The relevant maximum values in FRM-II must be assigned to the inner part of the plate and possibly to the plate ends. A result of these preliminary calculations is that the maximum of fission density in the meat is up to $2.0{\cdot}10^{21}$ cm^{-3} in a narrow area at the inner and outer border of the high density region. Test irradiations have to show whether the new fuel withstands the mentioned fission densities under full power conditions. Still the thermal flux is depressed by about 8.0% when compared to the actual HEU fuel, i.e. the aim of only marginal consequences for the scientific use is not yet met.

Actual Irradiation Program

For Phase I it was decided to plan an irradiation of four test plates of full size: For this, six plates are already produced by CERCA with UMo/Al dispersion fuel (8% wt. Mo) and wait to be irradiated.
The uranium densities are 8.0 g/cm^3 for 4 plates and 7 .0 g/cm^3 for the two other plates. Two of the 8.0 g/cm^3 plates contain the additive of a possible considerable "diffusion blocker". Those blockers are presently object of research and development worldwide. We used 2% of silicon additive in the Al matrix. Including a safety margin a FD of $2.3{\cdot}10^{21}$ cm^{-3} shall be reached by the test irradiations. According to calculations of CEA this will be reached in a remarkable area of the plates within four cycles of the MTR reactor OSIRIS at CEA-Saclay.
In case any of the 8.0 g/cm^3 plates will fail during the irradiation, it can be replaced by the two 7.0 g/cm^3 plates in the test facility.

6

Instrument Development

6.1 MIRA – the "very cold" beamline

Robert Georgii [2, 1], **Nikolas Arend** [1], **Peter Böni** [1], **Helmut Fußstetter** [2], **Thomas Hils** [1], **Daniel Lamago** [2, 1], **Sebastian Mühlbauer** [1], **Heinz Wagensonner** [2, 1]

[1] *Technische Universität München, Physics Department, Institute E21, D-85747 Garching, Germany*
[2] *Technische Universität München, ZWE FRM-II, D-85747 Garching, Germany*

Introduction

The construction of MIRA in its basic configuration has been finished early in the year. We also tested the position sensitive detector, having an active area of 18×18 cm^2 with a resolution of 1.5 to 1.8 mm, and integrated it in the instrument successfully. The instrument control software was also brought to working level. Thus the instrument was ready for neutrons:

On March, 2 2004 the FRM-II became critical for the first time at a thermal power of 1kW. On March, 8 the first neutrons have been measured at MIRA at a power of 50 kW and despite the low neutron intensity first tests of the monochromator were already possible.

In August the final power of 20 MW was reached and then kept constant for 4 weeks. This gave us the possibility to perform several demonstration experiments showing the performance of MIRA, already using different options of the instrument including different sample environments as low temperature and magnetic field (see Fig. 1). Such the performance of the whole instrument was successfully tested under realistic conditions.

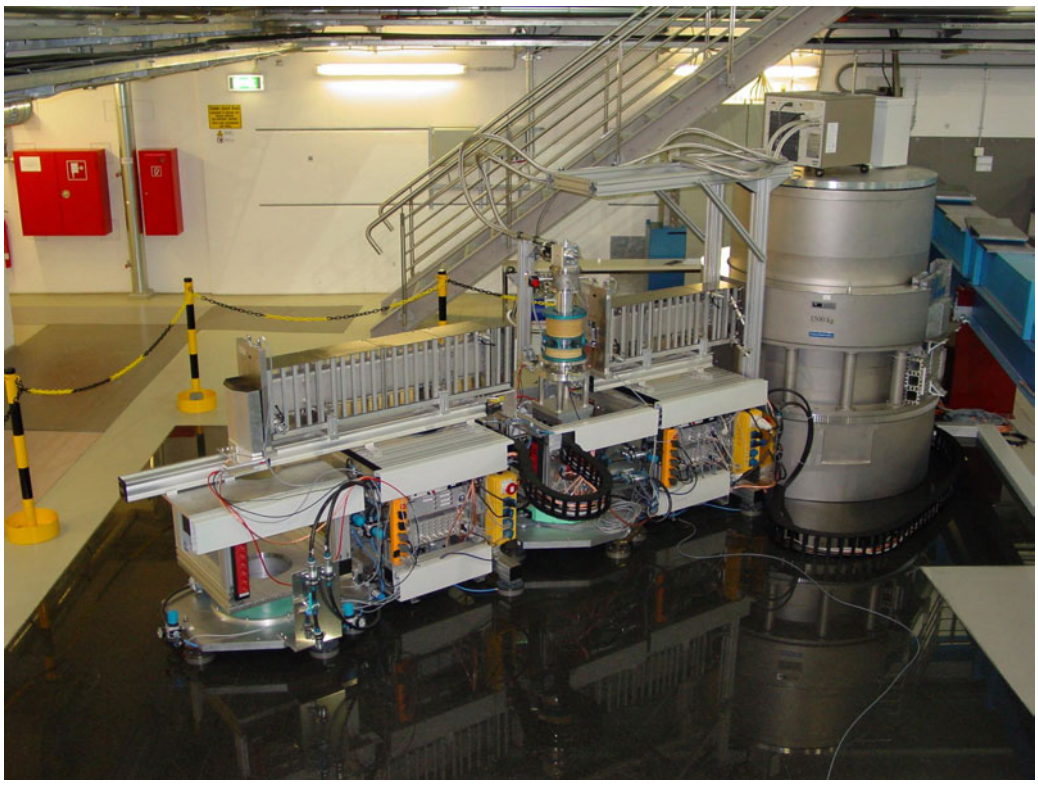

Figure 1: MIRA in the polarised reflectometer option equipped with a magnet and a closed cycle cooling machine.

Current improvements of the instrument are setting up a neutron spin-echo option (N. Arend, sec. 6.2), a multi-SANS set-up (Th. Hils, sec. 6.3) and building an improved water-cooled electromagnet up to 0.25 T (S. Mühlbauer).

Experiments

In the following the demonstration experiments performed are shortly described. A more detailed description can be found in the contributions of D. Lamago (sec. 1.1, 1.2), S. Mühlbauer (sec. 1.5) and Ch. Schanzer (sec. 2.3, 6.6, 2.4, 2.5,) in this report.

1. Reflectivity measurements on a magnetic multilayer (Ch. Schanzer): Unpolarisied neutron reflectivity measurements on a Ti/FeCoV/NiO/FeVoV/Ti magnetic multilayer have been performed partly in order to prepare later planned magnetic experiments and partly to improve the chemical lateral structure determination of the sample obtained with X-ray reflectometry.

2. The flux line lattice of Nb (S. Mühlbauer): A Nb sample cooled down to 6 K was measured in SANS geometry. Around the central beam a six-fold symmetry of the scattered neutron intensity could be observed. This is the footprint of the flux line lattice in the Shubnikov-phase of a type II superconductor.

3. The helical ferromagnet MnSi (D. Lamago): A MnSi single crystal at 10 K was measured in SANS geometry. Four scattering peaks were found indicating with their relative intensities the existence of the helical ferromagnetic phase.

6.2 Multi-MIEZE and NRSE options at MIRA

Nikolas Arend [1], **Robert Georgii** [1, 2], **Heinz Wagensonner** [2], **Thomas Keller** [3]
[1] *Technische Universität München, Physics Department, Institute E21, D-85747 Garching, Germany*
[2] *Technische Universität München, ZWE FRM-II, D-85747 Garching, Germany*
[3] *Max-Planck-Institute for Solid State Research, D-70569 Stuttgart, Germany*

The instrument MIRA is currently being equipped with a multi-MIEZE (Modulation of IntEnsity with Zero Effort [1]) and NRSE (Neutron Resonance Spin Echo) option. A crucial part of every NRSE based instrument are the NRSE coils. The FRM-II hosts two other instruments with Neutron Resonance Spin Echo (NRSE) capabilities, NRSE-TAS and RESEDA. Although not identical and optimised for the respective wave lengths, the NRSE coils installed at both instruments share a common basic design.
The DC coils are wound of an 8 mm by 0.5 mm aluminum band, coated with an Al_2O_3 layer to ensure electrical insulation. This coating is known to have two properties not ideal for application in neutron science (e.g. Small Angle Neutron Scattering (SANS)), especially with cold neutrons being utilised: The insulation layer is grown using a electro-chemical technique (anodising) and therefore features homogenously distributed pikes on its surface, forming a scattering grid-like structure. Furthermore it contains significant amounts of crystal water, which is intrinsic to the manufacturing process. The aluminum band must be specially treated before using it for coil winding, namely exposition to a D_2O atmosphere at high temperature (> 120 °C) in order to exchange H_20 by D_20, which has a significantly lower scattering cross section. Furthermore, since the winding density is relatively low, high currents (≈ 100 A) must be used to achieve the nominal DC field of 0.03 T.
The decision to develop a new NRSE coil design for MIRA was driven by the following goals:

- improvement of the neutron scattering/absorption properties at long neutron wave lengths
- since the construction of the RESEDA/NRSE-TAS coils requires some technical experience (especially with the winding process), a simpler and better reproducible design was desired, using standardised industrial materials and production engineering
- decrease the required current to achieve the same nominal field strength

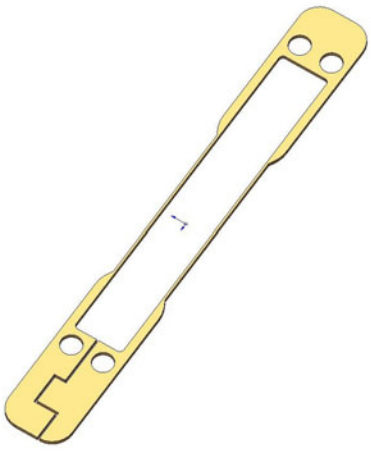

Figure 1: Winding geometry of the MIRA DC coils.

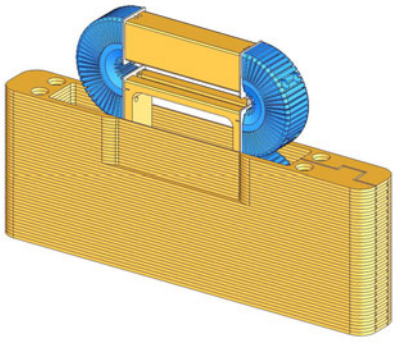

Figure 2: Assembled MIRA NRSE coil.

Fig. 1 and 2 show the current design, it is based on both an approach developed at the Max-Planck-Institute for Metal Research in Stuttgart [2] and the RESEDA/NRSE-TAS layout [3].
The idea is to form the DC coil by stacking single windings (Fig. 1) made out of 2 mm aluminum sheets. The contacting is done by point-wise welding and each layer is isolated against the next. The body of the DC coil, formed by the single Al sheets, does contain water cooling channels that will also serve as an alignment aid during assembly. Fig. 2 depicts a sketch of a partially assembled MIRA NRSE coil, including the radio frequency coils, whose layout is an enhanced version of the RESEDA coils. The window, where neutrons will penetrate the coil, is indicated in the center. Fig. 3 shows a test assembly of the DC coil, on which investigations of electrical and thermal properties can be performed.

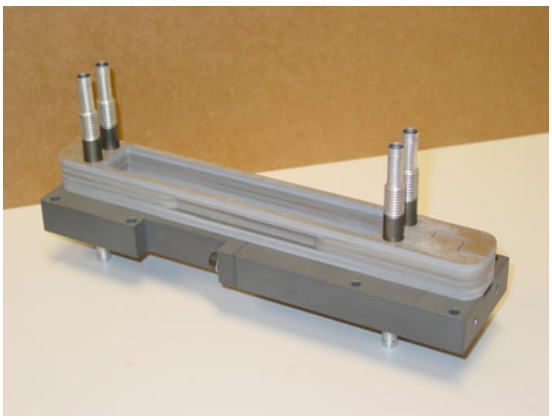

Figure 3: DC coil test assembly.

References

[1] Thomas Keller, Robert Golub, and Roland Gähler. In Roy Pike and Pierre Sabatier, editors, *Scattering and Inverse Scattering in Pure and Applied Science*, pages 1264–86. Academic Press, San Diego, CA, 2002.
[2] M. Wahl. Master's thesis, Max-Planck-Institut für Metallforschung, Stuttgart, Germany/Institut für Theoretische und Angewandte Physik, Universität Stuttgart, Germany, February 2003.
[3] R. Gähler and R. Golub. *J. Physique*, 49:1195, 1988.

6.3 Multiple Small Angle Neutron Scattering

Thomas Hils [1], **Roland Gähler** [2]
[1] *Technische Universität München, Physics Department, Institute E21, D-85747 Garching, Germany*
[2] *Institut Laue-Langevin, 38042 Grenoble Cedex 9, France*

Research on polymers, colloid systems, cements, microporous media, are examples of a rising field, where μm correlations play a crucial role. Small angle X-ray and neutron scattering (SAXS and SANS) typically measure lateral correlation lengths in the 0.01 to 1 μm range, the q-resolution ranging up to 10^{-3} Å^{-1}. To measure larger μm correlations with neutrons, the q-resolution has to be improved and various specific instruments have been designed. The technique is commonly known as USANS (ultra small angle neutron scattering). However these methods are sensitive to scattering only in one dimension and often suffer from intrinsic small angle scattering due to structure material in the beam.

Here we propose MSANS (Multi hole SANS), a new USANS option for a standard long baseline SANS instrument. It uses the common SANS infrastructure except for the detector, which requires enhanced spatial resolution. We aim at improving the q-resolution to about 10^{-5} Å^{-1} at 10 Å so correlations up to 60 μm should be possible. The system is sketched in Fig. 1.

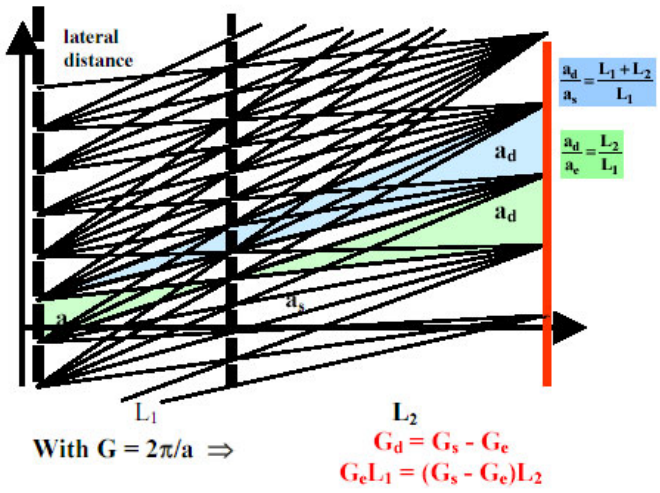

Figure 1: Condition for the lattice constants a_e and a_s and distances L_1 and L_2 for 'focussing' in the detector plane d

It is based on multi-hole apertures at the entrance (M_e) of the collimator and near the sample (M_s) with lattice constants a_e and a_s and hole diameters d_e and d_s respectively. With the choice

$$G_{e,s} = \frac{2\pi}{a_{e,s}}\,;\; G_e \cdot L_1 = (G_s - G_e)L_2\,;\; G_d = G_s - G_e$$

an intensity pattern of well separated peaks with lattice constant a_d in the detector plane is observed (a_d=$2/G_d$). The equations holds separately for x and z-direction, i.e. the lattice constants in both dimensions can be chosen according to the requirements. The validity of the above equations may be directly seen from Fig. 1.

Short range correlations in the sample may lead to significant overlap, however typical SANS intensities drop very rapidly with increasing q, and overlap will not be fatal in many cases. Sets of apertures with different relations $a_{e,s}/d_{e,s}$ (d diameter of hole apertures) can be used to adapt the pattern to the demand. In MSANS, resolution is decoupled from intensity, as long as the transmission of apertures is kept constant. The increase in q-resolution in MSANS is typically one order of magnitude, compared to SANS at equal intensity. The gain originates from the reduction in q-range in MSANS and the increase of the input guide cross section and its divergence. Diffraction from the aperture holes of typically 1 mm are not yet crucial, as the beam correlation length is only in the μm range.

Prototypes of a set of multihole-apertures based on cadmium and coated with typ. 13 μm 10B were produced with the following properties: hole diameter $d_{e,s}$ = 0.5/1mm; lattice constant $a_{e,s}$ = 2.5/5 mm.

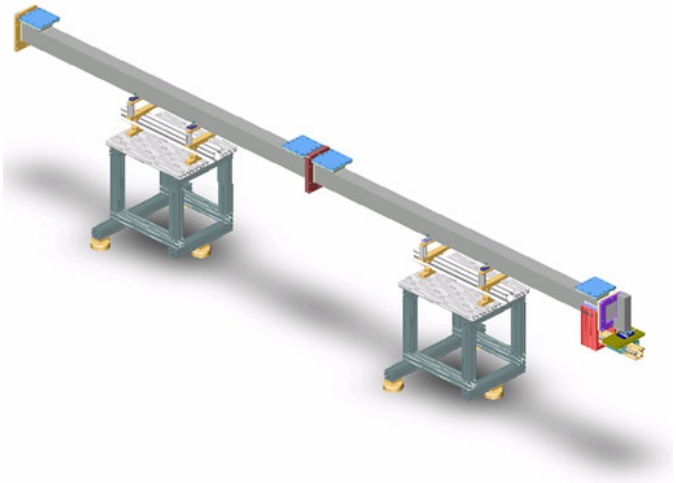

Figure 2: Setup MSANS.

In 2004 a basic test-design consisting of flight-tubes, the multihole-apertures, position-sensitive detector and the appropriate auxiliaries like tables, mountings etc. are being constructed and are to be manufactured.

6.4 Measurements on a short remanent solid state neutron polarizer at the POSY Refletometer at the IPNS in Argonne

Markus Bleuel [1], **Jyotsana Lal** [1], **Peter Böni** [2]
[1] *Intense Pulsed Neutron Source, Argonne National Laboratory IL-60439 Argonne, USA*
[2] *Technische Universität München, Physics Department, Institute E21, D-85747 Garching, Germany*

In order to test the performance of a versatile, compact polarizer, a series of measurements were conducted at the Posy I reflectometer (Fig. 1) at Argonne National Laboratory, USA [1]. Beside the alignment of the polarizer in the neutron beam there are two parameters having a serious impact on the performance of the polarizer:

- bending radius of the wavers
- amplitude of the guide field at the position of the polarizer

The incident neutron beam is polarized using a mirror that provides a polarization $P_{in} > 98\%$ in the range 3-10 Å. The flight time of the neutrons is converted into the wavelength λ of the neutrons and the intensity is recorded by means of an area detector located approximately 1.5 m from the remanent polarizer.

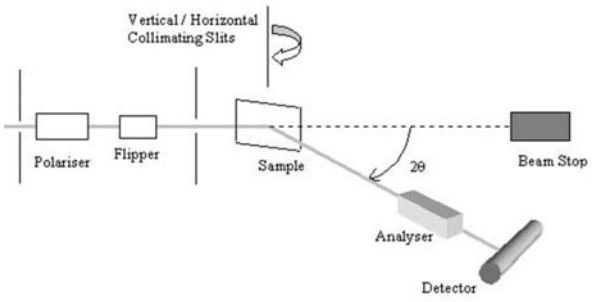

Figure 1: Setup of the Posy I reflectometer. For details see [2].

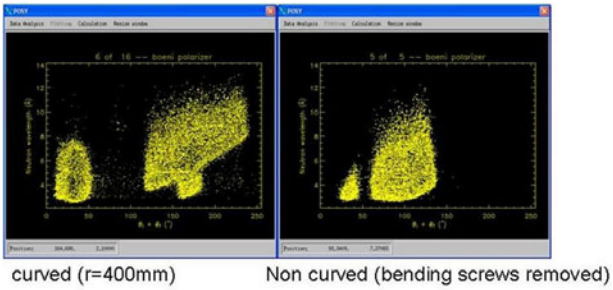

Figure 2: The figure shows the intensity of the neutrons (polarized anti-parallel to B_g) on the postion sensitive detector (PSD). The horizontal axis indicates the scattering angle (107 channels correspond to 1°), the vertical axis indicates λ. The left peak in each figure is the transmitted beam. The left figure shows the broad wavelength band reflected from the polarizing mirrors as discussed in Fig. 3 leading to an increased and unwanted transmission at large λ compared to the flat polarizer.

Fig. 2 shows the effect of different bending radii R of the silicon wavers on the transmitted and reflected neutron beam with polarization spin-down. Neutrons with small λ are not reflected because their angle of total reflection Θ_c is very small. With increasing λ more and more neutrons are reflected. By releasing the screws that push the wafers against a bent surface, R can be reduced. The results show that the reflected intensity is increased with decreasing R.
By looking at the right figure you can also estimate the angle of inclination: The difference between the middle positions of the transmitted and reflected beams is about 80 channels. This can be estimated to $\Theta_{in} + \Theta_{out} = 80/107^\circ \simeq 0.75^\circ$, so $\Theta_{in} \simeq 0.38^\circ$.
Fig. 3 gives an explanation for the dependence of the polarization on bending radius: If the mirrors are bent, the incoming angle between the neutron beam and the mirror surface depends on the position of the point of reflection in the polarizing channel. With increasing angle the critical λ (minimum λ reflected by the mirror) increases too. This means, that the neutrons are not reflected properly, if R becomes too large starting with the short wavelengths.

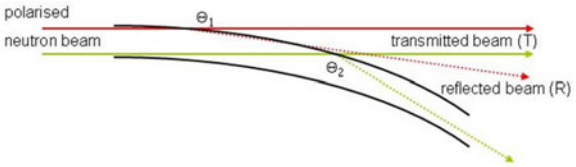

Figure 3: If the polarized neutron beam hits the supermirror, it splits into a reflected (R) and a transmitted (T) beam. For a curved supermirror the scattering angle changes with position ($\Theta_1 < \Theta_2$). This leads to a range of angles under which the polarized neutron beam hits the mirror surfaces.

Fig. 4 shows that the polarization increases with increasing guide field $B_g = 20$ G $\Rightarrow 100$ G. Note that the measurements in Fig. 2 were done with a guide field of 300 G.
In conclusion, we were able to successfully perform first tests on a compact remanent polarizer, with good polarizing efficiency ($P > 0.95$) for $\lambda > 4$ Å and $B_g = 300$ G. This performance may even increase with a new waver holder, since the reflected broad peak in the right Fig. 3 indicates, that the wavers indeed show some waviness.

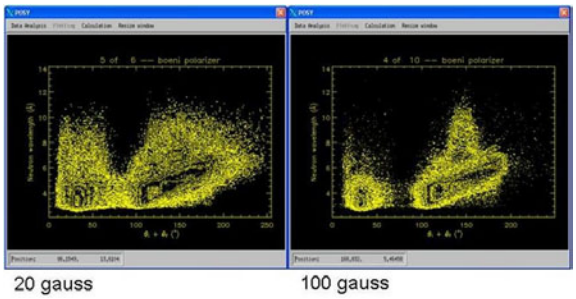

Figure 4: This figure shows an increasing polarization, if B_g is first reduced to 20 G and then increased to 100 G.

References

[1] G. P. Felcher, R. O. Hilleke, R. K. Crawford, J. Haumann, R. Kleb, and G. Ostrowski. The Polarized Neutron Reflectometer, a New Instrument to Measure Magnetic Depth Profiles. *Review of Scientific Instruments*, 58:609, 1987.
[2] http://www.pns.anl.gov/instruments/posy/.

6.5 RESEDA - the Neutron Resonance Spin Echo Spectrometer

Wolfgang Häußler [1, 2], **Peter Böni** [1], **Bodo Gohla-Neudecker** [2], **Heinz Wagensonner** [2]
[1] *Technische Universität München, Physics Department, Institute E21, D-85747 Garching, Germany*
[2] *Technische Universität München, ZWE FRM-II, D-85747 Garching, Germany*

RESEDA, the quasielastic Neutron Resonance Spin Echo (NRSE)-spectrometer at the FRM-II is located in the neutron guide hall. The neutron guide NL 5b leading to the instrument is bent, in order to provide a sufficient number of reflections, and to prevent direct sight to the neutron source. Thanks to its length (65 m, polarizing part 40 m), the bending radius of NL 5b is large ($r = 1640$ m), providing a broad neutron wavelength band ($\lambda = 2.5 - 15$ Å) with polarization being presumably better than 96%.

One part of the activities in 2004 at RESEDA was concentrated on the radiation shielding of NL 5b. Due to the results of first measurements of the radiation background performed just after the reactor start in May 2004, both guide and shielding were changed. The first part of the polarizing guide (8 m) was moved into the casemate, the lead shielding along the other part of the guide was doubled and a neutron shielding was mounted. New magnetic components needed for the polarizing guide, were installed, and the magnetic field was properly adjusted along the whole neutron guide.

Another major part of the activities was concentrated on the construction of the selector housing (s. Fig. 1). Base plate, aluminum support, rotary table and neutron shielding were built. The housing was modified in order to close openings in the shielding. In addition, cable channels were added. At the same time, the beam shutter in front of the selector was designed and constructed. In order to have enough space for the shutter, the neutron guide between selector housing and RESEDA was moved by 10 cm. The magnetic guide field inside the selector housing was modeled, and the necessary components were produced. The vacuum system of the selector was purchased and installed. In December, all components of the selector were mounted and tested. Finally, the three-dimensional model of the selector housing and all installations was actualized, because in the previous model, several dimensions were wrong, and major components were missing.

At RESEDA, several mechanical parts were reengineered. For example, the drive mechanics was modified, because the long (4 m) and heavy secondary spectrometer arms did not move properly. Both motors and encoders were substituted by a friction wheel drive and an absolute encoder. Concerning the extensive work on the electronics, we put into operation the RF-circuits. Both the existing RF coils were modified, in order to eliminate short circuits and new RF coils were constructed. For the first time, the RF coils were connected to the amplifiers by means of RF transformers. The circuits were tested and the resonance frequencies, resistances, and currents were determined. The RF transformers were adapted to the measured resistances. Bugs in the capacitor switches were eliminated. Two complete sets of coils and electronic components were selected, that have identical resonance frequencies. Finally, due to problems with the supplier of the RF amplifiers, new amplifiers were ordered from a different company.

Another major part of the activities was concentrated on the development of a new instrument-control program. It was decided to skip the non-functioning fragments of the existing code, and to start the development of TACO servers being the FRM-II standard, also for RESEDA. These activities are still going on and will be finished before the first measurements.

Figure 1: The velocity selector and the neutron guide leading towards RESEDA.

6.6 Elliptic neutron guides - a next generation in neutron optics

C. Schanzer [1], **U. Filges** [2], **T. Hils** [1], **P. Böni** [1]
[1] *Technical University Munich, Faculty for Physics E21, D-85747 Garching, Germany*
[2] *ETHZ&PSI, Laboratry for Neutron Scattering, CH-5232 Villgen PSI, Switzerland*

Sophisticated neutron guide systems take advantage of supermirrors being used to increase the neutron flux. However, the finite reflectivity of supermirrors becomes a major loss mechanism when a large number of reflections occur, e.g. in long neutron guides and for long wavelengths. In order to reduce the number of reflections, ballistic neutron guides have been proposed [1]. Usually linear tapered sections are used to enlarge the cross section and finally focus the beam to the sample. The disadvantages of linear tapering are an inhomogeneous phase space at the sample position and a decreasing flux with increasing distance from the exit of the guide.

We investigate the properties of i) a ballistic guide with linear tapering, ii) a ballistic guide with parabolic tapering and iii) an elliptic guide. Fig. 1 shows the various geometries.

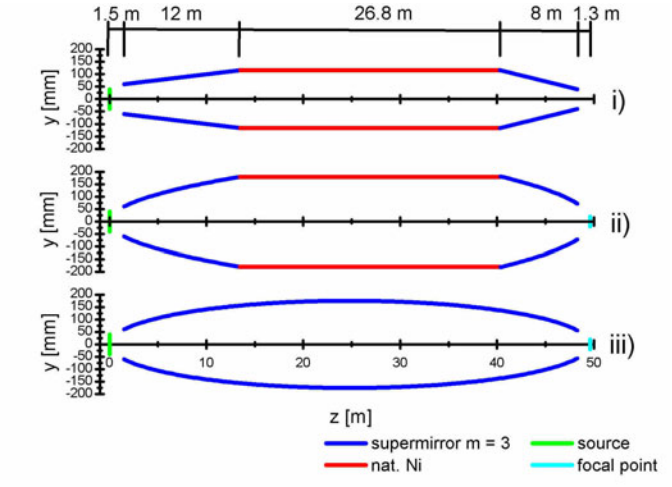

Figure 1: Various geometries for advanced neutron guides as described in the text: i) a ballistic guide with linearly tapered divergent/convergent sections, ii) a ballistic guide, where the divergent/convergent sections are parabolically shaped in two dimensions and iii) a neutron guide of elliptical shape.

Wavelength dependent gain factors of the different geometries with respect to a straight supermirror guide are shown in Fig. 2. The elliptic neutron guide is superior to the others and a gain up to a factor of five is achievable. In addition, we compare the phase space of the neutron beam provided by the various guide geometries. Fig. 3 shows the intensity distribution versus the divergence. A very inhomogneous distribution is obtained for ballistic guides with linear or parabolic tapering whereas the elliptic guide has a very homogeneous distribution and the highest intensity. In summary we can demonstrate by means of Monte Carlo simulation the beneficial properties of elliptic guides with respect to a gain of total intensity and the homogeneity of the phase space. Additionally the spot of highest intensity is shifted away from the guide exit for elliptic guides which allows an optimized beam handling with adjacent neutron optics. Further details of our investigations can be found in [2].

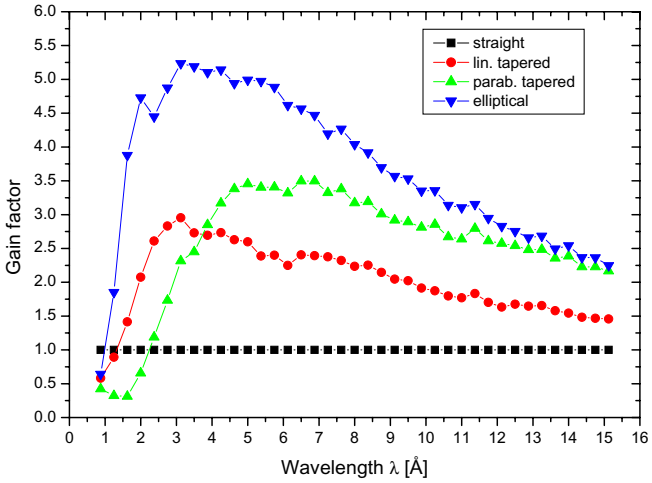

Figure 2: Gain factors of various guide geometries with respect to a straight supermirror guide ($m = 2$). Gain factors are calculated from integrated intensities (10×40 mm^2) at a distance of 0.5 m from the guide exit.

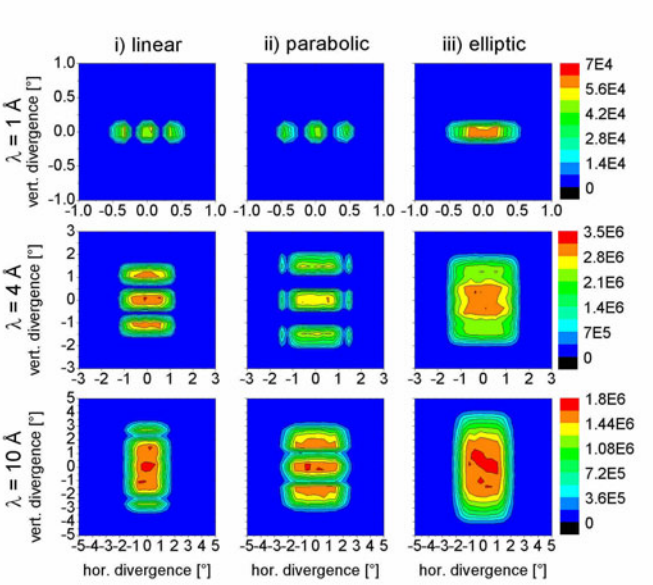

Figure 3: Vertical and horizontal intensity distribution (colour coded) versus the divergence for wavelengths $\lambda = 1$ Å, 4 Å, 10 Å of ii) ballistic guide with linearly tapered divergent and convergent sections, iii) ballistic guide with parabolic divergent and convergent sections, iv) elliptic guide. The intensity is spatially integrated over an area 10×40 mm^2 at a distance of 0.5 m from the guide exit. The divergence of the elliptic guide is rather homogeneous and the intensity is highest when compared with i) and ii)

References

[1] F. Mezei. *J. Neutron Res.*, 6:3, 1997.
[2] C. Schanzer, P. Böni, U. Filges, and T. Hils. *Nucl. Instr. and Meth. A*, 529:63–68, 2004.

7

Activities 2004

7.1 Lectures, Courses and Seminars

N. Arend	Practical course „Physikalisches Anfängerpraktikum“
P. Böni	Lecture „Magnetic Excitations: Theory and Experiment I“ Tutorial „Magnetic Excitations: Theory and Experiment I“ Lecture „Magnetic Excitations: Theory and Experiment II“ Tutorial „Magnetic Excitations: Theory and Experiment II“ Seminar „Neutrons in Research and Industry“, together with Profs. Böning, Petry, and Schreckenbach Seminar „Experimentelle Methoden der Festkörperphysik“, together with C. Hugenschmidt
K. Böning	Lecture „Reaktorphysik I und neue Konzepte in der Kerntechnik“ Seminar „Neutrons in Research and Industry“, together with Profs. Böni, Petry, and Schreckenbach
J. Brunner	Practical course „Elektronikpraktikum“
R. Georgii	Seminar „Neutronen in Forschung und Industrie“
F. Grünauer	Practical course „Physikalisches Anfängerpraktikum“
C. Hugenschmidt	Seminar „Experimentelle Methoden der Festköperphysik“
V. Kargl	Tutorial „Experimental Physics I“
T. Keller	Practical course „Elektronikpraktikum“
D. Lamago	Practical course „F-Praktikum Superfluid Helium“ Tutorial „Experimental Physics for Construction Engineers“
K. Lorenz	Practical course „Elektronikpraktikum“
W. Potzel	Practical course „Elektronikpraktikum“
C. Schanzer	Practical course „Demonstrationspraktikum für Lehramt Physik“
B. Schillinger	Practical course „Elektronikpraktikum“
K. Schreckenbach	Seminar „Neutrons in Research and Industry“, together with Profs. Böni, Böning, and Petry
N. Wieschalla	Tutorial „Reaktorphysik I und neue Konzepte in der Kerntechnik“

7.2 Seminar „Neutronen in Forschung und Industrie“ 2004

Date	Speaker	Title
26.1.	Arno Hiess (ILL, TU Dresden)	Herausforderungen und Möglichkeiten der Dreiachsenspektroskopie illustriert am Beispiel des Wechselspiels zwischen Magnetismus und Supraleitung in UPd2Al3
9.2.	W. Treimer (FH Berlin, HMI)	Neue Wege in der Neutronentomographie am HMI
16.2.	Stefan Janssen (PSI)	FOCUS: a Versatile Time-of-Flight Spectrometer at SINQ/PSI
23.2.	A. Kumar (MPI für Mikrostrukturphysik)	Spin-wave dispersion by spin-polarized electron energy loss spectroscopy
1.3.	Peter Kneschaurek (Klinikum rechts der Isar, TUM)	Hadronen in der Strahlentherapie - warum und wofür?
22.3.	Alexander Petoukhov (ILL)	Search for physics beyond the Standard Model at ILL
29.3.	Christian Rüegg (PSI)	Spin Dynamics across the Quantum Critical Points in S=1/2 Dimer Spin Systems
5.4.	Marc Janoschek (ILL, TUM)	MUPAD - 3D Polarisationsanalyse in magnetischer Streuung
10.5.	Georg Ehlers (SNS)	Untersuchungen der magnetischen Spindynamik von topologisch frustrierten Magneten mit Hilfe der Neutronen-Spinecho Methode
17.5.	V. Lauter-Pasyuk (ILL, TUM)	Monitoring of the internal magnetic structure in various magnetic nanosystems
24.5.	I. Goncharenko (LLB)	Neutron diffraction under extreme pressures
14.6.	A. Bradshaw (IPP, Garching)	ITER, why, how and where?
28.6.	Nico Wieschalla (FRM-II, TUM)	Entwicklung von neuen hochdichten Brennstoffen für Forschungsreaktoren
5.7.	Uwe Stuhr (PSI)	POLDI: A tof-diffractometer with multiple frame overlap for residual stress investigations
21.7.	P. Albers (Degussa AG)	Beispiele für den praktischen Einsatz der inelastischen, inkohärenten Neutronen-Streuung in der chemischen Industrie
19.7.	P. Strunz (Nuclear Physics Institute Rez, Czech Republic)	In-situ SANS application to investigation of high-temperature microstructure in superalloys and ceramic coatings
26.7.	M. Schwaiger (Klinikum rechts der Isar, TUM)	Radioaktivität und Bilder in der Medizin
13.9.	Shane Kennedy (ANSTO, Australien)	Neutrons from down under: progress report from the new Australian Research Reactor
20.10.	Staatsminister a.D. Dr. h.c. Hans Zehetmair	Festkolloquium
8.11.	Michael Meißner (BENSEC, HMI)	Neutronenstreuug bei höchsten Magnetfeldern: das N25T/N40T-Projekt bei BENSC
15.11.	Christian Schanzer (E21)	Untersuchung von FeCoV/NiO/FeCoV-Schichten mittels polarisierter Neutronenreflektometrie
29.11.	Kell Mortensen (Danish Polymer Centre, Risø National Laboratory)	Shear-Induced Texture and Shear-Induced Phase Transitions observed in Block Copolymer Melts and Networks

7.3 Publications 2004

[1] P.A. Alekseev, J.-M. Mignot, K.S. Nemkovski, E.V. Nefeodova, N.Y. Shitsevalova, Yu.B. Paderno, R. Bewley, R.S. Eccleston, E.S. Clementyev, and V.N. Lazukov. Yb-Yb correlations and crystal-field effects in the Kondo insulator YbB12 and its solid solutions. *J. of Physics: Condensed Matter*, 16:2631–2646, 2004.

[2] N. Arend, R. Gähler, T. Keller, R. Georgii, T. Hils, and P. Böni. Classical and quantum-mechanical picture of NRSE - measuring the longitudinal Stern-Gerlach effect by means of TOF methods. *Physics Letters A*, 327/1:21–27, 2004.

[3] P. Böni, C. Reich, B. Roessli, and E. Rastelli. Anti-renormalization of paramagnetic fluctuations in $CsMnBr_3$. *Physica B*, 350:59–62, 2004.

[4] E. S. Clementyev, P. A. Alekseev, P. Allenspach, G. Lapertot, and V. N. Lazukov. Single ion anisotropy and soft-mode-driven magnetic ordering in PrNi. *Physica B*, 350:e83–86, 2004.

[5] E. S. Clementyev, P. Böni, F. Demmel, and G. Shirane. Mapping of magnetic excitations in single-Q chromium. *Physica B*, 350:e67–69, 2004.

[6] R. Georgii, P. Böni, D. Lamago, S. Stüber, S.V. Grigoriev, S.V., Maleyev, A.I. Okorokov, H. Eckerlebe, P.K. Pranzas, B. Roessli, and W.E. Fischer. Critical small-angle scattering of polarised neutrons in MnSi. *Physica B*, 350:45–47, 2004.

[7] T. Hils, P. Böni, and J. Stahn. Focusing parabolic guide for very small samples. *Physica B*, 350:166–168, 2004.

[8] H. Hiraka, P. Böni, K. Yamada, S. Park, S-. H. Lee, and G. Shirane. Asymmetry of low-energy magnetic excitations in chromium. *Phys. Rev. B*, 70:144–413, 2004.

[9] C. Hugenschmidt, G. Kögel, R. Repper, K. Schreckenbach, P. Sperr, B. Straßer, and W. Triftshäuser. NEPOMUC - The New Positron Beam Facility at FRM II. *Mat. Sci. Forum*, 445-446:492–494, 2004.

[10] C. Hugenschmidt, G. Kögel, R. Repper, K. Schreckenbach, P. Sperr, B. Straßer, and W. Triftshäuser. The neutron induced positron source at Munich - NEPOMUC. *Nucl. Instr. Meth. B*, 221:160–164, 2004.

[11] V. Kargl, A. Mirmelstein, P. Böni, D. Sheptyakov, A. Amato, S. Kazakov, J. Karpinski, and A. Erb. Neutron diffraction, specific heat and μSR study of the spin chain compounds $Ca_{2+x}Y_{2-x}Cu_5O_{10}$. *Physica B*, 350:e257–e259, 2004.

[12] M. Senthil Kumar, P. Böni, and M. Horisberger. Neutron Reflectivity and Interface Roughness in Ni/Ti and FeCoV/TiN_x Supermirrors. *Nucl. Inst. and Meth. A*, 529:90–93, 2004.

[13] M. Senthil Kumar, V. R. Shah, C. Schanzer, P. Böni, T. Krist, and M. Horisberger. Polarized neutron reflectivity of FeCoV/Ti multilayers. *Physica B*, 350:e241–244, 2004.

[14] L. Liszkay, G. Kögel, P. Sperr, W. Egger, C. Hugenschmidt, and W. Triftshäuser. Positron Beam Splitter at the High Intensity Positron Beam in Munich. *Mat. Sci. Forum*, 445-446:480–482, 2004.

[15] P. Maier-Komor, I. Altarev, A. Bergmaier, P. Böni, G. Dollinger, R. Krücken, S. Paul, and W. Schott. Antireflection foils with multi-layer converter for ultracold neutron detectors. *Nucl. Instr. and Meth. A*, 521:242–246, 2004.

[16] A. I. Okorokov, S. V. Grigoriev, S. V. Maleyev Yu. O. Chetverikov, R. Georgii, P. Böni, D. Lamago, K. Pranzas H. Eckerlebe, and B. Roessli. The spin chirality in MnSi single crystal probed by small angle scattering with polarized neutrons. *Physica B*, 350:E323–E325, 2004.

[17] J. Padiyath, J. Stahn, P. Allenspach, M. Horisberger, and P. Böni. Influence of Mo in the Ni sublayers on the magnetization of Ni/Ti neutron supermirrors. *Physica B*, 350:E237–E240, 2004.

[18] J. Padiyath, J. Stahn, P. Allenspach, M. Horisberger, and P. Böni. Novel Monochromator Design. *Physica B*, 345:262–265, 2004.

[19] B. Roessli and P. Böni. Applications of Polarized Inelastic Neutron Scattering in Magnetism. *Pramana - J. Phys.*, 63:125–132, 2004.

[20] B. Roessli, P. Böni, W. E. Fischer, and Y. Endoh. Magnetic Field Dependence of Chiral Fluctuations in MnSi. *Physica B*, 345:124–127, 2004.

[21] A. Röhrmoser, W. Petry, K. Böning, and N. Wieschalla. Increasing depletion. *Nuclear Engineering International*, pages 28–30, December 2004.

[22] C. Schanzer, P. Böni, U. Filges, and T. Hils. Advanced geometries for ballistic neutron guides. *Nucl. Instr. and Meth. A*, 529:63–68, 2004.

[23] C. Schanzer, V.R. Shah, P. Böni, and T. Krist. Investigation of magnetization reversal in FeCoV/Ti multilayers. *Physica B*, 350:e221–e224, 2004.

[24] B. Schillinger, J. Baumann, H. Gebele, R. Schaetzing, H. Schaller, and M. Schuster. A new fast and large area neutron detector using a novel image plate readout technique. *J. Appl. Rad. Isotopes*, 61:451–454, 2004.

[25] B. Schillinger, E. Calzada, F. Grünauer, and E. Steichele. The design of the neutron radiography and tomography facility at the new research reactor FRM-II at Technical University Munich. 61:653–657, 2004.

[26] B. Schillinger, N. Kardjilov, and A. Kuba. Region of interest tomography of bigger than detector samples. *J. Appl. Rad. Isotopes*, 61:561–565, 2004.

7.4 Conference, Workshop and Seminar Contributions 2004

[1] N. Arend, R. Gähler, T. Keller, R. Georgii, and P. Böni. Preparation of short neutron pulses using the multi-level MIEZE principle. Conference on Precision Measurements with Slow Neutrons, Gaithersburg, MD, USA, April 2004. Poster.

[2] P. Böni. Excitations in Itinerant Systems. EASTMAG-2004, Krasnojarsk, Russia, Aug. 24 2004.

[3] P. Böni. Neutron Scattering from Magnetic Materials. ESRF, Grenoble, France, March 24-26 2004.

[4] P. Böni. SINQ, Supermirrors and the Consequences. Albert Furrer Symposium, Paul Scherrer Institute, Villigen, Switzerland, Oct. 6 2004.

[5] P. Böni. Spindynamik in magnetischen Materialien: Ein Spielplatz für Neutronen. Tag der Physik, Technische Universität München, Garching, July 16 2004.

[6] P. Böni, J. Brunner, and Ch. Schanzer. Präsentation für neuberufene Professoren. Technische Universität München, Garching, Feb 17 2004.

[7] P. Böni, B. Roessli, D. Lamago, and R. Georgii. Magnetic excitations and critical behavior in non-centrosymmetric MnSi. Workshop on MnSi, University of Geneva, Switzerland, March 19 2004.

[8] J. Brunner. Characterization of image quality in neutron radiography. International Topical Meeting of Neutron Radiography 2004, Munich, Germany, July 2004.

[9] J. Brunner. Dynamic neutron radiography of a combustion engine. Proceedings of the World Conference of Non Destructive Testing 2004, Montreal, Canada, September 2004.

[10] J. Brunner. Neutron radiography and tomography at FRM-II. Posters for the FRM-II inauguration, Tag der Physik, Tag der offenen Tür, 2004.

[11] J. Brunner. Neutron radiography at FRM-II. Seminar contribution at Hahn Meitner Institute, Berlin, Germany, May 2004.

[12] E.S. Clementyev, P.A. Alekseev, P. Allenspach, and V.N. Lazukov. Magnetic excitations in singlet ground state ferromagnet PrNi. 2^{nd} Euro-Asian Symposium „Trends in Magnetism“ (EASTMAG-2004), Krasnoyarsk, Russia, August 24-27 2004. Conference talk.

[13] E.S. Clementyev and G. Lapertot. Interplay between the RKKY and Kondo interactions in Gd1-xCexNi. International Conference on Strongly Correlated Electron Systems (SCES'04), Karlsruhe, Germany, July 26-30 2004. Conference Poster.

[14] Robert Georgii. Critical spin fluctuations in MnSi. Deutsche Neutronenstreutagung, September 2004. Talk.

[15] R. Gilles, C. Schanzer, W. Petry, and G. Eckold. The new small-angle scattering instrument SANS-1 at the FRM-II. Poster. canSAS-IV, Rutherford Appleton Laboratory, 12.5.-14.5.2004.

[16] R. Gilles, C. Schanzer, W. Petry, and G. Eckold. The new small-angle scattering instrument SANS-1 at the FRM-II. Poster. Deutsche Neutronenstreutagung, Dresden, 1.9.–4.9.2004.

[17] F. Grünauer. Image Deconvolution and Coded Apertures in Neutron Radiography. ITMNR5, July 26-30 2004. Conference talk.

[18] C. Hugenschmidt. Erste Positronen an NEPOMUC. Maier-Leibnitz-Kolloquium der Ludwig-Maximilians Universität und der Technischen Universität München, November 2004. Invited Talk.

[19] C. Hugenschmidt. NEPOMUC - Die neutroneninduzierte Positronenquelle und Experimente mit Positronen. Seminar des Max-Planck-Instituts für Kernphysik, Heidelberg, June 2004. Invited Talk.

[20] C. Hugenschmidt. NEPOMUC - Neutron Induced Positron Source Munich and Experiments with Positrons. Seminar at the Department of Physics, University of California, San Diego, USA, July 2004. Invited Talk.

[21] C. Hugenschmidt and M. Stadlbauer. Positronenspektroskopische Untersuchung von Magnesiumdruckgusslegierungen mit einem Koinzidenz-Doppler-Spektrometer. Frühjahrstagung der Deutschen Physikalischen Gesellschaft, Regensburg, March 2004. Conference Poster.

[22] V. Kargl, A. Mirmelstein, P. Böni, B. Roessli, and D. Sheptyakov. Magnetic neutron diffraction in $Ca_{2+x}Y_{2-x}Cu_5O_{10}$. Conference on strongly correlated electron systems, Karlsruhe, Germany, July 2004.

[23] D. Lamago, P. Böni, R. Georgii, S.V. Grigoriev, A.I. Okorokov, and S.V. Maleyev. Magnetic phase transitions in the itinerant ferromagnet MnSi. International conference on Strongly Correlated Electron Systems, Karlsruhe, Germany, July 2004.

[24] D. Lamago, P. Böni, R. Georgii, S.V. Grigoriev, A.I. Okorokov, and S.V. Maleyev. Magnetic susceptibility and specific heat of the weak ferromagnet MnSi. 3^{rd} Summer School on Condensed Matter Research - Phase Transitions, Zuoz, Switzerland., August 2004.

[25] K. Lorenz. Non-destructive testing with neutron phase contrast imaging. International Topical Meeting of Neutron Radiography 2004, Munich, Germany, July 2004.

[26] K. Lorenz. Non-destructive testing with neutron phase contrast imaging. Poster presentation at the XTOP conference in Prague, September 2004.

[27] C. Schanzer. Neutron optics - Liouville and its application. Invited talk. Summer school on neutron scattering 2004, Chalk River, 20.6.–25.6.2004.

[28] C. Schanzer. Untersuchung von FeCoV/NiO/FeCoV-Schichten mittels polarisierter Neutronenreflektometrie. Seminar talk. Seminar E21/FRM-II: Neutronen und deren Anwendungen in Wissenschaft und Industrie, Garching, 15.11.2004.

[29] C. Schanzer. Untersuchung von FeCoV/NiO/FeCoV-Schichten mittels polarisierter Neutronenreflektometrie. Seminar talk. Seminar Walther-Meissner-Institut: Aktuelle Probleme der Tieftemperatur-Festkörperphysik, Garching, 26.11.2004.

[30] C. Schanzer, P. Böni, U. Filges, and N. Kardjilov. Advanced geometries for ballistic neutron guides. Invited talk. International Conference on Neutron Optics NOP 2004, Tokyo, 12.1.-16.1.2004.

[31] C. Schanzer, V.R. Shah, P. Böni, H.B. Braun, T. Gutberlet, and M. Gupta. Magnetic depth profiling of FM/AF/FM trilayers by PNR. Poster. PNCMI 2004, Washington, 1.6.-4.6.2004.

[32] B. Schillinger. Experimental Setup and adjustment. International Topical Meeting on Neutron Radiography 5 (ITMNR-5), Garching, Germany: Workshop on Neutron Radiography and Tomography, 2004. Lecture.

[33] B. Schillinger. Image processing for radiography and tomography. International Topical Meeting on Neutron Radiography 5 (ITMNR-5), Garching, Germany: Workshop on Neutron Radiography and Tomography, 2004. Lecture.

[34] B. Schillinger. The principles of Tomography. International Topical Meeting on Neutron Radiography 5 (ITMNR-5), Garching, Germany: Workshop on Neutron Radiography and Tomography, 2004. Lecture.

[35] V. R. Shah. An overview on „Spintronics“. Seminar at E21 meeting, March 16 2004.

[36] V. R. Shah, C. Schanzer, P. Böni, and H. B. Braun. Interface and magnetic characterization of FeCoV/NiO/FeCoV trilayers,. 2^{nd} Euro-Asian Symposium „Trends in Magnetism“ (EASTMAG-2004), Krasnoyarsk, Russia, August 24-27 2004.

[37] V. R. Shah, C. Schanzer, P. Böni, and H. B. Braun. Interface and magnetic characterization of multilayered magnetic films. NATO Advanced Research Workshop - „Smart Materials for Ranging Systems“ (NATO-ARW), Krasnoyarsk, Russia, August 29- September 1 2004.

[38] V.R. Shah, C. Schanzer, P. Böni, and H.B. Braun. Magnetization reversal in FM/AF/FM trilayers: dependence of AF thickness. Poster. 5^{th} International Symposium on Metallic Multilayers 2004, Boulder, 7.6.–11.6.2004.

[39] B. Straßer, C. Hugenschmidt, and K. Schreckenbach. Konventionelle und positroneninduzierte Auger-Elektronenspektroskopie am System Kupfer-Gold. Frühjahrstagung der Deutschen Physikalischen Gesellschaft, Regensburg, March 2004. Conference Poster.

[40] Nico Wieschalla. Entwicklung von hochdichten Brennstoffen für Forschungsreaktoren. Seminarvortrag in „Neutronen in Forschung und Industrie“, TU-München, July 2004. Seminar Talk.

[41] Nico Wieschalla. FRM-II - short introduction. Saclay, CEA, France, September 2004. Invited Talk.

[42] Nico Wieschalla. Irradiation with heavy ions. Cadarache, CEA, France, October 2004. Invited Talk.

[43] Nico Wieschalla. Picture Analysis of U-Mo fuels. Cadarache, CEA, France, November 2004. Invited Talk.

Participants of ITMNR-5, held from July 26-30 2004 at TUM in Garching

7.5 Committee Memberships

P. Böni
- Nutzerausschuss deutsches Kontingent, Institut Laue Langevin, Grenoble, France
- Instrument Subcommittee, Institut Laue Langevin, Grenoble, France
- Referee for GKSS, Geesthacht, Germany
- SINQ Scientific Committee, Villigen, Switzerland
- Projektbegleitender Beirat FRM-II, Garching
- Instrumentierungsausschuss FRM-II, Garching
- TUM-Beirat für den FRM-II, Garching
- Coordinator of Work Package on Neutron Optics, Joint Research Project JRA3: NMI3 FP6
- International Conference on Neutron Optics NOP2004, Tokyo: Scientific Advisory Committee
- Conference on Polarized Neutrons in Condensed Matter Research PNCMI 2004, Washington: Scientific Advisory Committee
- Chairman of the International Topical Meeting on Neutron Radiography ITMNR-5 in Garching (together with Prof. Dr. A. Türler, RCM)
- Organisation of the symposium "Tomographic Methods in Materials Science" at the DPG-Meeting, March 4-9 2005 (together with Prof. Dr. J. Banhart, HMI)
- Gutachter, Wolfram-Prandl-Preis des Komitee's für die Forschung mit Neutronen

K. Schreckenbach
- Chairman of the 'Arbeitgemeinschaft Forschungsreaktoren' (German research reactor operation group)
- Chairman of the 'Expert Advisory Comittee' at the Institut Laue Langevin, Grenoble.

B. Schillinger
- Board member of the International Society for Neutron Radiography
- Vice President of the European Society for Neutron Radiology
- Conference Organizer and Editor for the 5th International Topical Meeting on Neutron Radiography (Garching, July 2005)

7.6 Accomplished PhD Theses

Sergey Prokudaylo Calculations for Neutron Spin Echo

Summary: Optimisation of the magnetic field geometries and preparations and analysis of experiments on crystal lattice dynamics.

7.7 Accomplished Master's Theses

Martin Engelhardt Imaging of dynamic processes with a timescale of microseconds at a thermal neutron beam

Marc Janoschek MuPAD 3D Polarization Analysis in Magnetic Neutron Scattering

Martin Stadlbauer Aufbau eines ortsauflösenden Doppler-Koinzidenzspektrometers zur Untersuchung der Positronenzerstrahlung in Festkörpern

7.8 Guided Tours at FRM-II

The FRM-II is open for everybody to come and visit the scientific and experimental facilities (Experimental Hall and Neutron Guide Hall). Therefore, Guided Tours are organised by a specially established division, the „Besucherdienst“, and conducted by the scientists and the technical personnel of FRM-II.

In 2004, the members of E21 guided approx. 130 officially registered tours and several others at various occasions, thus contributing a significant amount of time and personal effort to help making the Neutron Source FRM-II a publically transparent and accepted research facility.

7.9 E21 Members

Phone/Fax: +49-89-289-

Name	Phone	Fax	Room	email
Arend Nikolas, Dipl. Phys.	-12180	-13776	RS, 124	Nikolas.Arend@frm2.tum.de
Axtner Markus	-12125	-13776	RS, 140	maxtner@frm2.tum.de
Böni Peter, Prof. Dr.	-14711	-14713	PH 1, 2215	Peter.Boeni@frm2.tum.de
Böning Klaus, Prof. Dr.	-12150	-12191	FRM-II, UBA 0325	Klaus.Boening@frm2.tum.de
Brunner Johannes, Dipl. Phys.	-12106	-13776	RS, 146b	Johannes.Brunner@frm2.tum.de
Clementyev Evgeni, Dr.	-14722	-14713	PH 1, 2207	eclement@frm2.tum.de
Engelhardt Martin, Dipl. Phys.	+49-89-636-48015	+49-89-636-53810	–	zfp.student@mchp.siemens.de
Gläser Wolfgang, Prof. emerit.	-12476	-12474	PH 1, 2227	wglaeser@ph.tum.de
Grünauer Florian, Dipl. Phys.	-12115	-13776	RS, 140	Florian.Gruenauer@frm2.tum.de
Hils Thomas, Dr.	-14721	–	Flachbau, 17	thomas.hils@hils-consult.de
Jones Sylvia, Secretary	-14712	-14713	PH 1, 2217	Sylvia.Jones@frm2.tum.de
Kargl Verena, Dipl. Phys.	-12515	-14713	PH 1, 2373	Verena.Kargl@frm2.tum.de
Krimmel Sven, Dipl. Phys.	+49-89-636-45791	+49-89-636-53810	–	xray.external@mchp.siemens.de
Lamago Daniel, Dipl. Phys.	-14740	-13776	PH 1, 2207	Daniel.Lamago@frm2.tum.de
Lorenz Klaus, Dipl. Phys.	-14741	-13776	RS, 146b	Klaus.Lorenz@frm2.tum.de
Mühlbauer Martin, Diplomand	-14718	-13776	RS, 146b	Martin.Muehlbauer@frm2.tum.de
Mühlbauer Sebastian, Diplomand	-12515	–	PH 1, 2373	Sebastian.Muehlbauer@frm2.tum.de
Pfleiderer Christian, Prof. Dr.	-14712	-14713	PH 1, n/a	Christian.Pfleiderer@frm2.tum.de
Reingen Gabriel	-12656	–	PH 1, 1321	–
Russ Barbara, Dipl. Ing.	-14717	-14713	PH 1, 2207	Barbara.Russ@frm2.tum.de
Schanzer Christian, Dipl. Phys.	-14725	–	PH 1, 2214	Christian.Schanzer@frm2.tum.de
Schreckenbach Klaus, Prof. Dr.	-12183	-12191	FRM-II, UBA 0323	Klaus.Schreckenbach@frm2.tum.de
Schulz Michael, Diplomand	-14718	-13776	RS, 146b	Michael.Schulz@frm2.tum.de
Stadlbauer Martin, Dipl. Phys.	-14631	-13776	RS, Flachbau 16	Martin.Stadlbauer@frm2.tum.de
Steichele Erich, Dr.	-12141	-12112	–	Erich.Steichele@frm2.tum.de
Straßer Benno, Dr.	-12137	-13776	RS, Flachbau 16	Benno.Strasser@frm2.tum.de
Stüber Sebastian, Diplomand	-14723		PH 1, 2205	Sebastian.Stueber@frm2.tum.de
Valloppilly Shah, Dr.	-14723	-14713	PH 1, 2205	shah@frm2.tum.de
Wieschalla Nico, Dipl. Phys.	-12111	-13776	RS, 124	Nico.Wieschalla@frm2.tum.de

PH: Physics Department
RS: Reactor Station

7.10 Associated Members at FRM-II

Phone/Fax: +49-89-289-

Name	Phone	Fax	Room	email
Calzada Elbio, Dipl. Ing.	-14611	-13776	RS, 126	Elbio.Calzada@frm2.tum.de
Georgii Robert, Dr.	-14986	-14989	NL-Halle, UYH 0336	Robert.Georgii@frm2.tum.de
Häußler Wolfgang, Dr.	-14921	-14989	NL-Halle, UYH 0334	Wolfgang.Haeussler@frm2.tum.de
Hugenschmidt Christoph, Dr.	-14609	-13776	RS, 103	Christoph.Hugenschmidt@frm2.tum.de
Morkel Christoph, Dr. habil.	-12157		FRM-II, UBA 0324	Christoph.Morkel@frm2.tum.de
Röhrmoser Anton, Dr.	-14890	-14995	FRM-II, UYH 0328	Anton.Roehrmoser@frm2.tum.de
Schillinger Burkhard, Dr.	-12185	-13776	RS, 127	Burkhard.Schillinger@frm2.tum.de
Wagensonner Heinz, Dipl. Ing.	-14915	-14995	NL-Halle, UYH 0336	Heinz.Wagensonner@frm2.tum.de

PH: Physics Department
RS: Reactor Station

7.11 Guests

Phone/Fax: +49-89-289-

Name	Phone	Fax	Room	email
Gähler Roland, Dr. habil.	+33-4-7620-7189	+33-4-7648-3906	–	gahler@ill.fr
Keller Thomas, Dr.	-12164	-13776	RS, 106	Thomas.Keller@frm2.tum.de

PH: Physics Department
RS: Reactor Station

7.12 Guest Scientists

Name	Institute	Duration of stay
Demmel Franz, Dr.	Institute Laue-Langevin (ILL), France	November 1 2003 – January 31 2004
Klimko Sergey, Dr.	Institute Laue-Langevin (ILL), France	November 1 2004 – June 30 2005

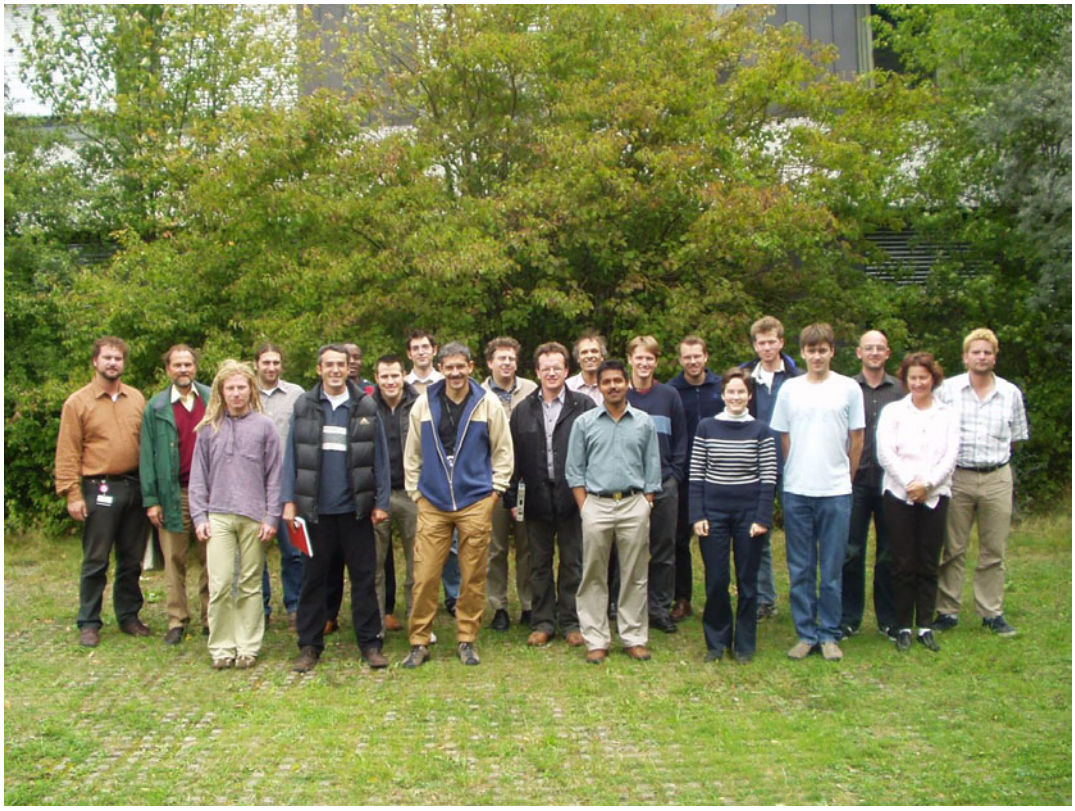

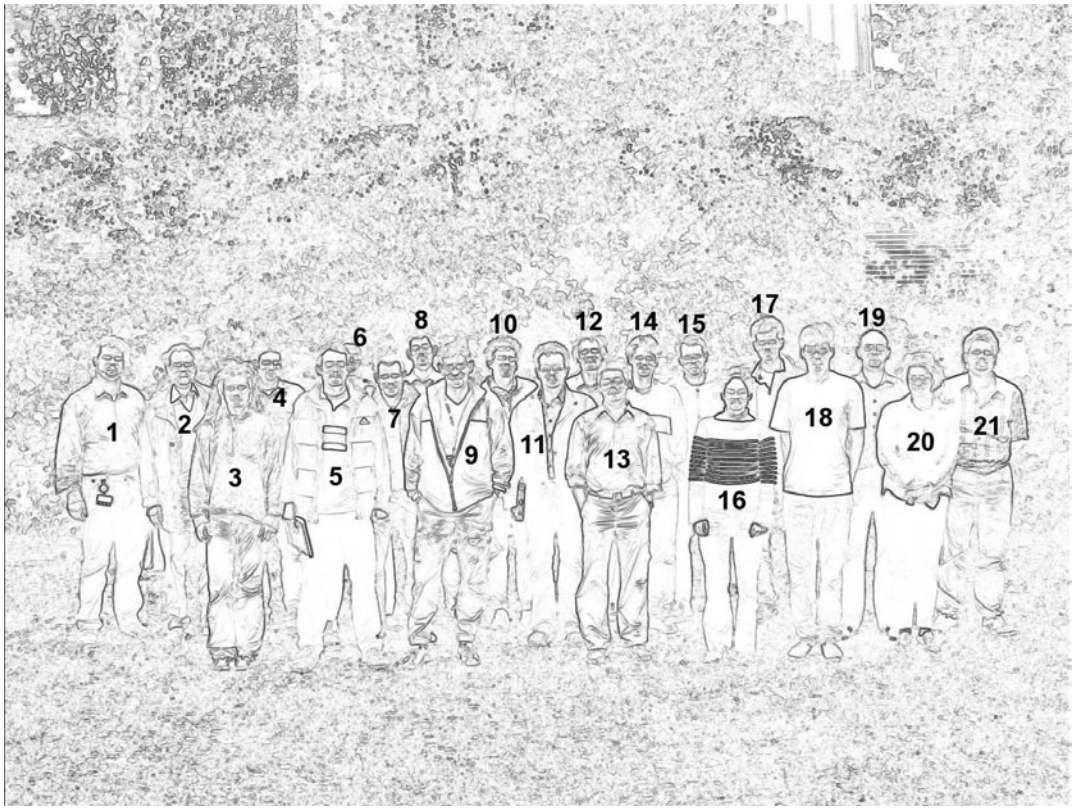

1	B. Schillinger	8	S. Stüber	15	N. Arend
2	K. Schreckenbach	9	E. Calzada	16	V. Kargl
3	M. Schulz	10	R. Georgii	17	K. Lorenz
4	M. Mühlbauer	11	C. Hugenschmidt	18	E. Clementyev
5	J. Brunner	12	P. Böni	19	C. Schanzer
6	D. Lamago	13	S. Valloppilly	20	S. Jones
7	M. Stadlbauer	14	S. Mühlbauer	21	F. Grünauer

Missing: H. Wagensonner, B. Gohla-Neudecker, T. Keller, B. Russ, K. Böning, M. Axtner, C. Pfleiderer, T. Hils, N. Wieschalla, W. Häußler, B. Straßer